UC Merced

UC Merced Electronic Theses and Dissertations

Title

Understanding the impact of single kinesin detachment kinetics on kinesin-based transport

Permalink

https://escholarship.org/uc/item/7903c2pq

Author

Wilson, John Olan

Publication Date

2023

Copyright Information

Peer reviewed|Thesis/dissertation

UNIVERSITY OF CALIFORNIA, MERCED

Understanding the impact of single kinesin detachment kinetics on kinesin-based transport

A dissertation submitted in partial satisfaction of the requirements
for the degree of Doctor of Philosophy

in

Physics

by

John Wilson

Committee in charge:

Professor Jay Sharping, Chair
Professor Ajay Gopinathan
Professor Jing Xu, Advisor

2023

The dissertation of John Wilson is approved, and it is acceptable in quality and form for publication on microfilm and electronically:

_____

Professor Ajay Gopinathan   Date

_____

Professor Jing Xu   Date

_____

Professor Jay Sharping, Chair   Date

University of California, Merced

2023

Table of Contents

List of figures

Acknowledgments

First, I would like to thank my PhD advisor Jing Xu, whose mentorship and guidance has made my journey through graduate school possible. Over the years Jing has maintained a balance between being supportive and pushing me to be a better researcher. I would also like to express my sincere gratitude to my thesis committee members: professor Jay Sharping and professor Ajay Gopinathan for their insightful comments and suggestions.

Next, I would like to thank Michael Li, a former graduate student in the Xu lab, whose guidance was helpful in getting started in my PhD.

I would like to thank my family who were all very supportive of my goal of obtaining my PhD. This was particularly important given the challenges my family faced over the past several years. Without their love and support it is unlikely, I would have completed college as a first-generation college student, let alone pursue my doctoral degree.

Finally, I would like to thank the friends I made over the course of graduate school. Having a group of friends who understood the challenges, and the importance of each successful step in my journey, was critical to my success.

Curriculum Vitae

Education

PhD, Physics, UC Merced   May 2023
BS, Physics, CSU Sacramento   May 2015
AS, Computer Science, Sierra College   May 2012

Skills

Python, C, C++, Java, SQL, Linux, Bash
Numerical simulations, Monte Carlo, Dynamic simulations
Data analysis & visualization, Bootstrapping, Machine learning, Regression
Matplotlib, Numpy, Scikit-learn, SciPy, Pandas

Certificates

Advanced Data Science with IBM Specialization   July 2022
Scientific Computing and Simulation, CSU Sacramento   May 2015
Computer Science: Embedded Systems, Sierra College   May 2012

Experience

Graduate Student Researcher, Biophysics, UC Merced   2017 – present
- Employed Monte Carlo simulations to examine molecular motor biophysics
- Carried out parallel computing on a multi-node computing cluster
- Developed analysis pipelines to perform parametric & non-parametric statistical analysis
- Developed a data visualized pipeline using matplotlib and Origin Pro
- Published two first-author papers, with two more publications in preparation
- Presented at nine international/national conferences (one invited talk)
- Supervised 11 undergraduates in research

Senior research project, Astrophysics, CSU Sacramento   2014-15
- Employed Monte Carlo simulations to examine populations of neutron stars
- Developed an analysis pipeline to perform least square fits
- Developed a data visualized pipeline using matplotlib
- Presented at a research symposium at CSU's

Honors research projects, Computer Science, Sierra College   2010-12
- Developed an N-body dynamic simulation to visualize orbiting planets
- Developed an agent-based simulation to visualize ant colony
- Developed an operating system to interface with an 8-bit computer

Awards and Honors

Faculty Diversification Graduate Fellowship	Bakersfield College	2021-22
NSF CREST: CCBM Graduate Fellowship	UC Merced	2018, 2019
Physics Graduate Group Summer Fellowship	UC Merced	2019
Summer Bridge Fellowship	UC Merced	2016
Senior Award, Physics	CSU Sacramento	2015
Honors Society Member	Sigma Pi Sigma	2014
Edwin Iloff Scholar, Physics	CSU Sacramento	2014
Vanderberg Scholar, Physics	CSU Sacramento	2014
Maxwell Scholar, Physics	CSU Sacramento	2012-14

Diversity and Outreach

Graduate teaching fellow at Bakersfield College   2021-22

- Taught a class of 30 students (20 minority, 10 female) in introductory physics class

Graduate mentor for high school students and undergraduate at UC Merced   2018-19

- Mentored one high school student (female, minority) in summer research
- Mentored 11 undergraduates in research (10 first generation, 4 females, 8 minority)

Science fair project judge at Merced County STEM fair   2019

- Evaluated 10 science fair projects for high school students from the Merced County

Publications

^{UG}: *Undergraduates supervised by JO Wilson*;   *: *co-senior author*

<u>JO Wilson</u>*, S. Deocampo^{UG}, J. Bartres^{UG}, D. Bercasio^{UG}, S. V. Valencia^{UG}, J Xu*, "Understanding the impact of molecular crowding on kinesin-based cargo transport", *in preparation*

Q Li, JT Ferrare, J Silver, <u>JO Wilson</u>, L Arteaga-Castaneda^{UG}, W Qiu, M Vershinin, SJ King, KC Neuman, J Xu, "Cholesterol in the cargo membrane reduces kinesin-1 binding in the presence of tau", *PNAS,* (2023)

<u>JO Wilson</u>, A Zaragoza^{UG}, J Xu, "Tuning ensemble-averaged cargo run length via fractional change in mean kinesin number", *Physical Biology* (2021)

<u>JO Wilson</u>, D Quint, A Gopinathan, J Xu, "Cargo diffusion shortens single-kinesin runs", *Scientific Reports* (2019)

Presentations

American Physical Society Annual March Meeting
  2020 "Cargo diffusion shortens single-kinesin runs"

2021 "Tuning ensemble-averaged cargo run length via fractional change in mean kinesin number"

Biophysical Society Annual Meeting

2020 "Cargo diffusion shortens single-kinesin runs"
2021 "Tuning ensemble-averaged cargo run length via fractional change in mean kinesin number"
2023 "Increased microtubule-detachment rate of kinesin under hindering load reduces multiple-kinesin cargo velocity"

American Physical Society Far West Annual Meeting

2018-19 "Cargo diffusion shortens single-kinesin runs"
2020 "Tuning ensemble-averaged cargo run length via fractional change in mean kinesin number"

Gordon Research Conference on Motile and Contractile Systems

2019 "Cargo diffusion shortens single-kinesin runs"

Bay Area Cytoskeleton Symposium (Invited Talk)

2019 "Cargo diffusion shortens single-kinesin runs"

Abstract

Understanding the impact of single kinesin detachment
kinetics on kinesin-based transport

by

John Wilson

Doctor of Philosophy in Physics

University of California, Merced

Jay Sharping, Chair

Molecular motors such as kinesin-1 drive the active and long-range transport of materials inside of our cells. This transport process is highly regulated, as these cellular cargos need to reach their destinations in a timely manner to maintain the proper function of the cell. Indeed, dysfunctions in this process have been linked to neurodegenerative diseases such as Lou Gehrig's disease. Kinesins single motor properties play a central role in this regulatory process, as these regulatory factors often act by altering these properties. A major focus of my research was how kinesin-1 detachment rate increases with force and how it is sensitive to the direction of the force. In my thesis study I employed Monte Carlo simulations to investigate the role of kinesins force-detachment kinetics in tuning key transport metrics such as the distance the cargo travels and the velocity of the cargo. I found that kinesins asymmetric force response results in a shorting effect on the cargos run length, as a result of the cargo random thermal motion (chapter 3). This diffusion-based shortening is countered by viscous drag, leading to an unexpected, non-monotonic variation in run length as viscous drag increases. Next, I found that the cargos run length is sensitive to slight changes in the average number of motors on the cargo and how this sensitivity can be tuned by kinesins detachment and attachment rates (chapter 4). Next, I explore how alterations to kinesins force-detachment kinetics, which can arise from macromolecular crowding, can impact the average velocity of cargos carried by more than one motor (chapter 5). Finally, a major part of my PhD experience has been mentoring undergraduates in simulation-based research, for many students this is their first-time doing research. Thus, I have created a guide of useful resources to engage future undergraduate students in similar simulation-based research projects (chapter 7).

Chapter 1 Introduction

1.1 Background

1.1.1 Active motion is a hallmark of life

One of the hallmarks of life is motion, specifically the ability to actively use energy to engage in this motion. We see this every day all around us. For example, we might observe an eagle in flight. With each beat of the eagle's wings, it consumes energy, which of course came from the food it consumed. What we don't often think about is the motion that happens at the microscopic level.

Zooming in on this microscopic level we will find a world full of cells in active motion [1-4]. Cells have evolved many different mechanisms to move themselves, such as flagella and cilia [3, 4]. These mechanisms allow cells to move towards nutrients, away from toxins, and interact with other cells [4]. Flagella and cilia are hair-like structures that extend from the surface of many cells, such as those in our respiratory tract, or sperm cells [3, 4]. These structures can move in a whip-like motion, propelling the cell forward or creating currents in the surrounding fluid [3, 4].

Another important aspect of cellular motility is the ability of cells to sense and respond to their environment [4]. This is accomplished through a variety of mechanisms, including chemical signals, mechanical cues, and electrical fields [5]. For example, immune cells can detect the presence of pathogens through chemical signals, and then move toward them in order to engulf and destroy them [4].

If we zoom in even further, to the inside of cells, we will find a bustling world of molecular motion and activity [6-8]. Cells are like highly organized microscopic cities, with different components of the cell serving different functions [7, 8]. A critical part of this organization is the placement of the various organelles and the distribution of materials to support the function of those organelles [9]. Cells achieve this by utilizing molecular motors, such as kinesin, to move materials around [6, 7]. These molecular motors are tiny machines, which function by utilizing chemical energy [6, 7].

1.1.2 Active transport is critical to cell function

The active transport of materials is critical to the health and function of all human cells (Fig 1.1). The various organelles within cells, such as mitochondria, endoplasmic reticulum, and Golgi apparatus, all have specific functions that require them to move and interact with each other [6, 7, 9]. In addition to organelles, cells must maintain a proper

distribution of materials to support their overall function and, the functions of their organelles [6, 7, 9]. To maintain the proper distribution of these materials and organelles, cells need to be able to move these materials around [6, 7].
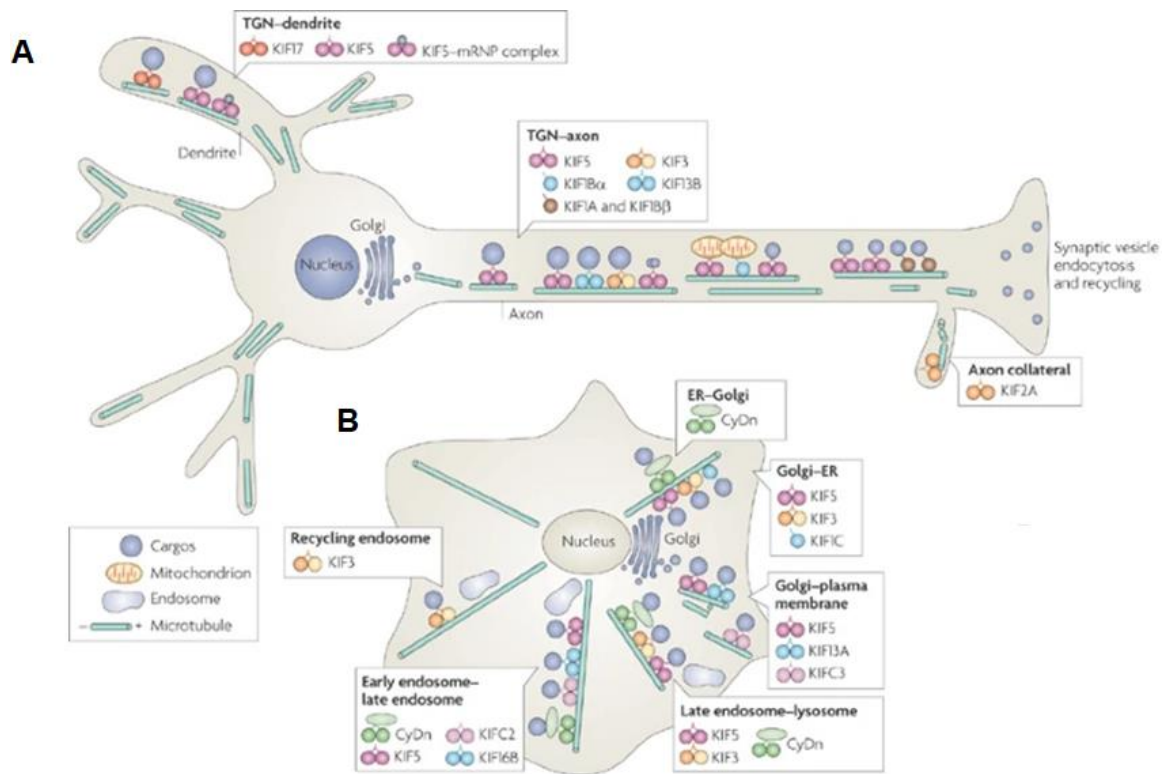
Figure 1.1: The transport of cargos by molecular motors is important across many cell types. Broadly these can broken down into two categories neuronal cells (A) and non-neuronal cells (B). Cargos being transported range from organelles (mitochondria for example) or other materials important to the function of the cells. This transport is carried out by many different types of motors including kinesin and dynein motors. A) In the axon (the long part of the neuron, kinesin motors transport their cargos from the cell body to the synaptic terminals. Dynein motors transport their cargos towards the cell body. B) In non-neuronal cells kinesin transports their cargos towards the cell body, while dynein transports their cargos towards the cell center. Diagram was reproduced with permission from Hirokawa, Nobutaka, et al. [10]. In my research, I focus on KIF5 also known as kinesin-1. Specifically, I use Monte Carlo simulations to investigate the impact of the impact of single kinesin detachment kinetics on kinesin-based transport.

Cells utilize molecular motors such as kinesin to actively drive the transport of materials and organelles [6, 7] (Figure1.3). Molecular motors transport their cargos, by "walking" along the cytoskeleton of the cell, consuming energy with each step. This active, and often long-range, transport of materials is critical to the cell's ability to maintain a proper distribution of materials.

Impressively, the process of active transport mediated by molecular motors can span several orders of magnitude in length scale, from nanometers to up to a meter in length in the case of neurons in the human body (Figure 1.3). This is one of the reasons cells must rely on active transport, as opposed to passive transport mechanisms such as diffusion. For example, it would take 2 years for a cargo to travel across a 10 cm neuron. With active transport, it would take approximately 3 hours.
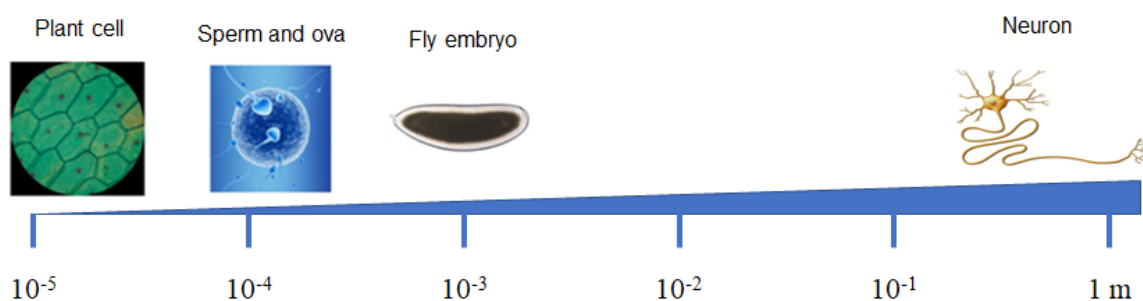
Figure 1.2: The active transport of material by molecular motors such as kinesin-1 spans 5 orders of magnitude and is important for many cell types. In my research, I aim to understand how kinesin-1's detachment kinetics acts as a regulatory mechanism in the transport process, which may help us better understand how transport by kinesin-1 motors can span this 5 order of magnitude length scale.

When this transport process becomes impaired, it can lead to severe consequences for the cell's health and function [11-13]. Neurons are elongated cells, which perhaps pose additional challenges in the transport process. It is conceivable that small mistakes in transported can result in the accumulation of cargos leading to major problems for the health of the neuron. Indeed, mutations in the gene associated with axonal transport machinery and errors in gene encoding have been linked to a large variety of neurodegenerative and neurodevelopmental diseases [11-13] (Table 1.1).

Table 1.1: Neurological diseases associated with dysfunctions in axonal transport.

Motor	Disease	Disease Type	References
Kinesin-1	Amyotrophic Lateral Sclerosis (ALS)	Neurodegenerative	[14, 15]
	Huntington	Neurodegenerative	[16]
	Alzheimer's	Neurodegenerative	[17]
	Spastic Paraplegia 10	Neurodegenerative	[18]
	Charcot-Marie-Tooth Type 2	Neurodegenerative	[19]
	Neonatal Intractable Myoclonus	Neurodevelopmental	[13]
Kinesin-3	Multiple Sclerosis	Neurodegenerative	[20]
	Meckel Syndrome 12	Neurodegenerative	[21]
	Primary Microcephaly 20	Neurodegenerative	[22]
	Charcot-Marie-Tooth Type 2a	Neurodevelopmental	[23]
Kinesin-4	Acrocallosal Syndrome	Neurodevelopmental	[24]
	Multiple Sclerosis	Neurodevelopmental	[25]
Kinesin-5	Microcephaly	Neurodevelopmental	[26]
Kinesin-7	Primary Microcephaly 13	Neurodevelopmental	[13]
Kinesin-12	Microcephaly and Thrombocytopenia	Neurodevelopmental	[27]
Kinesin-13	Cortical Dysplasia	Neurodevelopmental	[28]

1.2 Transport machinery in axons

The machinery supporting long-range transport of cargos in the axon consists of three primary components: the microtubules, the motors, and the cargos (Fig 1.4) [6, 7, 10]. In my thesis study, I focus on kinesin-1 motors as a model for understanding the transport process. Understanding the transport mechanisms of kinesin-1 motors is important because they are implicated in many neurological diseases (Table 1.1). Furthermore, we have a solid understanding of their single motor properties and have made significant progress in understanding what factors can influence these properties [29-34].

In the remainder of this section, I will discuss each of these transport components in turn, starting with the microtubules which act as a roadway for kinesin motors. Next, I will discuss kinesin motors. Finally, I will discuss the cargos and how they can impact the transport process.
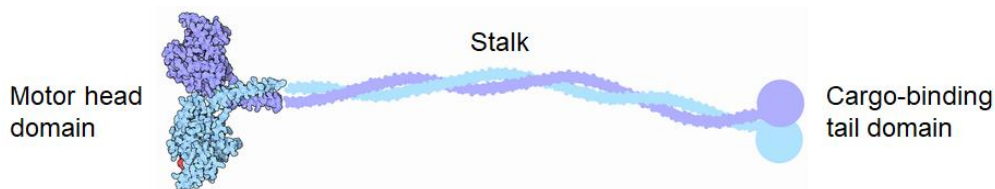
Figure 1.3: Kinesin-1 motor transport their cargos along a microtubule track. Each of these components plays an important role in the transport process Kinesins motor head domain allows it to step along the microtubule. In my thesis, I am focused on the force sensitivity in kinesins-1 detachment kinetics, and in particular the asymmetric response to the direction of the force. In my research I found that this asymmetric response introduces non-linearity in the transport process, suggesting that the force-detachment kinetics of kinesin motors plays an import role in the regulation of kinesin-based transport.

1.2.1 Microtubules are the molecular highway for kinesin motors

Microtubules are a critical component of the active transport of materials inside cells[8, 35-37]. They act as the highway for kinesin [38-40]. And thus plays a central role in maintaining the distribution of organelles and materials inside cells [7].

Microtubules are biopolymers that self-assemble from α- and β-tubulin dimers that polymerize to form long, hollow cylindrical structures [35, 37, 41]. These dimers can assemble into protofilaments, which then bundle together to form the microtubule [35]. Microtubules are polarized, with one end having a β-tubulin exposed, known as the plus end, and the other end having an α-tubulin exposed, known as the minus end [42].

The polarization of microtubules allows for the directional transport of cargos [6, 7, 10]. Typically, the plus end of microtubules is at the cell periphery and the minus is at the cell center. Kinesin motors are plus-end motors meaning they drive transport toward the cell periphery [6, 7, 10]. Dynein is minus end-directed motors driving transport toward the cell center. The opposing directionality of Kinesin and Dynein motors allows for the precise regulation of the transport process [43-46].

Just like the conditions of the roadway can impact traffic, the conditions of the microtubule can affect the transport of their cargos. Defects in the structure of microtubules can for instance cause transport to stall [47]. Further, the dynamics of transport can be regulated by MAPs. MAPs bind to the microtubule and play a critical role in their dynamics [48]. But they can also impact how molecular motors interact with them [49-55]. For example, MAP7 increases the binding rate of kinesin [50-52].

1.2.2 Kinesin-1 motors

Kinesin-1 (henceforth referred to as kinesin) motors are complex machines made up of several parts that work together to achieve their function [6, 7, 10, 56, 57]. Kinesin motors consist of two main regions: the motor domain and the tail domain (Figure 1.4). The motor domain has two heads, each of which can bind to the microtubule at specific locations.

The motor domain contains the microtubule-binding sites, while the tail domain is responsible for cargo binding [56]. Together, the motor domain, neck linker, and tail domain allow kinesin motors to move along microtubules and transport various cargos within cells [56].

1.2.2.1 Kinesins stepping rate

Kinesin motors step along the microtubule using a "hand-over-hand" motion [58-61]. This means that the two "heads" of the motor alternate in binding to the microtubule, with one head binding and propelling the other head forward, and then releasing and binding again in front of the first head. With each step, kinesin advances 8 nm along the microtubule while hydrolyzing one molecule of ATP [31, 34].

The hand-over-hand motion of kinesin motors along the microtubule is accomplished through a series of conformational changes in the motor domain, which is driven by the motor's chemomechanical cycle [57, 60, 62]. This cycle involves the binding of ATP to the motor domain, which induces a conformational change that allows the motor to bind to the microtubule and move forward [31, 34]. Hydrolysis of ATP then leads to a release of energy, which triggers a second conformational change that causes the motor to detach from the microtubule and move its trailing head forward [31, 34]. This process is then repeated as the motor takes additional steps along the microtubule. The coordination of this chemomechanical cycle with the hand-over-hand stepping mechanism allows kinesin motors to efficiently transport cargos over long distances within cells and produce a force of up to 7 pN [32, 33, 62].

Taken together the rate at which kinesin steps along the microtubule and its step size (8 nm), dictate kinesin's average velocity [31, 34]. Kinesin motors step along the microtubule at a rate that is limited by the amount of ATP available to them [63]. Kinesin's stepping rate is also sensitive to the force it experiences (see section 1.2.2.3) [29, 30].

1.2.2.2 Kinesins off-rate

During the chemomechanical cycle of kinesin motors, there are various points where the motor may become detached from the microtubule [29, 30, 61, 64]. For example, after hydrolyzing ATP and taking a step along the microtubule, the motor may release its grip on the microtubule if it fails to rebind to a new binding site on the microtubule. This process is captured in the motors detachment kinetics, which can be sensitive to force and other factors (section 1.2.2.3) [29, 30].

1.2.2.3 Force sensitivity of stepping and off-rates

It is common to model the chemomechanical cycle using simplified parameters such as detachment rate and stepping rate [45, 65]. These parameters can be adjusted to account for the effects of external forces on the motor's movement along the microtubule [29, 30]. For example, when kinesin motors experience a force, it can reduce their stepping rate and increase the likely hood of detaching from the microtubule [29, 30].

Notably, kinesin's response to force is asymmetric [29, 30]. Forces in the direction of their motion (assisting forces) lead to larger detachment rates than forces opposing their motion (hindering forces).

Kinesin's stepping rate is only impacted by hindering forces [29, 30]. Importantly, kinesin's force response can be modified by the cellular environment [66]. For example, macromolecular crowding can increase the rate at which kinesin detaches under hindering forces [66].

A   Assisting Force,   Hindering Force,
           $F > 0$ $F < 0$

B

$$v = v_0 \begin{cases} 1, & F > 0 \\ 1 - \left(\dfrac{F}{F_s}\right)^2, & F < 0 \end{cases}$$

C

$$\varepsilon = \varepsilon_\pm e^{\delta_\pm F / K_b T}$$
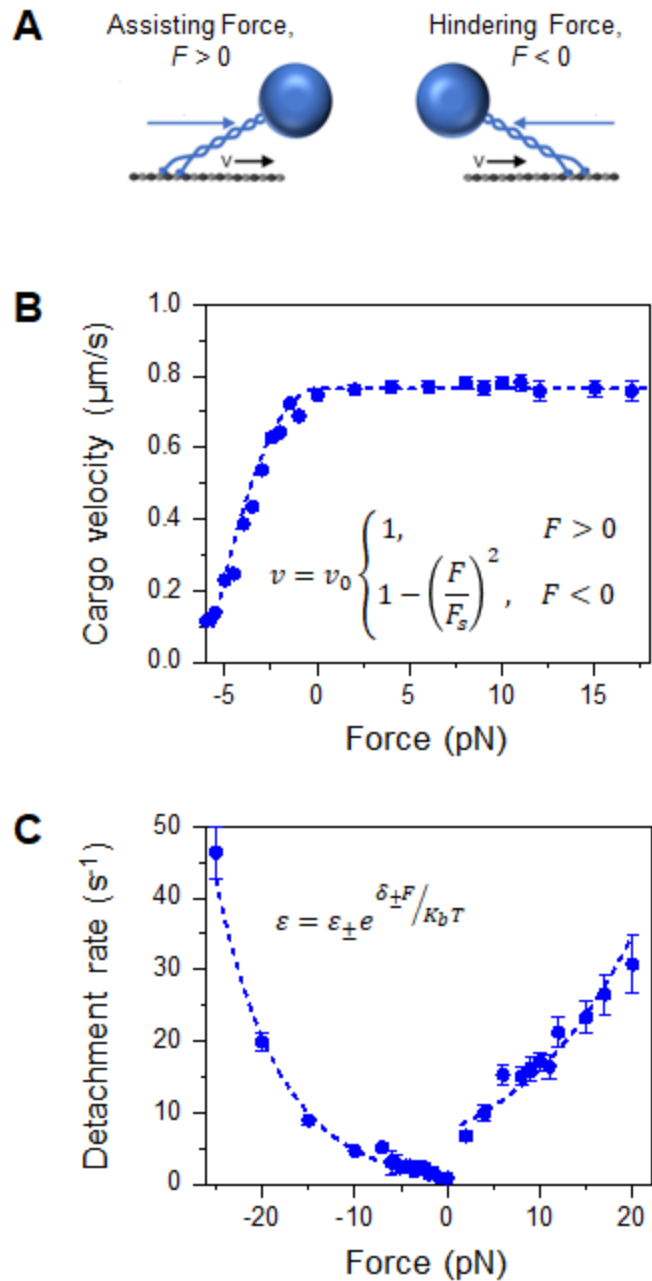
Figure 1.4: Motors experience a force when they become separated from the cargo by more than their rest length. Hindering forces result in a decreased stepping rate of the motor and an increased detachment rate. Assisting forces increase the motor's detachment rate, but don't impact the motor's stepping rate. In my thesis study, I explore how the cargos run length and velocity are sensitive to the asymmetric response of kinesins force-detachment rate.

1.2.2.4 Kinesin attachment rate

Another important parameter in kinesin-based transport is the rate at which motors bind to the microtubule or on-rate [67-69]. Motors unattached from the microtubule will be undergoing diffusion and when they come close to the microtubule there is a chance they can attach to the microtubule [55]. Many factors can impact this process. For example, the location of the motor on the cargo can impact the probability the motor will be near enough to the microtubule to bind [70]. Another factor could be the availability of binding sites [71]. Additionally, certain MAPs, such as MAP7 are known to recruit kinesin motors effectively increasing the on-rate [50-52]. Other MAPs, such as Tau, will decrease the kinesin's on-rate [53-55, 72].

1.2.3 Cargos

Kinesin motors are involved in the transport of a wide variety of cargoes in cells, including organelles, vesicles, and protein complexes [7, 10]. The identity of the cargo being transported can impact the activity of kinesin motors in several ways, including their velocity, processivity, and detachment kinetics [73].

1.2.3.1 Forces on the cargo

The size of the cargos that kinesin carries can vary greatly [74, 75]. Some cargos, such as small vesicles, may be only a few nanometers in size, while others, like organelles such as mitochondria, can be several micrometers in length. This size variation can impact the transport process in several ways, including the velocity and processivity of the motor, as well as the forces exerted on the motor by the cargo during transport.

This size variation of the cargos is import because the size of the cargo can impact the drag forces experienced by the cargo [74, 75]. The larger the cargo, the higher the drag force it experiences as it moves through a fluid, such as the cytoplasm of a cell [76]. Furthermore, high cytoplasmic viscosities can also increase the drag on the cargo [74, 77-79]. A large drag force on the cargo will lag behind the motor, and the motor will experience a force opposing its motion which can impact both the stepping and detachment kinetics of the motors [76, 80].

Cargo size can also impact the diffusion of the cargo which can also have important implications for kinesin-based transport [76]. Diffusion is the process by which particles move randomly due to their thermal energy, the rate of diffusion decreases with cargo size [81]. The diffusion of the cargo can impact kinesin-based transport because the cargos diffusion will cause it to exert both hindering and assisting loads on the cargo.

1.3.3.2 Biological nature of the cargo

Another factor that can impact transport is the composition of the cargo [55] [75]. For example, enclosing a cargo in a lipid membrane can enhance its velocity [82]. Furthermore, the surface fluidity of lipid membrane-enclosed cargos may reduce the mechanical interference between motors, thereby enhancing the cargo processivity [83]. The lipid membrane of cargos may also play an important role in the ability of the cargo to navigate obstacles along the microtubule, such as tau, during transport [55].

1.1.3 Regulations of transport target single-molecule functions

In cells, motor-based transport is highly regulated, ensuring that cargos reach its destinations in a timely manner [8, 73, 84]. There are many ways this transport is regulated, for example, cells can use chemical signals which lead to post-translational modifications in the motor [8]. Another way this transport process may be regulated is via microtubule-associated proteins (MAPs), which can affect how the motors interact with the microtubule [85-87]. Often these regulatory mechanism act by changing and impacting the single motor properties [84]. Thus, understanding how the single motor properties impact the transport process is critical to understanding how this transport process is regulated in cells.

1.3 Overview of my thesis study

In my thesis research, I used Monte Carlo simulations to investigate the role of single motor properties in regulating kinesin-based transport. Many factors which regulate kinesin-based transport do so by modifying kinesin's single-motor properties. My primary focus was on understanding how asymmetry in kinesins detachment kinetics introduced non-linearity during the cargo transport process. In this section, I introduce each of the major topics in my research.

1.3.1 Cargo diffusion shortens single-kinesin runs at low viscous drag

Molecular motors such as kinesin-1 drive active, long-range transport of cargos along microtubules in cells. Thermal diffusion of the cargo can impose a randomly directed, fluctuating mechanical load on the motor carrying the cargo. Recent experiments highlighted a strong asymmetry in the sensitivity of single-kinesin run length to load direction, raising the intriguing possibility that cargo diffusion may non-trivially influence

motor run length. To test this possibility, here we employed Monte Carlo-based simulations to evaluate the transport of cargo by a single kinesin. Our simulations included physiologically relevant viscous drag on the cargo and interrogated a large parameter space of cytoplasmic viscosities, cargo sizes, and motor velocities that captures their respective ranges in living cells. We found that cargo diffusion significantly shortens single-kinesin runs. This diffusion-based shortening is countered by viscous drag, leading to an unexpected, non-monotonic variation in run length as viscous drag increases. To our knowledge, this is the first identification of a significant effect of cargo diffusion on motor-based transport. Our study highlights the importance of cargo diffusion and load-detachment kinetics on single-motor functions under physiologically relevant conditions.

Figure 1.5: Cargo diffusion shortens single-kinesin runs at low viscous drag. A) Cargo diffusion can cause the motor to experience both assisting forces and hindering forces. B) Viscous drag on the cargo results in the motor experiencing hindering forces. In my thesis study, I explore how the relative sampling of both assisting and hindering forces from cargo diffusion, as tuned by the viscous drag, impacts the cargos run length. I found when viscous drag is low, the frequent sampling of assisting forces results in a shorting of the cargo's run length. Slight increases in viscous drag reduce this sampling increasing the cargos run length. Overall, I found that this asymmetric force-detachment rate results in a non-monotonic response in kinesin's run length as viscous drag is increased.

1.3.2 Tuning ensemble-averaged cargo run length via a fractional change in mean kinesin number

The number of motors carrying cargos in biological cells is not well-defined, instead varying from cargo to cargo about a statistical mean. Predictive understanding of motility in cells therefore requires quantitative insights into mixed ensembles of cargos. Toward this goal, here we employed Monte Carlo simulations to investigate statistical ensembles of cargos carried by a Poisson-distributed number of motors. Focusing on the key microtubule-based motor kinesin-1, our simulations utilized experimentally determined single-kinesin characteristics and alterations in kinesin's on- and off-rates caused by cellular factors and/or physical load. We found that a fractional increase in mean kinesin number enhances the ensemble-averaged cargo run length and amplifies run-length sensitivity to changes in single-kinesin on-rate and off-rate. These tuning effects can be

further enhanced as solution viscosity increases over the range reported for cells. Together, our data indicate that the physiological range of kinesin number sensitively tunes the motility of mixed cargo populations. These effects have rich implications for quantitative and predictive understanding of cellular motility and its regulation.

1.3.3 Force-dependent kinesin detachment critically influences the effect of cargo-mediated motor interactions on cargo velocity

Molecular motors such as kinesin-1 often work in small teams to drive the long-range transport of cargo along microtubules in cells. During transport these motors can undergo force-based interactions, mediated through the cargo, increasing the likelihood of one of the motors detaching from the microtubule. After a detachment event will be pulled toward the remaining motor. If these detachment events are biased toward one direction they can impact the average velocity of cargos transported under these conditions. This is potentially the case with macromolecular crowding which has been shown increase kinesin's detachment rate under hindering loads. This increase in detachment kinetics is thought to be responsible for the slow down of cargos transported by multiple kinesins under crowded conditions. Here, we used Monte Carlo simulations to examine how kinesin force-dependent detachment kinetics influence the effects of cargo-mediated motor interactions on the cargo's average velocity. We found increasing the motors detachment rate under hindering loads resulted in a slowdown under crowded conditions. This effect could be amplified by heterogeneity in kinesin's population which increases the cargo-mediated interactions between the motors. We also found that a small external forces on the cargo could also amplify the impact of the slowdown. Our study indicates that kinesin's force-dependent detachment rates may be an important and sensitive tuning factor influencing the velocity of cargos transported by multiple motors in the cell.

Motors become
separated

Leading motor
detaches

Cargo flops
backward
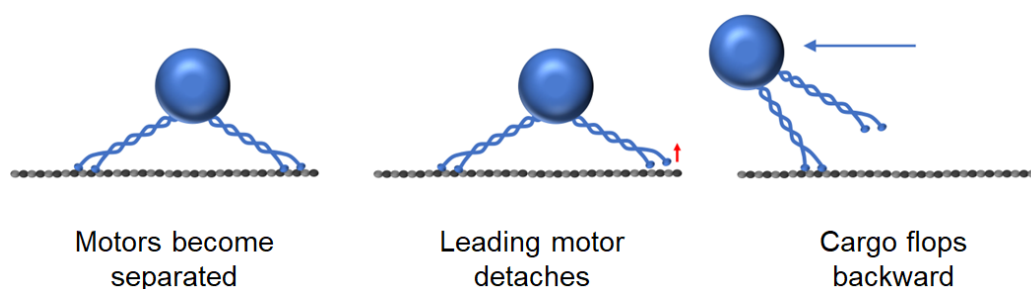
Figure 1.6: Force-dependent kinesin detachment critically influences the effect of cargo-mediated motor interactions on cargo velocity. When two motors transporting a cargo become separated, they will each experience a force, which may result in one of them detaching from the microtubule. When this happens the cargos position will change in response. In my thesis study, I am interested in how

kinesin's force-detachment kinetics may bias this process resulting in a change to the average velocity of the cargo.

Chapter 2 Methods

2.1 Kinesin Simulation

In my thesis project, I adapted a previously developed Monte Carlo-based simulation model to examine the regulating effects of kinesin's single motor parameters. In this section, I outline the algorithm employed in the kinesin simulations used in my thesis project.

2.1.1 Description of kinesin simulation

Here I will give an overview of the flow of my simulation, breaking it the simulation down into a series of key steps which are evaluated at each time step (Figure 2.1). Each of these steps are described in detail in sections 2.1.2-2.1.7.

Increased microtubule-detachment rate of kinesin under hindering load reduces multiple-kinesin cargo velocity
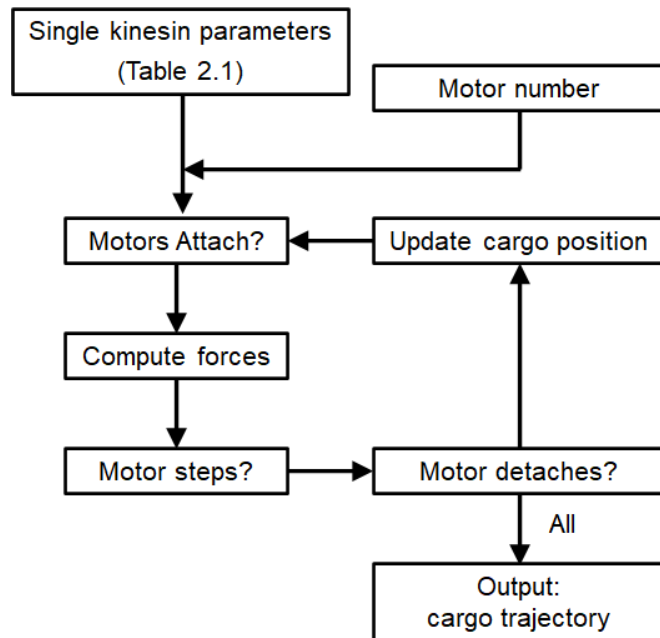
Figure 2.1: Flow chart for simulation the trajectory of a cargo carried by kinesin motors employed in my thesis study [65, 76, 88].

My simulation takes in the single motor properties, along with other key parameters to model the cargo transport process (Section 2.1.2). Before a cargo trajectory is initiated, all of the motors are unattached from the microtubule. The cargo trajectory is initiated when one (or more) of the motors attach to the microtubule (Section 2.1.3). The cargo is transported along a one-dimensional microtubule lattice, with motors stochastically stepping along the microtubule. The cargos trajectory is terminated when all of the motors become unbound. The motors are assumed to be idealized springs with an unstretched rest length and a linkage stiffness (Table 2.1). The motors are assumed to experience a force only when the displacement between the motor and its cargo is larger than the motor's rest length.

At each time step, unattached motors can stochastically attach to the microtubule (Section 2.1.3). Next the force between all attached motors and the cargo is evaluated (Section 2.1.4). Attached motors can become can take a step along the microtubule can take a step along the microtubule or become detached from the microtubule, the probability of either of these events occurring is based on the force on the motor. Next, the cargos trajectory is updated based on the force between the motor and the cargo (Section 2.1.5 & 2.1.6). Once the motile states of all kinesin molecules on the cargo have been updated, the simulation updates the cargo position by summing the deterministic drift motion and the random thermal motion of the cargo during the time step along the one-dimensional microtubule (Section 2.1.1.7). This process is repeated until all motors become detached from the microtubule. Finally, the trajectory of the cargo and motors are output to a file for latter analysis (Section 2.2).

2.1.2 Simulation parameters

The following table (Table 2.1) contains a list of the single kinesin and environmental parameters I used in my simulations unless otherwise noted in the text.

Table 2.1: Table of single kinesin and environmental parameters employed in my thesis study, unless otherwise noted in the text.

Parameter	Description	Values	References
v_0	Unloaded velocity of the motors.	800 nm/s	[34, 89]
ℓ_m	Rest length of the motors.	40 nm	[70, 89]
k	Spring constant of the motor.	0.32 pN/nm	[90-92]
ε_0	Unloaded off-rate of kinesin.	0.8 s^{-1}	[29, 30, 32]
δ_-	Characteristic distance between the attached and the detached states. F < 0	0.6 nm	[29, 30, 32]
δ_+	Characteristic distance between the attached and the detached states. F > 0	0.32 nm	[29, 30, 32]
k$_{on}$	Kinesins on-rate.	5 s^{-1}	[67, 93]
F_s	Kinesin stall force.	7 pn	[30]
Δx	Kinesin step size	8 nm	[31, 34]
N	Number of motors on the cargo.	1 - 4	[44, 75]
$k_B T$	Thermal energy in the system (room temperature).	4.11 pN·nm	
Δt	Simulation time step	10 μs	[65]
η	Viscosity of the surrounding fluid.	10^{-3} pa·s	[74, 77, 79, 94]
R	Radius of the cargo.	250 nm	[74, 75]

2.1.3 Motors attaching to the microtubule

At each simulation time step, an individual unbound kinesin binds the microtubule with a probability determined by its on-rate, within a region on the microtubule that can be explored by its rest length. The simulation time step is incremented, and the above evaluations are repeated until at least one kinesin on the cargo binds the microtubule, at which point the run is initiated.

2.1.4 Calculating the force between the motors and the cargo

The force between the motor and the cargo depends on the separation between the motor and the cargo. When this separation is greater than the motors rest length the motor will experience a force with a magnitude of

$$F = \begin{cases} 0, & |x_c - x_m| \leq \ell_m \\ k \cdot (|x_c - x_m| - \ell_m), & |x_c - x_m| > \ell_m \end{cases}, \quad (2.1)$$

where ℓ_m is the motors rest length, k is the motors spring constant, x_c is the position of the cargo, and x_m is the position of the motor. The force on the motor will be positive if $x_c > x_m$ and negative otherwise. The force on the cargo from the motor will have the opposite sign.

2.1.5 Kinesin's force-dependent stepping kinetics

The force-dependent stepping rate for kinesin has been previously determined by experimental [29, 32, 95] and modeling [45, 65, 76] studies:

$$k_{step}(F) = \begin{cases} 0, & F \leq -F_s \\ (v_0/\Delta x) \cdot (1 - (F/F_S)^2), & -F_s < F \leq 0 \\ v_0/\Delta x, & F > 0 \end{cases}, \quad (2.2)$$

where v_0 is the unloaded velocity, Δx is the step size, F_s is the stall force, and F is the force on the motor.

2.1.6 Kinesin's force-dependent detachment kinetics

The motor's load-detachment kinetics was as determined in recent experimental studies by Milic et al. [30] and Andreason et al. [29] for hindering forces between -25 pN and 0 pN, and for assisting forces between +2 pN and +20 pN. Extrapolation of measurements of these two ranges yields an apparent discontinuity [29] in kinesin's detachment rate at 0 pN. This apparent discontinuity has not yet been resolved experimentally: direct measurements of the motor's load-detachment kinetics are not yet available for the 0-2 pN assisting force range. To mitigate this apparent discontinuity, here we modeled the detachment rate of kinesin as a linear continuation between available experimental measurements at 0 pN and at 2 pN [29, 30]. Note that this linear-interpolation approach underestimates the effect of cargo diffusion uncovered in the current study. We summarize the motor's detachment rate under load used in the current study as the piecewise function

$$\varepsilon(F) = \varepsilon_0 \begin{cases} exp(|F|/F_{d-}), & F \leq 0 \\ 1 + 3.8247 \cdot F, & 0 < F \leq 2, \\ 7.4\, exp(|F|/F_{d-}), & F > 2 \end{cases} \quad (2.3)$$

where ε_0 is the unloaded single-kinesin detachment rate, F is the load on the motor, F_{d-} is the detachment force of kinesin in the hindering direction, and F_{d+} is the detachment force of kinesin in the assisting direction. The unit of detachment rates is s^{-1}, and the unit of forces is pN. All other numerical values are dimensionless. Positive force indicates load in the direction assisting motor motion, and negative force indicates load in the direction hindering motor motion. The unloaded detachment rate is determined as $\varepsilon_0 = v_0/l_0$, where v_0 is the unloaded single-kinesin velocity, and l_0 is the unloaded single-kinesin run length. The value of the detachment force in the hindering direction was defined by Schnitzer et al. [32] as $F_{d-}=k_BT/\delta_{l-}$, where k_BT is the thermal energy (4.11 pN·nm) and δ_{l-} is the characteristic distance between the attached and the detached states. The value of δ_{l-} was recently determined as 0.60 nm by Andreason et al. [29], approximately half of the value previously reported by Schnitzer et al. [32], likely reflecting the major technological advances in the force-clamping experiments used for these measurements [30, 96, 97]. The value of the detachment force in the assisting direction is similarly defined by Andreason et al. [29] as $F_{d+}=k_BT/\delta_{l+}$, where $\delta_{l+}=0.32$ nm.

2.1.7 Updating the cargos position

The cargos position is updated by taking into account the drift motion and the thermal motion of the cargo. The drift motion of the cargo opposes the kinesin motion and is determined as $\Delta t \cdot F/\xi$, where Δt is the simulation time step, F is the net load on the cargo, and $\xi = 9\pi\eta d$ is a friction constant determined by the solution viscosity η and cargo diameter d. In all simulations. The thermal motion of the cargo is uncorrelated to kinesins motion and is drawn from a normal distribution with a mean square displacement of $2D \cdot \Delta t$, where the cargo diffusion constant D is related to the friction constant ξ by the Einstein relation $\xi = k_BT/D$ [81].

2.2 Analysis

Here I go over the analysis methods common to each of my thesis studies. Other analysis methods, specific to one of my studies, can be found in the methods section of the chapter associated with that study.

2.2.1 Cargo run length

Run length was determined as the distance that the simulated cargo travels after binding to and before unbinding from the microtubule. Within the uncertainty arising from the thermal diffusion of the cargo, the motion of each simulated run was unidirectional and plus-end oriented (in the direction of kinesin motion). For each simulation condition, the cumulative probability distribution of the run lengths was fitted to the cumulative probability function of a single exponential distribution $1 - e^{-x/L}$. Mean run length was determined as the best-fit decay constant L. The associated standard error of the mean was determined via a bootstrap method [98].

2.5.2 Cargo velocity

The velocity of a simulated trajectory was determined as the best-fit slope of the trajectory. Only trajectories ≥ 0.2 s in duration were considered for analysis; of these trajectories, only those that moved ≥ 100 nm were analyzed. We determined the mean cargo velocity by fitting the cumulative distribution of each individual cargo velocity to a normal distribution $\frac{1}{2}\left(1 + erf\left(\frac{v - v_m}{\sigma\sqrt{2}}\right)\right)$, where v is the cargo velocity, v_m is the mean cargo velocity, and σ is the standard deviation of the cargo velocity. The associated standard error of the mean was determined via a bootstrap method [98].

2.5.3 Data representation

MATLAB functions corocet.m [99] and cmap2pal.m [100] were used to generate the perceptually uniform color maps in figure 2(a).

Chapter 3 Cargo diffusion shortens single-kinesin runs at low viscous drag

3.1 Background

Molecular motors such as kinesin-1 are mechanoenzymes that drive long-range transport of cargos in living cells [6, 7]. This transport process is challenging to accomplish, because motors must overcome substantial thermal diffusion to maintain directional transport. Thermal diffusion encompasses the set of random, non-directional motions that result from thermal agitation [101]. Thermal diffusion plays important roles in a variety of biological processes, including early embryonic patterning [102, 103], cell signaling [104], and metabolism [105]. For motor-based transport, thermal diffusion can manifest as random motions of the motor or of the cargo. A recent investigation highlighted a significant effect of thermal diffusion of individual motor domains on single-kinesin function in vitro [106]. How thermal diffusion of the cargo influences motor-based transport, however, has remained unclear. While previous numerical modeling [65] did not uncover a significant effect of cargo diffusion on single-motor function, recent modeling work [107] indicated that changing the solution viscosity significantly affects cargo navigation across three-dimensional microtubule intersections, suggesting a likely effect of cargo diffusion on motor function.

The functions of molecular motors are affected by external force, or "load" [29, 30, 32]. Until recently, kinesin-1 was thought to be affected by load oriented in the direction opposite ("hindering") of motor motion, but not by load oriented in the same ("assisting") direction. This notion was reflected in previous numerical modeling studies, including work that predicted a null effect of cargo diffusion on single-kinesin transport [65]. However, recent single-molecule investigations [29, 30] revealed a significant impact of assisting load on the distance traveled by a single kinesin ("run length"), revising our understanding of the dependence of single-kinesin function to load. Importantly, these recent studies demonstrate a strong and perhaps counterintuitive asymmetry in the effect of load on single-kinesin run length: under the same amount of load, kinesin's run length is significantly *shorter* when the load is in the direction assisting versus hindering motor motion [29, 30]. In the current study, we carried out the first investigation of how this asymmetric sensitivity combines with cargo diffusion to impact kinesin's motor function.

Thermal diffusion of the cargo can exert load on the motor. Importantly, because cargo diffusion is not correlated with motor motion [81, 108], the direction of the load from cargo diffusion can assist or hinder motor motion, depending on whether the cargo is leading in front of or lagging behind the motor. Given the recently identified asymmetric response of kinesin run length to load direction [29, 30], we hypothesized that cargo diffusion may non-trivially influence the run length of the kinesin carrying that cargo.

20

Here we employed Monte Carlo-based simulations to numerically examine the effects of cargo diffusion on transport by a single kinesin. Our study builds on previous numerical models [45, 65] and incorporates the recently uncovered effect of assisting load on single-kinesin run length [29, 30]. We carried out our simulations over a large parameter space that captures crucial transport characteristics in living cells, including variations in cytoplasmic viscosity [74, 77-79, 94, 109], cargo size [74, 75, 110-114], and transport velocity [115, 116]. Our simulations included the physiologically relevant viscous drag that is associated with these parameter choices. Our simulations revealed that cargo diffusion significantly shortens single-kinesin run length at low viscous drag; this diffusion-based shortening effect arises from the specific asymmetry in the response of kinesin run length to load direction.

3.2 Methods

3.2.1 Monte Carlo-based simulation

Simulations were as described in chapter 2.1 with the following exceptions. The number of motors on the cargo in each simulation was 1. The values of viscosity and cargo radius are indicated in the text.

A faster simulation time step of 10^{-6} s was used for simulations of stiffer motors (>0.32 pN/nm, Figure 4), which better resolved the position of the cargo under higher tension from the stiffer motor linkage (data not shown).

3.2.2 Data analysis

The cargo run length and velocity were determined as described in chapter 2.2.

The load on the motor for a given displacement of the cargo from the motor was determined as the length of the motor stretched beyond its rest value, multiplied by motor stiffness. The direction of the load was determined by the relative position of the cargo to the motor: "assisting" when the cargo position leads the motor, "hindering" when the cargo position lags behind the motor.

The effective detachment rate of the motor for a given distribution of displacements of the diffusing cargo from the motor (Figures 3 and 4) was determined as the weighted sum of kinesin's detachment rate at a particular displacement value, multiplied by the frequency of occurrence of the particular displacement value. Kinesin's detachment rate at a particular displacement value was calculated by first determining the load associated with the displacement value, then applying the motor's load-detachment kinetics as described above. The run length was calculated as the ratio of cargo velocity to its detachment rate.

3.2.3 Analytical model of the run length of single-kinesin cargos in the diffusion-free case

In the absence of cargo diffusion, the only load on the motor is imposed by viscous drag in the direction that hinders the motor's motion: $|F|=9\pi d\eta v$, as described above for the Monte Carlo-based simulations.

The run length of single-kinesin cargos was determined as $L=v/\varepsilon$, where v is the velocity and ε is the detachment rate of the motor carrying the cargo. Based on the experimentally measured load-detachment kinetics of kinesin for hindering loads [29, 30, 32] (described in the simulation model for $F<0$), the run length of single-kinesin cargos is

$$L = \frac{v}{\varepsilon_0} exp\left(\frac{-9\pi\eta dv}{F_{d-}}\right),$$

where ε_0 is the unloaded single-kinesin detachment rate and F_{d-} is the single-kinesin detachment force under hindering load, as described above for the Monte Carlo-based simulations.

The velocity of the motor under viscous load in the preceding equation was calculated as follows. The experimentally measured load-velocity kinetics of kinesin for hindering loads [95] is well approximated as [45]

$$v = v_0\left(1 - \left(\frac{F}{F_s}\right)^2\right),$$

where v_0 is the unloaded single-kinesin velocity, and F is the hindering load on the motor. The velocity of the motor under viscous load ($|F|=9\pi d\eta v$) is then described as

$$v = v_0\left(1 - \left(\frac{9\pi d\eta v}{F_s}\right)^2\right),$$

The solution to this above quadratic equation gives rise to the analytic description of the velocity of single-kinesin cargos in a viscous medium

$$v = \frac{v_0}{2}\left(\frac{F_s}{9\pi d\eta v}\right)^2\left(-1 + \sqrt{1 + 4\left(\frac{9\pi d\eta v}{F_s}\right)^2}\right),$$

3.3 Results

3.3.1 Thermal diffusion of the cargo shortens the run length of single-kinesin cargos

We used a previously developed Monte Carlo simulation [45, 65] to examine the effect of cargo diffusion on kinesin run length in a viscous medium (Chapter 2). In this simulation, the motor steps directionally along the microtubule track, while its cargo undergoes both random thermal diffusion and deterministic drift under load [81, 101, 108]. The direction and the value of the load on the cargo and the motor are determined by the displacement between them. The effect of load on run length is modeled by the motor's load-detachment kinetics (Chapter 2), which describes the probability of the motor detaching from the microtubule per unit time ("detachment rate") for a given load value and direction. Previously, this and similar numerical simulation models included kinesin's load-detachment kinetics under hindering load only and assumed that the motor's detachment rate is unaffected by assisting load [45, 65]. In the current study, we extended the load-detachment kinetics of the simulated motor (Chapter 2) to reflect recent experimental measurements of the motor's detachment rate under load oriented in both the assisting and the hindering directions [29, 30].

We first examined the run length of single-kinesin cargos over a physiologically relevant range of solution viscosities [74, 77-79, 94, 109], while holding cargo size and motor velocity constant at 0.5 µm in diameter and 0.8 µm/s when unloaded, respectively. These values are commonly captured in *in vitro* studies and are within the ranges measured for intracellular cargos [74, 75, 110-116].

Perhaps surprisingly, our simulations revealed a non-monotonic dependence of run length on solution viscosity (blue scatters, Figure 3.1A). Whereas the mean run length reached only 76±6% of the unloaded single-kinesin value at the viscosity of water, it recovered to 97±7% of the unloaded single-kinesin value at a viscosity ~22-fold higher than that of water, before declining with further increases in solution viscosity (blue scatters, Figure 3.1A). In contrast, when we did not include thermal diffusion of the cargo in our simulations, we detected only a simple monotonic effect of viscosity on run length; importantly, run length remained approximately the same as the unloaded single-kinesin value at low viscosity (magenta scatters, Figure 3.1A). Our simulations of the diffusion-free case were in excellent agreement with predictions of the analytical model that considers the motor's response to viscous load but not cargo diffusion (Section 3.2.3) (magenta line, Figure 3.1A). The reduction in run length for simulations carried out in the presence of cargo diffusion versus the diffusion-free case was pronounced at low viscosity (grey area, Figure 3.1A). This difference in run length vanished at higher viscosities, where viscous drag alone was sufficient to shorten cargo runs (magenta, Figure 3.1A).
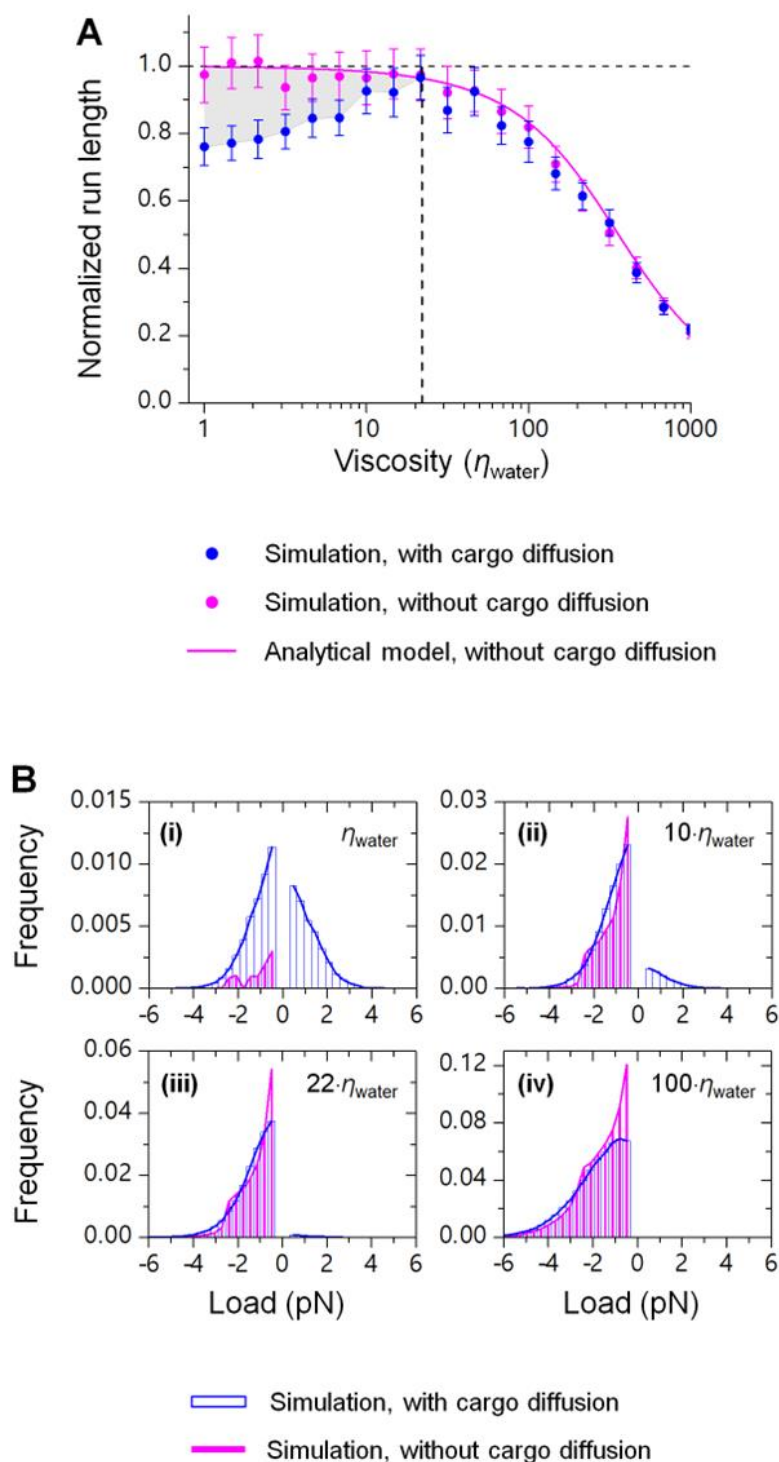
Figure 3.1: Cargo diffusion shortens single-kinesin run length at low viscosities (A) by imposing substantial assisting load on the motor (B). Simulations were carried out using a cargo 0.5 μm in diameter and a motor velocity of 0.8 μm/s unloaded. ηwater, the viscosity of water. (A) Run length (mean ± standard error of the mean) was normalized by the unloaded single-kinesin run length. N = 1000 for

each simulation condition. Grey area, the difference in run length between simulations with and without cargo diffusion. Vertical dashed line, a viscosity 22-fold higher than that of water (22·ηwater). (B) Thermal diffusion of the cargo increases the load on the motor at low viscosities. Positive values indicate load in the direction that assists motor movement; negative values indicate load in the direction that hinders motor movement.

Together, our data demonstrate that thermal diffusion of the cargo results in kinesin run lengths that are shorter than those achieved without diffusion. This effect is localized to the low-viscosity range (grey area, Figure 3.1A), yielding a non-monotonic dependence of run length on solution viscosity.

3.3.2 Cargo diffusion imposes assisting load on the motor that is absent in the diffusion-free case

How does cargo diffusion shorten single-kinesin run length? Molecular motors such as kinesin are affected by mechanical load; a shorter run length suggests a larger load on the motor [29, 30, 32]. We thus hypothesized that cargo diffusion increases the load on the motor, particularly at the low viscosities at which we detected substantial diffusion-based shortening (grey area, Figure 3.1A). To test this hypothesis, we compared the distribution of load on the motor between simulations with and without cargo diffusion.

We found that cargo diffusion introduced substantial assisting load on the motor at low viscosities (positive load, blue, Figure 3.1B, i-iii). For example, at the viscosity of water, the motor had a similar probability of experiencing load in the assisting direction as in the hindering direction (positive vs. negative load, blue, Figure 3.1Bi). In contrast, in the diffusion-free case, the motor experienced load only in the hindering direction (negative load, magenta, Figure 1Bi), which is expected because viscous drag always opposes cargo motion. Note that cargo diffusion also increased the hindering load on the motor at low viscosity. For example, at the viscosity of water, the motor had a higher probability of experiencing a greater hindering load in the presence of cargo diffusion than in the diffusion-free case (negative load, blue vs. magenta, Figure 3.1Bi). This observation is reasonable: thermal diffusion of the cargo is not correlated with the direction of motor motion[101] and can thus contribute to load in both directions. As viscosity increased, the difference in load distributions diminished more quickly in the hindering direction than in the assisting direction (negative load vs. positive load, Figure 3.1B, i-iii).

Taken together, our data demonstrate that cargo diffusion imposes substantial assisting load on the motor at low viscosities. Because assisting load *shortens* kinesin's run length more severely than does hindering load [29, 30], diffusion-based assisting load

supports the observed reduction in run length versus the diffusion-free case (grey area, Figure 3.1A).

3.3.3 The effect of cargo diffusion on run length depends non-monotonically on viscous drag

We next sought to understand how cargo size and/or motor velocity impact the run length of single kinesins carrying a cargo. While these parameters were held constant in the preceding simulations at 0.5 µm in diameter and 0.8 µm/s unloaded, respectively (Figure 3.1), their values are known to vary in living cells [74, 75, 110-116].

We first examined the impact of cargo size, while holding motor velocity constant at 0.8 µm/s unloaded. The effect of solution viscosity on run length remained non-monotonic for cargos 0.1-1 µm in diameter ($v_0 = 0.8$ µm/s, Figure 3.2A). Interestingly, the viscosity at which run length most closely approached the unloaded single-motor value ("critical viscosity") scaled inversely with cargo size (Figure 3.2A, left). Because viscosity (η) and cargo size (d) enter the problem via viscous drag on the cargo, which scales as the product ηd, a reasonable ansatz would be for run length to depend on this product. Consistent with this hypothesis, the simulated run lengths for each combination of solution viscosity and cargo size collapsed onto a single curve with ηd as the control parameter (Figure 3.2B, left).

We next examined the impact of motor velocity on our simulation results. For each unloaded motor velocity examined, the run length of single-kinesin cargos again varied non-monotonically with the combined parameter ηd (Figure 3.2, A and B, middle and right). Interestingly, the value of ηd at which run length approached the unloaded single-motor value correlated inversely with motor velocity (Figure 3.2C). This inverse scaling suggests that the effects of ηd and motor velocity (v) on run length may be again combined as that of their product $\eta d v$ [117], or equivalently the viscous drag experienced by the cargo (modeled as $9\pi\eta d v$, see Discussion). Consistent with this hypothesis, the run length for the three unloaded motor velocities (Figure 3.2B) collapsed onto a single curve with viscous drag as the single control parameter (Figure 3.2D).

Thus, our simulations demonstrate that the run length of single-kinesin cargos is influenced by three independent parameters: solution viscosity, cargo size, and motor velocity. The effect of these three parameters on run length is summarized as that of a single control parameter: the product of the three parameters, or viscous drag that arises from the active motion of the motor. This collapsed single-parameter curve differs substantially from model predictions for the diffusion-free case at low viscous drag (≤ 0.2 pN, Figure 3.2D). This difference diminishes when the effect of viscous drag on kinesin's run length becomes pronounced (scatters vs. solid line, Figure 3.2D).
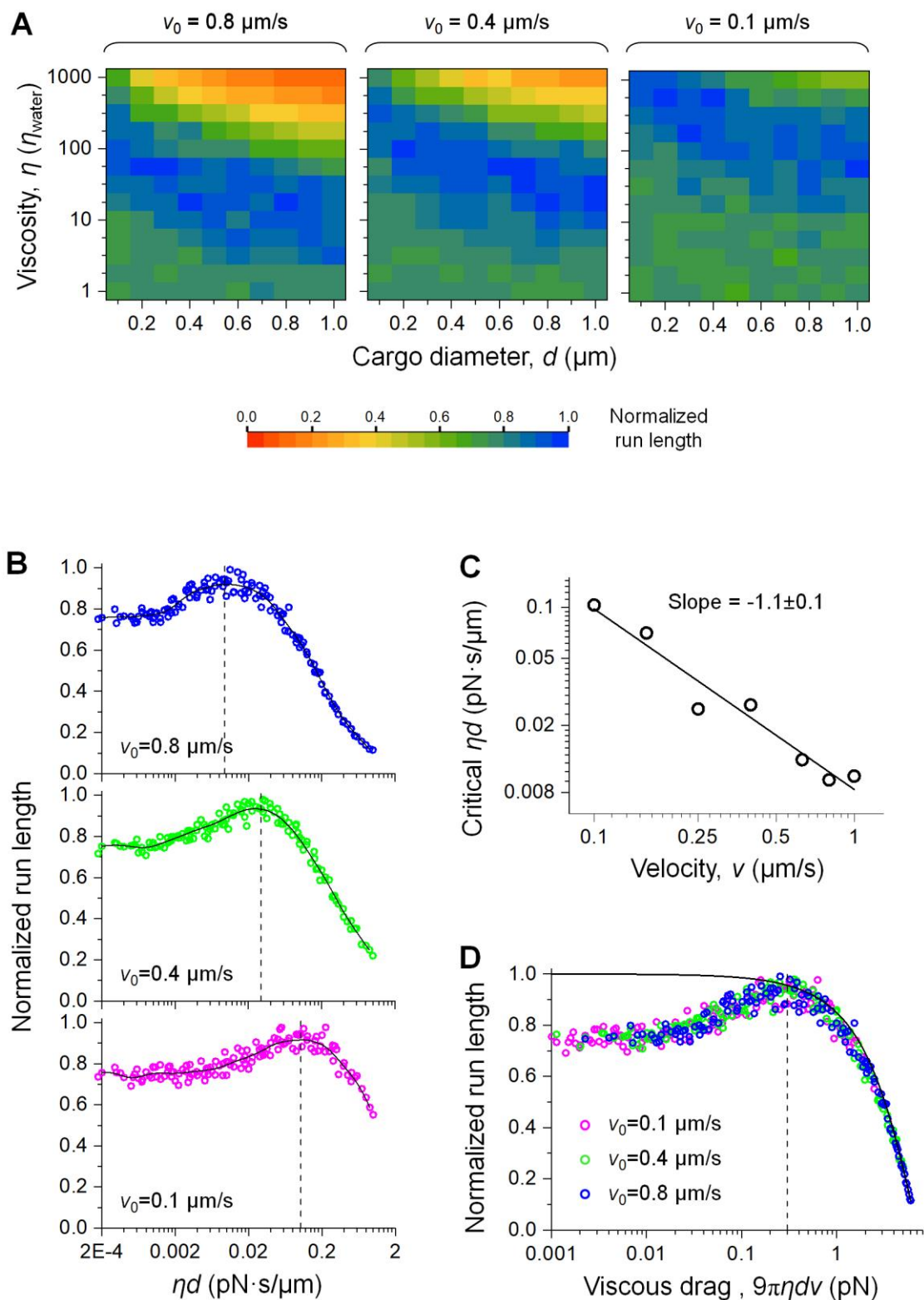
Figure 3.2: Non-monotonic variation in run length is general for physiologically relevant ranges of cargo size and motor velocity (A) and is summarized by the

single parameter of viscous drag (B-D). v_0 indicates the unloaded single-motor velocity. Run length was normalized by the unloaded single-motor value. $N = 1000$ for each simulation condition. (A) Dashed line, example inverse relationship between viscosity and cargo size as a guide to the eye. η_{water}, the viscosity of water. (B) For each unloaded motor velocity, the impact of solution viscosity and cargo size on run length (panel A) is summarized as that of their product ηd. Solid line, smoothed moving average of simulated run lengths to guide the eye. Vertical dashed line, critical ηd value, where run length approaches that of the unloaded single kinesin. (C) The critical ηd value scales inversely with motor velocity. Solid line, best linear fit with the indicated slope. (D) The impact of ηd and motor velocity (v) on run length (panel B) is summarized as that of viscous drag ($9\pi\eta dv$). Solid line, model prediction of run length for the diffusion-free case. Vertical dashed line, an approximate threshold (0.3 pN) where the shortening effect of viscous drag on kinesin run length exceeds 5% of the unloaded single-kinesin value.

3.3.4 Viscous drag biases thermal diffusion of cargo toward the hindering direction

We next sought to understand the impact of viscous drag on the displacement of the diffusing cargo from the motor; this displacement information is important because it determines the load on the motor.

We first carried out simulations for the case of zero viscous drag (Figure 3A). Here, the motor velocity was set at 0 µm/s to realize a zero drag force, and solution viscosity and cargo size were varied over the physiologically relevant ranges used in preceding simulations (1000- fold and 10-fold ranges, respectively). The resulting displacement distributions were symmetric about the motor position and exhibited two diffusion regimes: a uniformly distributed "free diffusion" range (grey area, Figure 3) where thermal motion of the cargo does not stretch the motor beyond its rest length (Chapter 2) and is thus effectively decoupled from the motor; and a normally distributed "tethered diffusion" range (cyan and yellow areas, Figure 4) where thermal excursion of the cargo is restricted by the motor that tethers the cargo to the microtubule [81]. Displacement distributions were not sensitive to cargo size or solution viscosity, with each distribution demonstrating a similar probability and a similar mean excursion of the cargo in the tethered diffusion range (~5% and ~3 nm, respectively and in both load directions, cyan and yellow areas, Figure 3.3A). These displacement distributions correspond to a 30% increase in the motor's detachment rate and a 26% reduction in motor run length from their unloaded values (Chapter 2). These values are in excellent agreement with the ~24% reduction in run length in our simulations at negligible viscous drag (1×10^{-3} pN, Figure 2D).
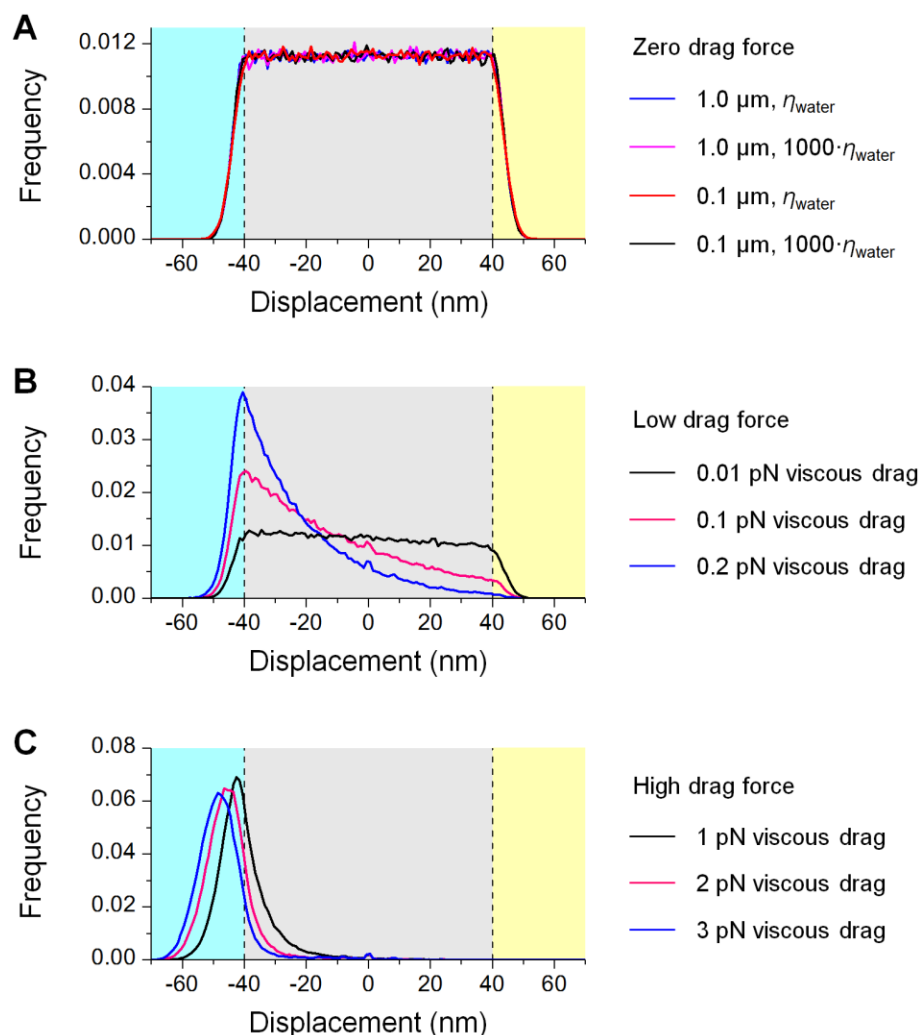
Figure 3.3: Distributions of the displacement of thermally diffusing cargo from the motor, simulated at zero viscous drag (A), low viscous drag (B), and relatively high viscous drag (C). Positive displacement reflects the cargo leading in front of the motor; negative displacement indicates that the cargo lags behind the motor. Grey area, free-diffusion range where the cargo does not impose load on the motor. Cyan (and yellow) area, tethered-diffusion range where the cargo imposes hindering (and assisting) load on the motor. (A) At zero viscous drag, the displacement of the diffusing cargo is symmetric about the motor position (0 nm) and is not sensitive to cargo size or solution viscosity. $N = 10$ for each simulation condition, with each simulation including 20,000 times steps. (B-C) At both low (B) and relatively high (C) viscous drag, the displacement of a diffusing cargo is biased toward the hindering direction (negative displacement). The extent of this bias increases as the viscous drag increases. $N = 1000$ for each simulation condition.

We next examined the case of low viscous drag (Figure 3.3B). Here, the motor velocity was kept constant at 0.8 μm/s, and solution viscosity and cargo size were chosen to capture the low viscous drag range that alleviates the shortening effect of cargo diffusion on kinesin run length (0.01-0.2 pN, Figure 3.2D). Within this force range, the effect of viscous drag on kinesin run length was ≤3% of the unloaded single-kinesin value (solid line, Figure 3.2D). The resulting displacement distributions were asymmetric about the motor position in both the free-diffusion range (grey area, Figure 3.3B) and the tethered-diffusion range (cyan and yellow areas, Figure 3.3B). As the viscous drag increased, the position of the diffusing cargo increasingly lagged behind the motor. At a drag force of 0.2 pN, the probability that the cargo will exert load in the assisting direction diminished to <0.4% (blue line, Figure 3.3B). Of note, despite the asymmetry in the displacement distribution, mean excursion of the cargo in the tethered-diffusion range remained similar between load directions (~2.9 nm in the hindering direction and ~3.2 nm in the assisting direction, cyan and yellow areas, Figure 3.3B) and similar to that for zero viscous drag (~3 nm in both load directions, cyan and yellow areas, Figure 3.3A). For comparison, at higher viscous drag (1-3 pN, Figure 3.3C), the displacement of the diffusing cargo was further biased toward the hindering direction (cyan area, Figure 3.3C); the mean excursion of the cargo in the hindering direction increased as the viscous drag increased (cyan area, Figure 3.3C).

Thus, our simulations indicate that viscous drag biases the diffusing cargo to lag behind the moving motor, which reduces the probability of the motor experiencing assisting load. At low viscous drag, this reduction in assisting load is accompanied by an increased probability, but not the magnitude, of hindering load on the motor.

3.3.5 The effect of cargo diffusion on run length is not strongly influenced by motor stiffness

Because the stiffness of the motor is a key determining factor for tethered diffusion [65, 81, 108], we hypothesized that the effect of cargo diffusion on run length may be influenced by motor stiffness. We carried out simulations at zero viscous drag to test this possibility. As experimental measurements of the stiffness of molecular motors (or other proteins) are still limited, here we examined a large, 100-fold range of values of motor stiffness, including available in vitro experimental measurements for single-kinesin transport [91] and multiple-motor transport [67, 118, 119].

Our simulations demonstrate that although motor stiffness impacts both the probability and the extent of cargo displacement in the load-imposing, tethered-diffusion range (Figure 3.4, A and B), these two factors do not combine to substantially alter the effect of cargo diffusion on single-kinesin run length (Figure 3.4C). As the motor linkage increased in stiffness, there was a higher probability of the cargo remaining in the free-diffusion range (grey area, Figure 3.4Ai; 0 pN, Figure 4Aii), and a lower probability of the cargo diffusing in the tethered range to exert load on the cargo (green, Figure 3.4B). These

observations are expected for tethered diffusion [65, 81, 108]. On the other hand, the magnitude of the load from the cargo increased as motor stiffness increased (blue vs. magenta, Figure 3.4Aii, and purple diamonds, Figure 3.4B), varying as the square root of motor stiffness as expected from equipartition theorem in statistical physics [108, 117] (solid line, Figure 3.4B). Thus, the stiffness of the motor has opposite effects on the probability of the cargo imposing load on the motor (green squares, Figure 3.4B) and the magnitude of the load that the cargo can impose (purple diamonds, Figure 3.4B). Over the 100-fold range of motor stiffnesses tested, these two opposing effects resulted in a modest, 3.5% change in the motor's detachment rate (black triangles, Figure 3.4C), corresponding to a similarly modest, 3.8% change in run length over the same stiffness range (red circles, Figure 3.4C).

Taken together—and contrary to our initial expectation—our data indicate that the effect of cargo diffusion on single-kinesin run length is not strongly influenced by motor stiffness.
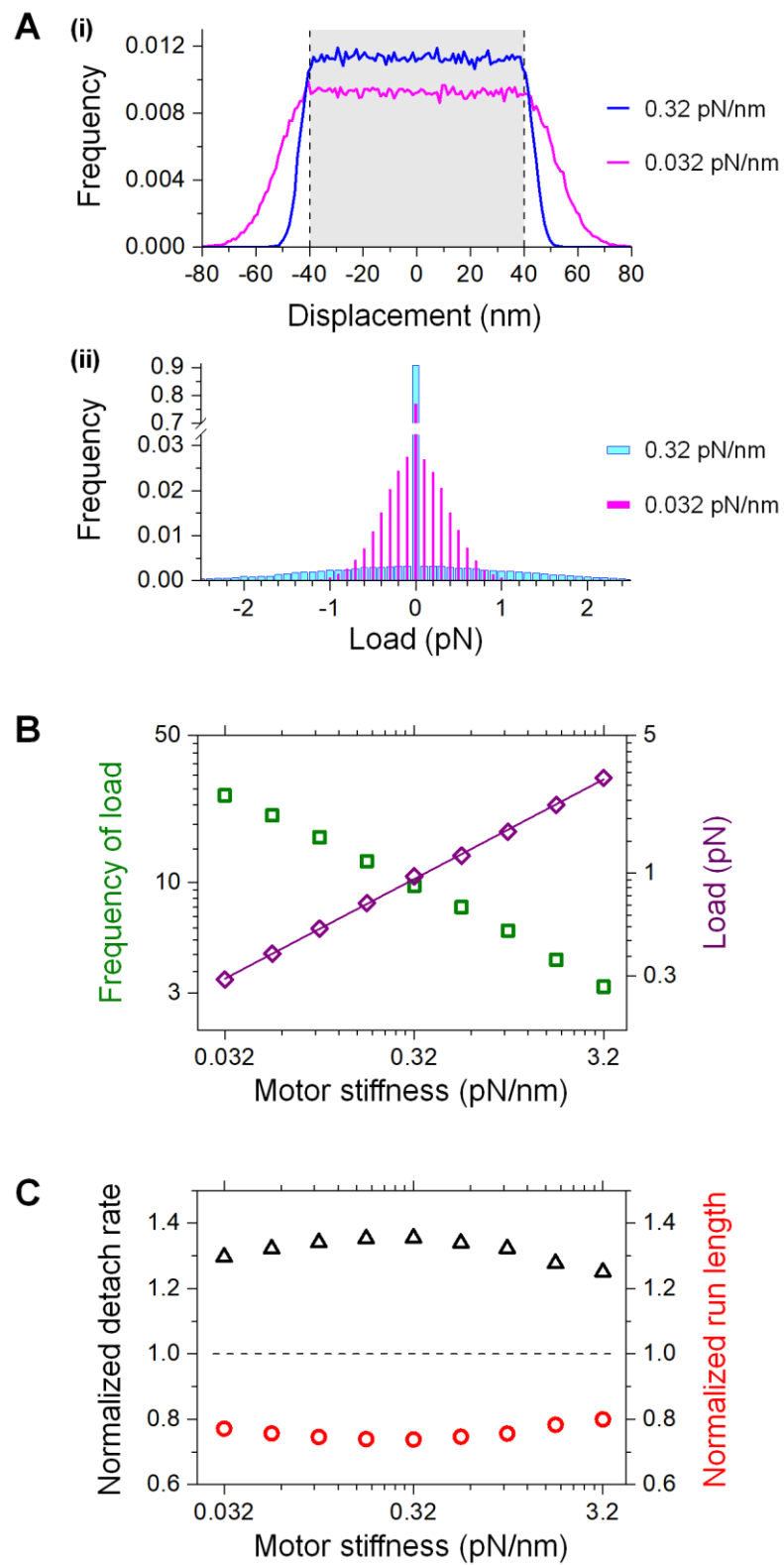
Figure 3.4: The effect of cargo diffusion on single-kinesin run length is not strongly influenced by motor stiffness. Simulations were carried out at zero viscous drag. N = 10 for each simulation condition, with each simulation including 20,000 times steps. (A) Motor stiffness impacts (i) the displacement of the diffusing cargo from the motor and (ii) the resulting load on the motor. Grey area, free-diffusion range where the cargo does not impose load on the motor. (B) Increasing motor stiffness decreases the frequency with which the diffusing cargo imposes load on the motor (green squares), while increasing the mean magnitude of the load on the motor (purple diamonds). Solid line, best linear fit with a slope of 0.505 ± 0.004. (C) The motor's detachment rate (black triangles) and run length (red circles) were largely unchanged over the range of motor stiffness tested. Detachment rate and run length were normalized by their unloaded single-motor values.

3.3.6 Non-monotonic variation in run length requires specific asymmetry in the motor's load-detachment kinetics

We next sought to understand how specific asymmetry in kinesin's load-detachment kinetics influences run length behavior. To address this, we varied the symmetry properties of the motor's load-detachment kinetics under otherwise identical simulation conditions. We duplicated our preceding simulations and the associated experimentally measured load-detachment kinetics for single kinesins [29, 30] for ease of comparison (Figures 3.1A and 3.5A).

We found that asymmetry in kinesin's load-detachment kinetics is necessary but not sufficient for the observed non-monotonic dependence of run length on viscous drag (Figure 3.5, B-D). We first examined the effect of symmetric load-detachment profiles on run length (Figure 3.5, B and C). Here, we duplicated the experimentally measured load dependence [29, 30] in the hindering direction (left, Figure 3.5B) or the assisting direction (left, Figure 3.5C). In both cases, the effect of viscous drag on run length increased monotonically, with run length maintaining its maximum value at the lowest viscous drag tested (right, Figure 3.5, B and C). As expected, the maximum run length of the single-motor cargo was substantially shorter when we assumed a higher sensitivity of the motor's detachment rate to load (right, Figure 3.5, C vs. B). We next implemented an asymmetric load-detachment profile that reversed the directional bias of kinesin's load dependence (left, Figure 3.5D); we again observed a monotonic dependence of run length on viscous drag (right, Figure 3.5D).

Hence, our simulations reveal that the specific asymmetry in the load-detachment kinetics of kinesin—steeper sensitivity for assisting versus hindering load [29, 30] (inset, Figure 3.5A)—underlies the non-monotonic dependence of run length on viscous drag uncovered in the current study.
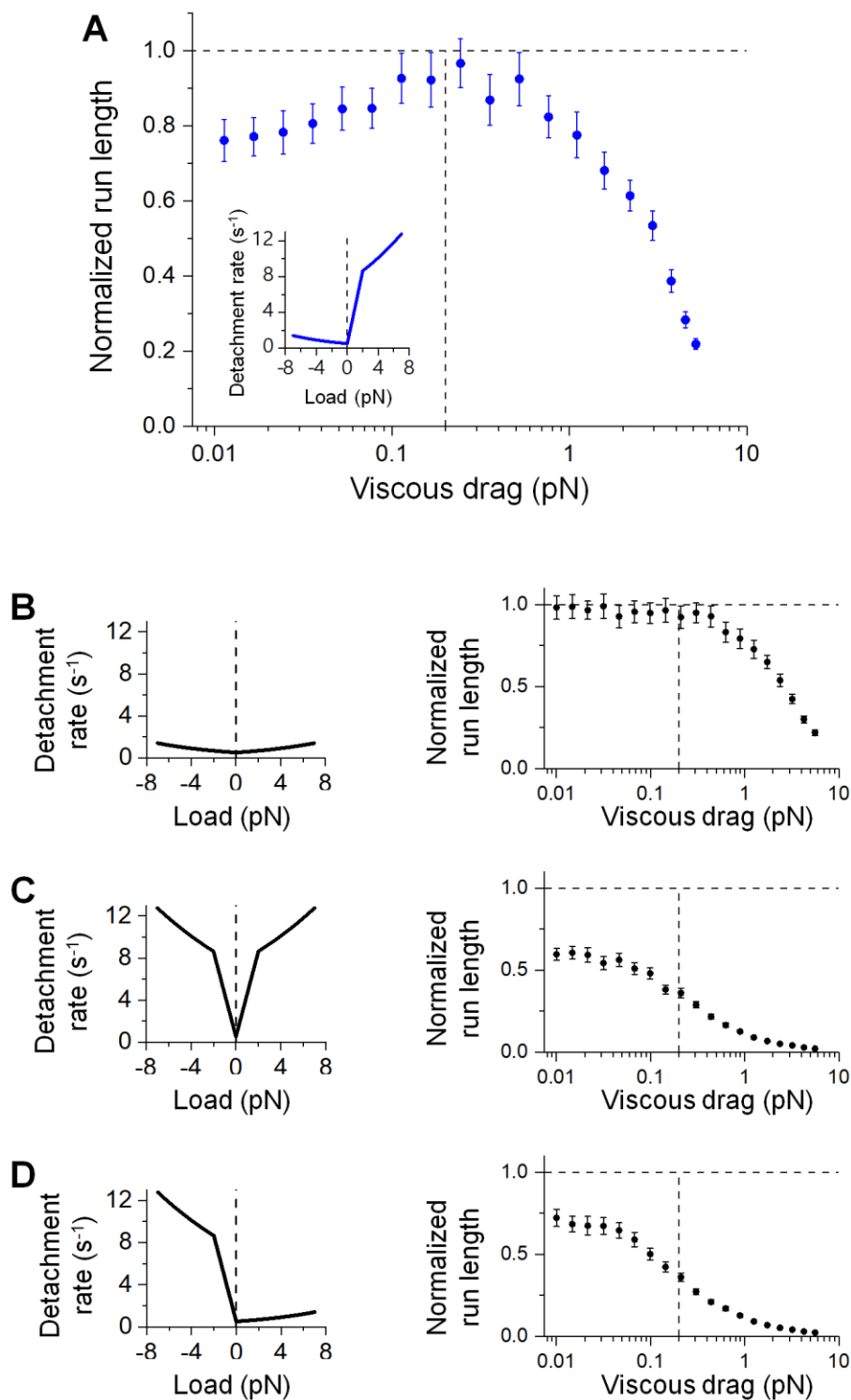
Figure 3.5: Non-monotonic dependence of run length on viscous drag reflects a specific asymmetry in the motor's load-detachment kinetics. Vertical dashed lines

in run-length panels, the critical viscous drag force (0.2 pN, Figure 2D) that separates the region where the effect of thermal diffusion dominates (left) from the region where the effect of viscous drag dominates (right). (A) Experimentally measured load-detachment kinetics [29, 30] (inset) give rise to a non-monotonic dependence of run length on viscous drag. Data are duplicated from Figure 1A (blue scatter). (B-C) Symmetric load-detachment kinetics (left) cannot support a non-monotonic dependence of run length on viscous drag (right). (D) Asymmetric load-detachment kinetics with reduced sensitivity for assisting versus hindering load (left) also cannot support a non-monotonic dependence of run length on viscous drag (right). For all panels, run length (mean ± standard error of the mean; N = 1000 for each simulation condition) was normalized by the unloaded single-kinesin value.

3.4 Discussion

Here we used Monte Carlo-based simulations to examine the effect of thermal diffusion of the cargo on the run length of a single kinesin carrying the cargo. To our knowledge, this is the first identification of a significant effect of cargo diffusion on motor-based transport. We found that cargo diffusion shortens single-kinesin runs by imposing substantial load in the direction of transport; this load is absent in the diffusion-free case. This diffusion-based shortening is countered by viscous drag, which biases the effect of the diffusing cargo toward the hindering load. Combined, our simulations revealed an unexpected, non-monotonic variation in run length, which is impaired at low and high viscous drag, but recovers to the unloaded single-motor value at intermediate viscous drag. We determined that the shortening effect of cargo diffusion on run length is not strongly sensitive to motor stiffness, and that the specific asymmetry in kinesin's load-detachment kinetics underlies the non-monotonic variation of run length uncovered in the current study.

Our simulations reveal a novel, dual effect of viscous drag on molecular motor-based transport. Because viscous drag opposes cargo motion, it is generally examined in the context of impairing motor-based transport [80, 120, 121]. Consistent with this notion, we observed substantial impairment at high viscous drag (Figure 3.2D). However, at lower viscous drag that does not significantly influence motor functions, our simulations indicate a novel, "recovery" effect of viscous drag on run length (Figures 3.2D). The resulting non-monotonic variation in run length may be important for understanding the diverse characteristics of transport in living cells, where highly variable conditions can combine to alter viscous drag—and hence run length—non-trivially. Such predictions may be tested experimentally by combining fluorescence-based run length measurements [122, 123] with ~10-fold variations in solution viscosity [80, 121], cargo size [124], and motor velocity). This would allow one to achieve a 1000-fold variation in viscous drag needed to explore the full range of the non-monotonic variation of run length (Figure 3.2D). Note that we modeled the viscous drag on the cargo as the Stoke's drag near a hard wall ($9\pi\eta dv$), which matches the experimental conditions for many in vitro studies but may not be appropriate

for in vivo scenarios. Nonetheless, because our study identifies the *magnitude of viscous drag* as the single parameter controlling the impact of cargo diffusion on single-kinesin run length (Figure 3.2D), we anticipate that the results of our study will hold for in vivo scenarios, even if the precise expression evaluating the drag force may be different.

An important implication of our study is that the specifics of load-detachment kinetics are likely critical for differentiating and fine-tuning the single-motor functions of distinct classes of motors under physiologically relevant conditions. The diffusion-based shortening of run length at low viscous drag arises from the motor's sensitivity to assisting load (Figure 3.1); the non-monotonic variation in run length with viscous drag reflects the specific asymmetry in the motor's load-detachment kinetics (Figure 3.5). The more likely the motor is to detach under load in the assisting versus the hindering direction, the greater the effect of cargo diffusion on shortening the motor's run length, and the greater the non-monotonic variation in cargo run length with viscous drag. We thus predict similar non-monotonic variations in run length for other classes of motors whose detachment rates are more sensitive to assisting load than to hindering load, such as kinesin-2 [125] and cytoplasmic dynein [126]. The specifics of non-monotonicity in run length likely depend on the specific functional forms of their respective load-detachment kinetics. A potential sensitivity of the load-detachment kinetics to nucleotide concentrations, such as that experimentally identified [127, 128] and theoretically examined [129] for the load-velocity dependence of kinesin-1, may drive further fine-tuning of single-motor functions in vivo.

Our findings at the single-molecule level are likely directly relevant for transport by small teams of kinesin-1, which is on average accomplished via the action of a single kinesin [63, 130, 131]. Thermal diffusion of multiple-motor cargos depends stochastically on the number of motors linking the cargo to the microtubule [67, 118, 119]. Because we did not detect a strong impact of motor stiffness on the shortening effect of cargo diffusion on run length (Figure 3.4C), we speculate that the effects uncovered here may not be substantially altered by changes in effective stiffness in multiple-motor transport versus single-motor transport.

The effects uncovered here also highlight diffusion-based load as a new consideration for understanding multiple-motor transport, particularly for mixed classes of motors that differ in their load-detachment kinetics. Recent investigations have focused on the importance of inter-motor strain [118, 132, 133] and local confinement [63, 67, 118] on team-motor functions. The current study suggests that, depending on the specifics of the load-detachment kinetics of the motor(s) present, thermal diffusion of the cargo may preferentially shorten the run length of a particular class of motor engaged in team transport, a bias that may be further tuned by viscous drag. We are developing simulations to explore this intriguing possibility.

In summary, our simulations revealed a previously unexplored, non-monotonic variation of run length that arises from the interplay between cargo diffusion and solution viscosity. As an additional consideration, the elastic nature of the cytoplasm, which is strongly influenced by spatial heterogeneity of the cytoskeleton [134], has been predicted

to impact the velocity of a single, cargo-free kinesin [135]. Future investigations combining solution viscoelasticity with cargo diffusion may reveal additional diversity or tunability in cargo transport, for single motors and for multiple motors functioning in teams.

Chapter 4 Tuning ensemble-averaged cargo run length via fractional change in mean kinesin number

4.2 Background

Kinesin-1 is a key microtubule-based motor that drives long-range delivery of cargos in cells [7, 10]. This intracellular motility is critical for eukaryotic cell function and survival; dysfunctions in this process are linked to human diseases including neurodegeneration [11, 12]. While the single-molecule characteristics of kinesin are reasonably well understood, many important questions still remain, including how the number of kinesins carrying a cargo impacts the distance over which the cargo travels before unbinding from the microtubule ("run length").

In cells, individual vesicular cargos are often carried by one or two kinesins, with the motor number varying among cargos in a population [44, 75, 136]. Although intuitively run length should increase as more motors carry a cargo, it is unclear how substantial such an increase would be, given that only a limited fraction of the cargo population is carried by more than one kinesin *in vivo [44, 75, 136]*. Further, for a given cargo carried by multiple kinesins, intra-motor strain can hinder cooperative function between kinesins and limit the contribution of additional kinesins to run length [63, 118, 131]. Additionally, the microtubule binding and unbinding kinetics of kinesin can be altered by cellular factors such as microtubule-associated proteins [50-52, 54, 137-139]. How the interplay of these single-motor alterations with a fractional change in mean kinesin number impacts cargo delivery is not currently understood.

Here we employed Monte Carlo-based simulations to investigate statistical ensembles of cargos, with each cargo carried by a Poisson-distributed number of kinesins. Our assumption of a Poissonian motor number is consistent with random processes [31, 70, 140] and with data available for biological scenarios [44, 75, 136]. We varied the mean number of kinesins on motile cargos between 1 and 1.3, corresponding to a modest range of 0-25% of the cargos in the population carried by two or more motors (figure 1(a)). We then characterized the run length of the cargo population as the ensemble average of the mean run lengths of cargos carried by one or more kinesins. Our simulations employed experimentally determined single-kinesin characteristics [29-32, 34, 70, 89-92, 95], including the load-dependent off-rate [29, 30] that limits the cooperative function of kinesins in a team. We varied the single-kinesin on-rate and unloaded off-rate over a large parameter space, capturing how these characteristics are altered by cellular factors [50-52, 54, 137-139]. Our simulations also included cargo diffusion [76] and viscous drag [74, 77, 79, 94], two sources of physical load that are important at the molecular level and present in all live cells. We found that a fractional change in mean kinesin number has important ramifications for the ensemble-averaged cargo run length, suggesting that the physiological range of kinesin number [44, 75, 136] provides crucial regulation of cargo delivery in cells.

4.3 Methods

4.3.1 Monte Carlo-based simulations

The kinesin simulation was the same as described in chapter 2.1 with the following exceptions. Cargos in a population were either transported by a fixed number of motors or using a poison distributed number of motors. Values for the single-kinesin on-rate, unloaded off-rate, and solution viscosity are indicated in the text.

4.3.1.1 Cargos carried by the same number of kinesins

Each cargo in a simulated population was carried by the same number of kinesins (1, 2, 3, 4, or 5). Simulations of individual cargo runs were carried out as described in section 3.2.1.2.

4.3.1.2 Cargos carried by a Poisson-distributed number of kinesins

For each simulated ensemble, the number of kinesins on each cargo in the population was drawn from the discrete Poisson distribution, $\lambda^k e^{-\lambda}/k!$, where the motor number k is a non-negative integer and λ is the Poisson mean. Only cargos assigned one or more kinesins were used to simulate runs. Simulations of individual cargo runs were carried out as described in section 3.2.1.2.

The mean number of kinesins on motile cargos was varied between 1 and 1.3, corresponding to a range of 0-25% of cargos in the populations carried by ≥ 2 kinesins (Figure 1(A)). There was a probability of <0.006% that a cargo is carried by ≥ 6 kinesins.

4.3.2 Analysis of cargo run length

4.3.2.1 Run length of individual simulated cargos

Run length was determined as the distance that the simulated cargo travels after binding to and before unbinding from the microtubule. Within the uncertainty arising from the thermal diffusion of the cargo, the motion of each simulated run was unidirectional and plus-end oriented (in the direction of kinesin motion). We detected no evidence of minus-end directed (in the direction opposite of kinesin motion) segments within individual simulated runs (data not shown), suggesting no substantial impact of intra-motor strain on the direction of cargo motion.

4.3.2.2 Mean run length of cargos carried by the same number of kinesins

For each simulation condition in which all cargos were carried by the same number of kinesins (Section 2.1.3), the cumulative probability distribution of the run lengths was fitted to that of a single exponential distribution $1 - A \cdot e^{-x/d}$. Mean run length was determined as the best-fit decay constant d. The associated standard error of the mean (SEM) was determined via a bootstrap method [98].

4.3.2.3 Ensemble-averaged run length of cargos carried by a Poisson-distributed number of kinesins

For each simulation condition in which cargos were carried by a Poisson-distributed number of kinesins (Section 2.1.4), the cumulative probability distribution of cargo run lengths was fitted to the following weighted sum:

$$P(x) = 1 - \sum_{k=1}^{5} P_k \cdot e^{-x/d_k}, \quad (4.3)$$

where P_k is the probability that a cargo is carried by k kinesins and d_k represents the mean run length of cargos carried by k kinesins. Note that the weighted sum considers up to 5 kinesins per cargo because the probability that a cargo is carried by 6 or more kinesins is negligible (<0.006%) over the range of mean kinesins examined in this study. Each probability P_k was determined as the fraction of simulated cargos carried by k kinesins. This approach accounts for stochasticity inherent in simulations of statistical ensembles; the resulting P_k values are in good agreement with those expected from Poisson distributions (data not shown). The value of each fitting parameter d_k was constrained to be within one SEM of the mean run length of cargos carried by a well-defined k number of kinesins (section 2.2.2). This approach accounts for stochasticity inherent in run-length simulations in section 2.1. The resulting best-fit determines the ensemble-averaged cargo run length, $\sum_{k=1}^{5} P_k \cdot d_k$. The associated SEM was determined via a bootstrap method [98].

4.4 Results

4.4.1 A fractional increase in mean kinesin number enhances the ensemble-averaged cargo run length

We first carried out run-length simulations using the commonly reported values for single-kinesin on-rate (5 s^{-1} [67, 93]) and unloaded off-rate (0.8 s^{-1} [34]). Our simulations utilized a solution viscosity of water (1 mPa·s), capturing the lower limit of cytoplasmic

viscosity [74, 77, 79, 94]. Under these conditions, we previously showed that load arising from cargo diffusion shortens single-kinesin runs from the unloaded value of 1 µm to 0.8 µm [76].

We found that the ensemble average of cargo runs substantially lengthened as the mean number of kinesins on the cargo fractionally increased from one (Figure 4.1). For cargos carried by a single motor (0% with ≥2 kinesins, Figure 4.1(A)), the run-length distribution was well described by a single exponential fit (Figure 4.1(B) and (C)), with a mean that was in excellent agreement with our prior work (0.80±0.04 µm, Figure 4.1(B), inset; compare with 0.8 µm in [76]). As we increased the fraction of cargos with ≥2 kinesins (5-25%, Figure 4.1(A)), the run-length distributions shifted toward longer runs (Figure 1(b)), were well-described by a weighted sum of several exponentials (Equation (4.3); solid lines, figure 4.1(C)), and deviated from a single-exponential fit (grey lines, Figure 1(C)). These changes in run-length distributions are consistent with increases in the mean number of kinesins for the cargo population [140, 141]. The reduction in run length due to cargo diffusion was mitigated when the fraction of cargos with ≥2 kinesins increased to a modest 10%, with the ensemble-averaged cargo run length returning to the unloaded single-kinesin value (1.07±0.08 µm, Figure 4.1(B), inset). Overall, the ensemble-averaged cargo run length increased by 1.9-fold (±0.2) as the fraction of cargos carried by ≥2 kinesins increased from 0% to 25% (Figure 4.1(B), inset).
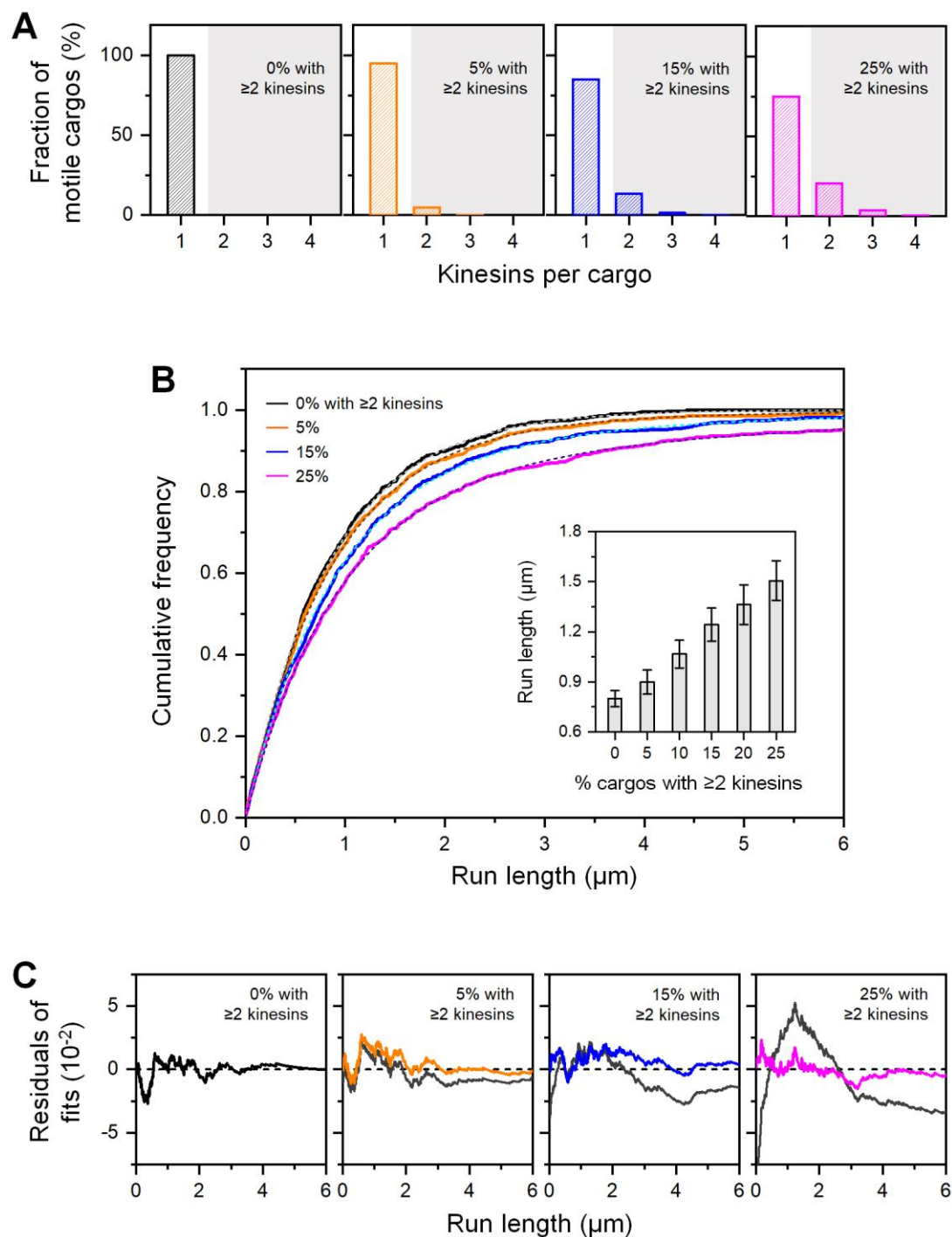
Figure 4.1: The ensemble-averaged cargo run length increases as the fraction of cargos with ≥2 kinesins increases. Simulations were carried out using an on-rate of 5 s-1 and an unloaded off-rate of 0.8 s-1 for a single kinesin, and a solution viscosity of 1 mPa·s. (A) Fraction of motile cargos carried by the indicated number of kinesins, for mean kinesin numbers between 1.0 and 1.3. Grey regions indicate the

fraction of cargos with ≥2 kinesins. (B) Cumulative frequency distributions of cargo run length, for the four distributions of kinesin numbers in (A). Dashed lines indicate best-fit to a single exponential (0% with ≥2 kinesins) or a weighted sum of several exponentials (Equation (4.4)) (5, 15, 25%). N = 1000 for each distribution. Inset: Mean run length of single-kinesin cargos (0% with ≥2 kinesins) and ensemble-averaged run length of cargos with contributions from ≥2 kinesins (5, 15, and 25%). Error bars indicate SEM. N = 5000 for each simulation condition in the inset. (C) Residuals of fits from (B). Grey solid lines indicate deviations from a single-exponential fit (5, 10, 25%).

4.4.2 A fractional increase in mean kinesin number amplifies the impact of single-motor alterations on run length

We next examined how changes in single-kinesin binding and unbinding kinetics impact the ensemble-averaged cargo run length. To allow direct comparison with the simulations in Figure 4.1, we carried out this set of simulations at the same solution viscosity (1 mPa·s). We varied the single-kinesin on-rate between 1 s^{-1} and 8 s^{-1} and the unloaded off-rate between 0.5 s^{-1} and 1.6 s^{-1}, guided by how these single-motor rates are altered by cellular factors such as microtubule-associated proteins [50-52, 54, 137-139].

The run-length increase that we observed in Figure 4.1 was general over a wide parameter space of single-motor on-rates and off-rates (Figure 4.2). For each rate combination, the larger the fraction of cargos with ≥2 kinesins, the greater the increase in the ensemble-averaged cargo run length over that of single-kinesin cargos (Figure 4.2(A)). Moreover, the sensitivity of cargo run length to these rate changes was amplified by the fraction of cargos carried by ≥2 kinesins (Figure 4.2(B)). For example, over an 8-fold change in the single-kinesin on-rate and a 3-fold change in its unloaded off-rate, the run-length increase remained largely constant when only a limited fraction of cargos was carried by ≥2 kinesins (Figure 4.2(B), left). In contrast, the run-length increase was strongly sensitive to changes in single-motor on- and off-rates when the fraction of cargos with ≥2 kinesins increased to 25% (Figure 4.2(B), right).
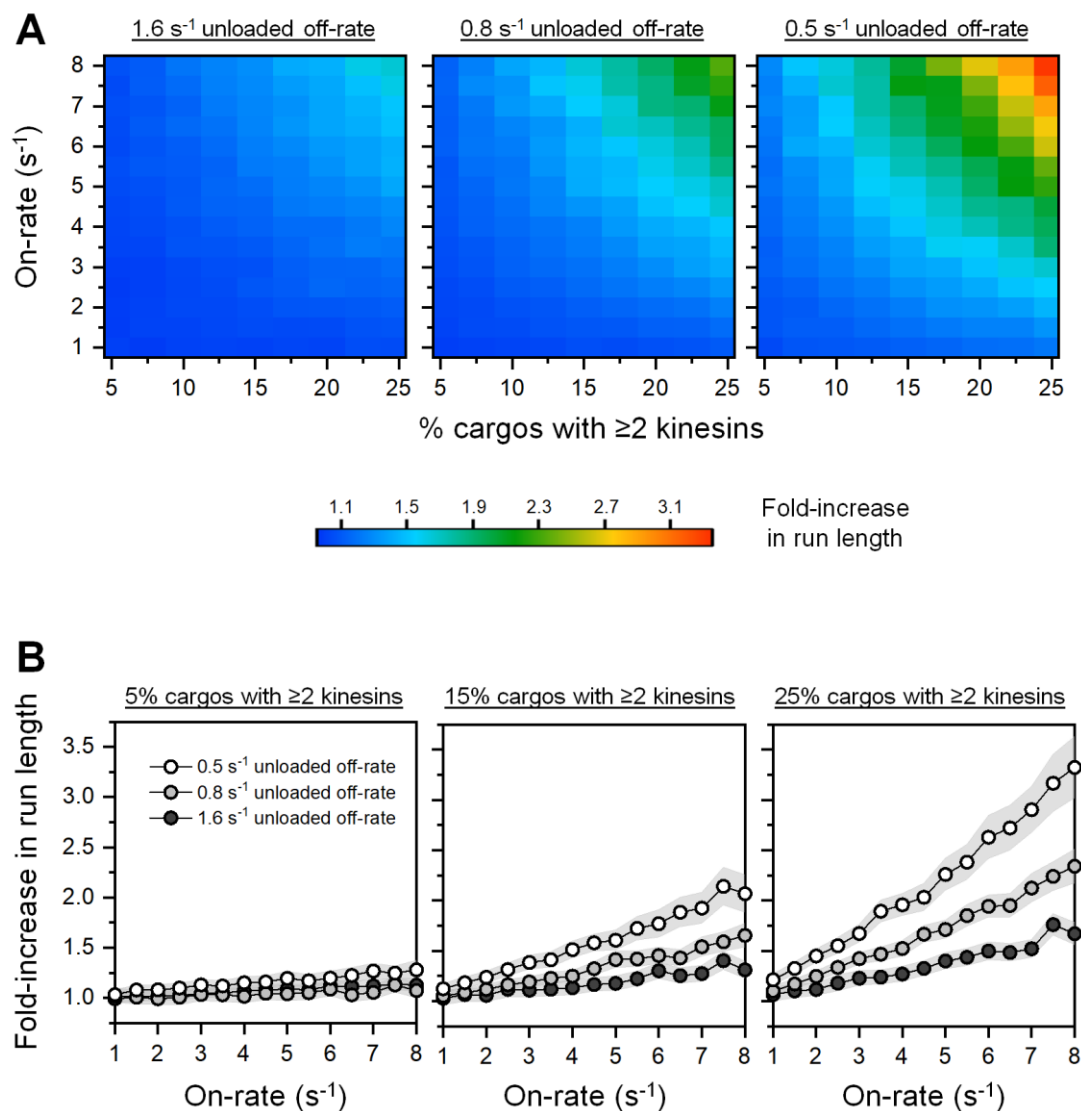
Figure 4.2: The impact of single-motor alterations on the ensemble-averaged cargo run length is amplified by the fraction of cargos carried by ≥ 2 kinesins. Simulations were carried out using a solution viscosity of 1 mPa·s. Fold-increase in ensemble-averaged run length is determined relative to the mean run length of single-kinesin cargos. (A) Fold-increase in run length as a function of the single-kinesin on-rate and the fraction of cargos carried by ≥ 2 kinesins, evaluated for three unloaded off-rates of a single kinesin. $N = 5000$ for each simulation condition. (B) Fold-increase in ensemble-averaged run length from (A), replotted as a function of single-kinesin on-rate, for three fractions of cargos with ≥ 2 motors and three unloaded off-rates of the single kinesin. Shaded regions indicate SEM.

4.4.3 Solution viscosity can enhance the effects of mean kinesin number on run length

We next explored whether our findings in Figures 4.1 and 4.2 are sensitive to changes in solution viscosity. Thus far, our simulations were conducted at the viscosity of water. In contrast, cytoplasmic viscosities can be up to ~300-fold higher than that of water [76]. We previously showed that, due to the interplay between cargo diffusion and viscous drag, the run length of cargos carried by a single kinesin varies non-monotonically with solution viscosity [76].

We found that the effects of kinesin number on run length (Figures 4.1 and 4.2) can increase as solution viscosity increased over the range reported for cells (Figure 4.3). As in our previous work [76], here we observed a non-monotonic effect of viscosity on the run length of single-kinesin cargos (dashed line, Figure 4.3(A)). This non-monotonic variation in run length persisted for mixed ensembles of cargos (5-25% with $\geq$2 kinesins, Figure 4.3(A)). For each solution viscosity tested, the ensemble-averaged cargo run length increased as the mean number of kinesins on the cargo increased fractionally from one. This run-length increase was sensitive to both solution viscosity and single-kinesin characteristics, for example remaining constant for a combination of 5 s^{-1} on-rate and 0.8 s^{-1} unloaded off-rate (grey scatter, Figure 4.3(B)), but increasing at higher viscosity for a combination of 8 s^{-1} on-rate and 0.5 s^{-1} unloaded off-rate (open scatter, Figure 4.3(B)). These effects were again amplified by the fraction of cargos carried by $\geq$2 kinesins (Figure 3(B)).
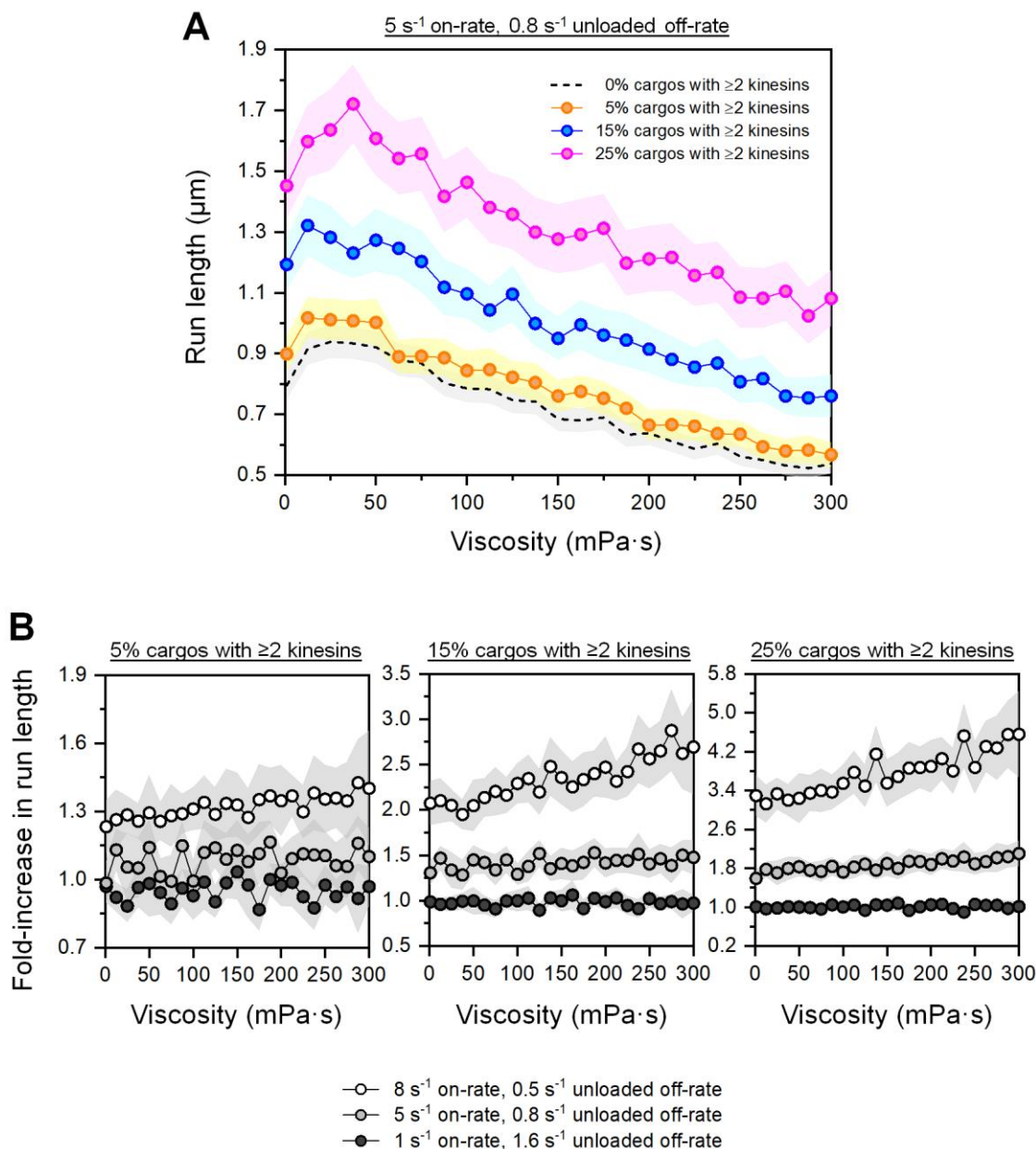
Figure 4.3: Solution viscosity can enhance the effects of kinesin motor number on run length. (A) Ensemble-averaged cargo run length as a function of solution viscosity, for three fractions of cargos with ≥2 kinesins. Simulations were carried out using an on-rate of 5 s^{-1} and an unloaded off-rate of 0.8 s^{-1} for a single kinesin. Shaded regions indicate SEM. $N = 5000$ for each simulation condition. (B) Fold-increase in the ensemble-averaged run length as a function of solution viscosity, for three fractions of cargos with ≥2 kinesins and three combinations of single-kinesin on-rate and unloaded off-rate. Fold-increase in run length is determined relative to the run length of cargos carried by a single motor. Shaded regions indicate SEM. $N = 5000$ for each simulation condition.
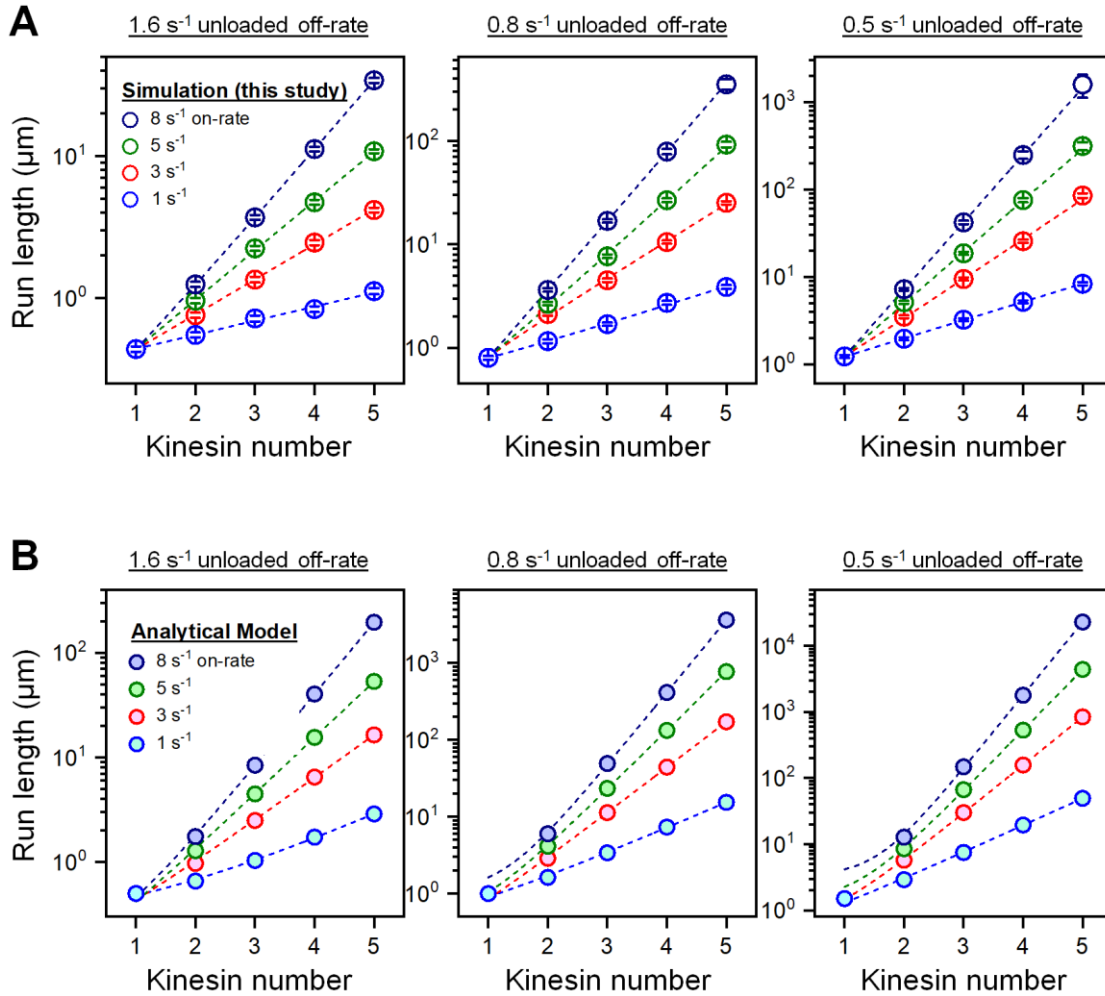
Figure 4.4: Mean run lengths of cargos carried by exactly 1, 2, 3, 4, or 5 kinesins, evaluated for four on-rates and three unloaded off-rates of a single kinesin. (A) Simulation results from the current study. Simulations were carried out using a solution viscosity of 1 mPa·s. Error bars indicate SEM. $N = 5000$ for each simulation condition. (B) Analytical calculations developed by Klumpp et al. [142] describing the mean run length of cargos carried by exactly N motors as $\frac{v}{\varepsilon}\left[1 + \sum_{n=1}^{N-1} \prod_{i=1}^{n} \frac{(N-i)\pi_{ad}}{(i+1)\varepsilon}\right]$, where $v = 0.8$ μm/s is the single-kinesin velocity, ε is the motor's unloaded off-rate, and π_{ad} is the motor's on-rate. We verified that the mean cargo run lengths from our simulations in panel (A), which included intra-motor strain that hinder motor cooperativity, are substantially shorter than those determined from analytical calculations that do not consider intra-motor strain [142] in panel (B). Mean run lengths in (A) were used to determine the ensemble-averaged run length of mixed cargo populations in Figures 4.1-3 in the main text.
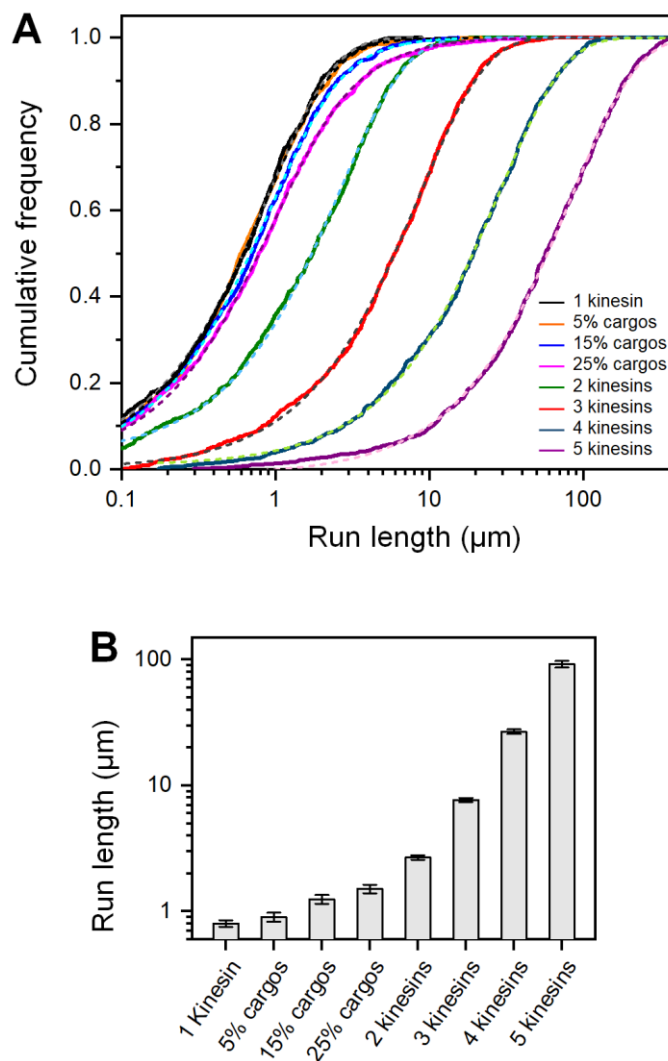
Figure 4.5: Run lengths of cargos carried by exactly 1, 2, 3, 4, or 5 kinesins. Simulations were carried out using an on-rate of 5 s^{-1} and an unloaded off-rate of 0.8 s^{-1} for a single kinesin, and a solution viscosity of 1 mPa·s. (A) Cumulative frequency distributions of cargo run length, for five defined kinesin numbers. For reference, run-length distributions for mixed ensembles of cargos are replotted from Figure 4.1(B) in the main text (5, 15, and 25% cargos). Dashed lines indicate best-fit to a single exponential (1, 2, 3, 4, or 5 kinesins) or a weighted sum of several exponentials (Equation (4.4) in the main text) (5, 15, 25% cargos). $N = 1000$ for each distribution. (B) Mean cargo run length, for five defined kinesin numbers. For reference, the ensemble-averaged run lengths of cargos with contributions from ≥ 2 kinesins (5, 15, and 25% cargos) are replotted from Figure 4.1(B) in the main text. Error bars indicate SEM. $N = 5000$ for each simulation condition.
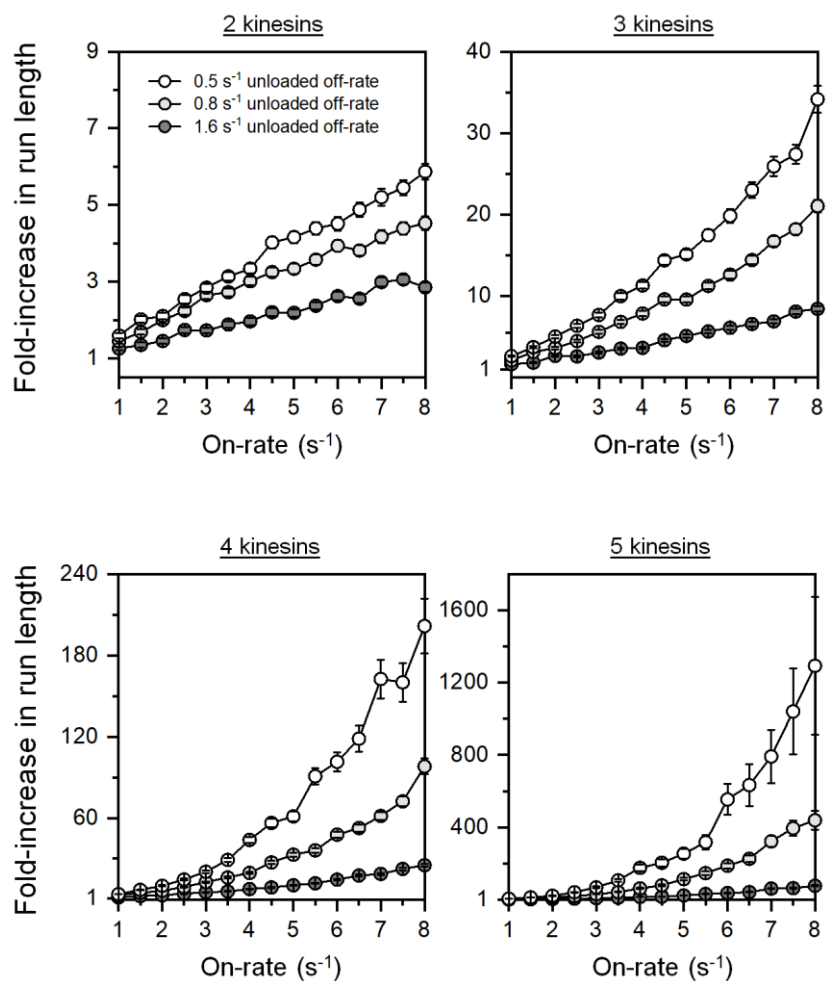
Figure 4.6: The impact of single-motor alterations on mean run length, for cargos carried by exactly 2, 3, 4, or 5 kinesins. Simulations were carried out using a solution viscosity of 1 mPa·s. Single-kinesin on-rates and unloaded off-rates are as indicated. Fold-increase in run length is determined relative to the mean run length of single-kinesin cargos. Error bars indicate SEM. $N = 5000$ for each simulation condition.
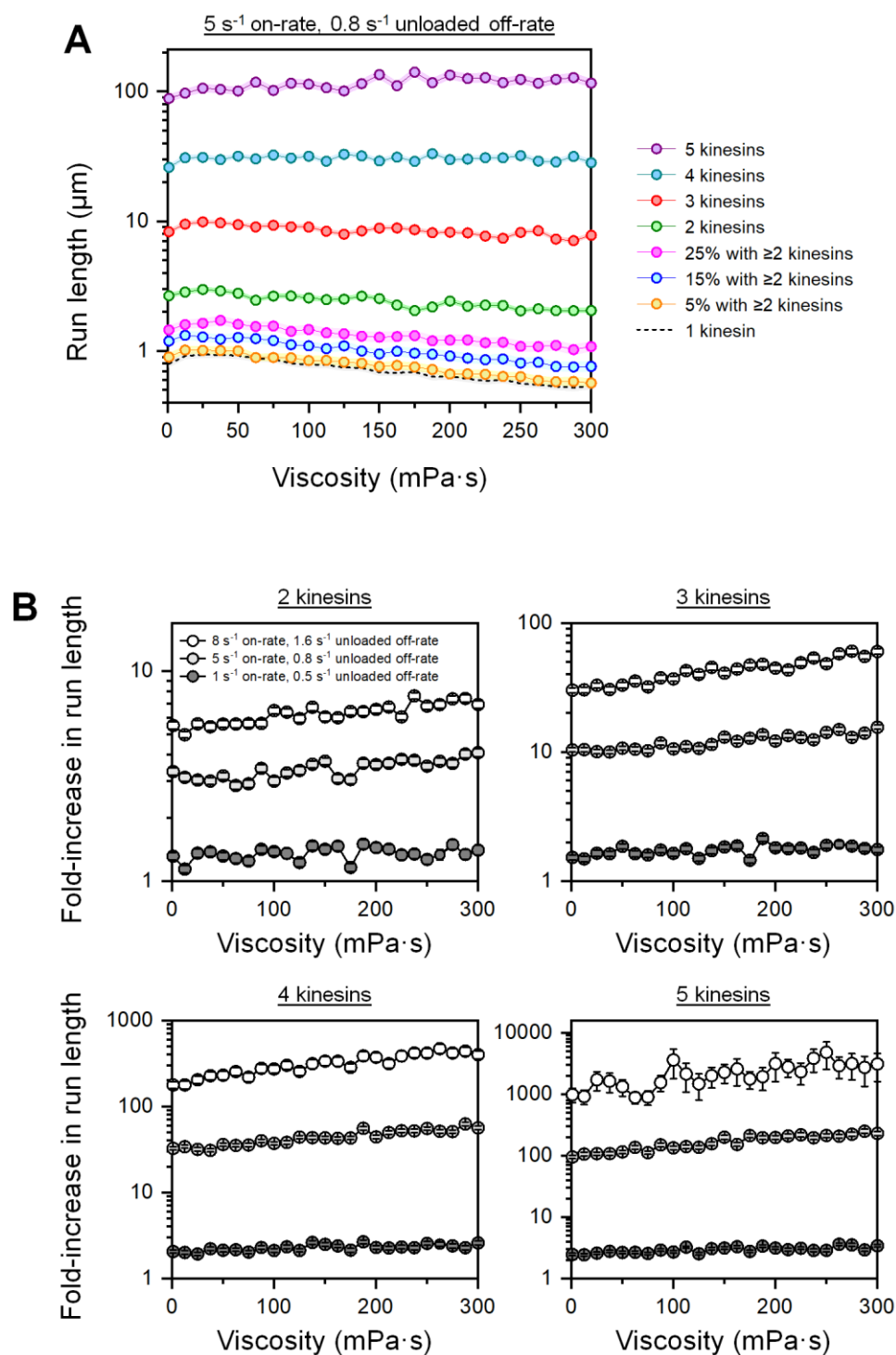
Figure 4.7: The impact of solution viscosity on mean run length, for cargos carried by exactly 1, 2, 3, 4, or 5 kinesins. (A) Mean cargo run length as a function of solution viscosity, for five defined kinesin numbers. For reference, ensemble-averaged run lengths of mixed cargo populations (5%, 15%, 25% with ≥2 kinesins) are replotted from Figure 4.3 (A) in the main text. Simulations were carried out

using an on-rate of 5 s^{-1} and an unloaded off-rate of 0.8 s^{-1} for a single kinesin. Shaded regions indicate SEM. $N = 5000$ for each simulation condition. (B) Fold-increase in the mean run length of cargos as a function of solution viscosity, for four defined kinesin numbers and three combinations of single-kinesin on-rate and unloaded off-rate. Fold-increase in run length is determined relative to the mean run length of cargos carried by a single motor. Error bars indicate SEM. $N = 5000$ for each simulation condition.

4.5 Discussion

Here we present *in silico* evidence that mean kinesin number is an important and sensitive tuning parameter for the ensemble-averaged distance that cargos travel in biological cells. Compared to the single-motor case, a fractional changes in mean kinesin number enhances both the ensemble average of cargo run length and its sensitivity to single-kinesin alterations (Figures 4.1 and 4.2). Thus, although kinesin is thought to function non-cooperatively [63, 118], our study indicates that a modest change in mean kinesin number can have important ramifications for the motility of mixed ensembles of cargos, which reflects the biological scenario. We found that the effects of kinesin number on cargo run length can be further enhanced over the range of solution viscosities reported for living cells (Figure 4.3).

Our results may be understood by considering the interplay between the microtubule-binding and -unbinding kinetics of individual kinesins. The load-dependent off-rate of kinesin [29, 30] limits cooperative function in an ensemble. However, because the on-rate of the motor can be several-fold faster than the unloaded off-rate (5 s^{-1} [67, 93] versus 0.8 s^{-1} [34]), the presence of an additional motor increases the probability that the cargo remains tethered to the microtubule, thereby lengthening the run without necessarily contributing to the number of kinesins simultaneously driving motility. Thus, under otherwise identical conditions, the faster the on-rate of the motor, the longer the individual runs of cargos carried by ≥2 kinesins, and the greater the ensemble-averaged run length of the cargo population. Our results in Figure 4.2 capture this interplay.

The effects of viscosity (Figure 4.3) further highlight the interplay between kinesin's binding and unbinding kinetics. Solution viscosity imposes load on the cargo and increases the off-rate of kinesin carrying the cargo [76, 143]. The presence of additional motors on the cargo can reduce the impact of viscous load on kinesin's off-rate by enabling load sharing between kinesins [65]. The higher the solution viscosity and/or fraction of cargos carried by ≥2 kinesins, the more effective load sharing can be, and the larger the contribution that each additional motor can make to run length. These effects are pronounced when kinesin's on-rate is substantially faster than its off-rate, enabling the load sharing that can only take place between motors simultaneously driving motility.

Taken together, we anticipate that the effects uncovered here will have rich implications for delineating the motility of cellular cargos. In particular, because cellular factors impact kinesin function on the single-molecule level, quantitative insights into how these single-kinesin alterations combine with the biological range of kinesin number are critical for predictive understanding of motility and its regulation in cells. The range of tuning by kinesin number will likely expand as we learn more about the regulation of single-molecule characteristics, including the microtubule binding and unbinding kinetics of the kinesin motor highlighted here.

Chapter 5 Force-dependent kinesin detachment critically influences the effect of cargo-mediated motor interactions on cargo velocity

5.1 Background

Kinesin-1 is a key microtubule-based motor that drives the long-range delivery of cargos in cells [6, 7, 44]. Cargo transport is critical for eukaryotic cell function and survival, as dysfunctions in this process are linked to human diseases, including neurodegeneration [11, 12]. Cargo velocity is an important factor governing timely cargo delivery. For cargos transported by a single motor, research has demonstrated which factors (such as forces on the motor) impact cargo velocity [29, 33, 95]. However, we still lack a complete understanding of the factors that influence the velocity of cargos transported by more than one motor.

In cells, individual vesicular cargos are often transported by a small team of molecular motors [44, 75]. Up until recently, the velocity of cargos transported by multiple motors was largely thought to reflect the single motor velocity [63, 130, 144]. However, recent evidence has emerged suggesting non-linearity in the team motor velocity may arise in multi-motor transport under certain conditions [53, 65, 66, 82, 131, 145, 146]. Force-based interactions, mediated through the cargo, among the motors are likely a critical factor underlying non-linearity in the team motor velocity. During transport the motors step asynchronously and can get separated along the microtubule, resulting in force-based interactions mediated through the cargo [118]. In cells, these force-based interactions are likely a frequent occurrence given the inherent heterogeneity in kinesins population [145]. Furthermore, multiple types of molecular motors may be active on any given cellular cargo, leading to force-based interaction between different types of motors [44]. Importantly, these force-based interactions make it likely that one of the motors will detach from the microtubule because the detachment rates of molecular motors increase with force [29, 30, 147]. As one of these motors detach, the cargo will be pulled towards the remaining motor (cargo flop). It is conceivable that if these cargo flops occur frequently enough and with a preference for one direction, they could alter the average cargo velocity. Indeed, recent evidence has emerged that this may indeed be the case with macro-molecular crowding [66]. Cells are composed of macromolecules which may limit the available volume to molecular motors [148-153]. Recent efforts have begun to determine the impact of macromolecular crowding on molecular motors [106, 152, 154, 155]. A recent experiment showed that macromolecular crowding can increase the likelihood the leading motor will detach during force-based interactions (due to entropic forces in the crowded medium), potentially causing the cargo to flop back more frequently than it flops forward [66]. It has become clear the details of kinesins detachment kinetics critically influence the impact of cargo-mediated interactions among the motors on the cargo's velocity.

In this work, we used Monte Carlo-based simulations to examine how the details of kinesin detachment kinetics and cargo-mediated motor interactions impact cargo velocity. For this purpose, we first captured the entropic effect of macromolecular crowding in our simulations by increasing the kinesin detachment rate for motors experiencing a hindering force [66]. In this scenario, we characterized the cargo velocity as the detachment rate increased for cargos transported by up to four motors (see Methods). Next, we examined how the separation between two motors carrying a single cargo impacts detachment events for the leading and lagging motors. Here, we examined changes in cargo position after a detachment event and the detachment frequency for leading and lagging motors. We then assessed the impact of heterogeneity in the single-motor velocity on cargo-mediated motor interactions when one cargo is carried by two motors. Specifically, we examined how this heterogeneity impacts the cargo velocity. The single-motor detachment was varied to mimic non-crowded versus crowded. Finally, we assessed the effect of crowding when an external force biases the cargo position to be behind the central position of the motors, making it more likely for the motors to experience hindering forces. Overall, we found that the kinesin detachment kinetics indeed play a central role in how cargo-mediated interactions impact cargo velocity. Additionally, for the first time, we directly capture how reductions in cargo velocity arise from an increased detachment frequency of the leading motor. Our findings here suggest that the velocity of vesicles in cells is sensitive to environmental factors inside the cell, which can modify the kinesin force-detachment rate or otherwise influence cargo-mediated interactions among the motors.

5.2 Methods

5.2.1 Monte Carlo-based simulations

Kinesins simulations were as described in chapter 2.1 but with the following change to kinesins force detachment kinetics.

We modeled kinesin's force-dependent off-rate as an exponential function that is asymmetric for positive and negative forces [66]:

$$\varepsilon(F) = \begin{cases} \varepsilon_0 \cdot \exp\left(\frac{\delta_H |F|}{k_B T}\right), & F < 0 \\ \varepsilon_0 \cdot \exp\left(\frac{\delta_A |F|}{k_B T}\right), & F > 0 \end{cases} \quad (5.1)$$

where ε_0 is the unloaded off-rate and F is the force on the motor. Positive values of F indicate a force oriented in the direction of kinesin motion; negative values of F indicate a force oriented in the direction opposite to motor motion. F is given in units of pN. $k_B T$ is the thermal energy at room temperature (4.11 pN·nm). δ_H and δ_A are the characteristic distance between attached and unattached states under hindering and assisting loads, respectively. δ_H/δ_A was varied from 0.5 to 2 with $\delta_A = 2.0$ nm [29, 32].

5.2.2 Analysis of cargo velocity

We determined the velocity of an individual cargo by fitting the cargo position as a function of time. We determined the mean cargo velocity by fitting the cumulative distribution of each individual cargo velocity to a normal distribution: $\frac{1}{2}\left(1 + erf\left(\frac{v - v_m}{\sigma\sqrt{2}}\right)\right)$, where v is the cargo velocity, v_m is the mean cargo velocity, and σ is the standard deviation of the cargo velocity.

5.2.3 Analysis Motor detachment events

For each detachment event in which two or more motors were attached to the cargo, we tracked the positions of the cargo and all motors at the time of detachment and the cargo position 5 ms after the detachment event. For two-motor cargos, we calculated the separation between the motors and the change in cargo position. We next calculated the frequency of detachment events for each motor separation depending on whether the detached motor was the leading or lagging motor. The detachment frequency was defined as the number of detachment events for a given motor separation (for leading vs. lagging detachments) divided by the total number of detachment events (including both leading and lagging motor detachments). The associated standard error of the mean (SEM) was determined via a bootstrap method [98].

5.3 Results

5.3.1 Multi-motor cargo velocity is sensitive to the parameters of single-motor detachment

Here we examined how increasing a motor's detachment rate, for hindering forces, impacted the velocity of multi-motor cargos. In our simulations, we modeled the motor's force detachment rates using an exponential function (Equation 5.1). We assumed that all motors were identical and used a previously established force-velocity dependence for the motors (Equation 2.2). We simulated cargo runs for cargos carried by 1, 2, 3, or 4 motors and increased the motor's characteristic distance parameter in the hindering direction (Figure 5.1A, δ_H) such that from 0.6 to 4.0 nm, reflecting uncrowded and crowded conditions. We held the motor's characteristic distance parameter in the assisting direction constant (Figure 5.1A, δ_H = 2 nm). Under these conditions, we determined the cumulative velocity distribution of the cargos and found the average cargo velocity (Figure 5.1B&C, see Methods).
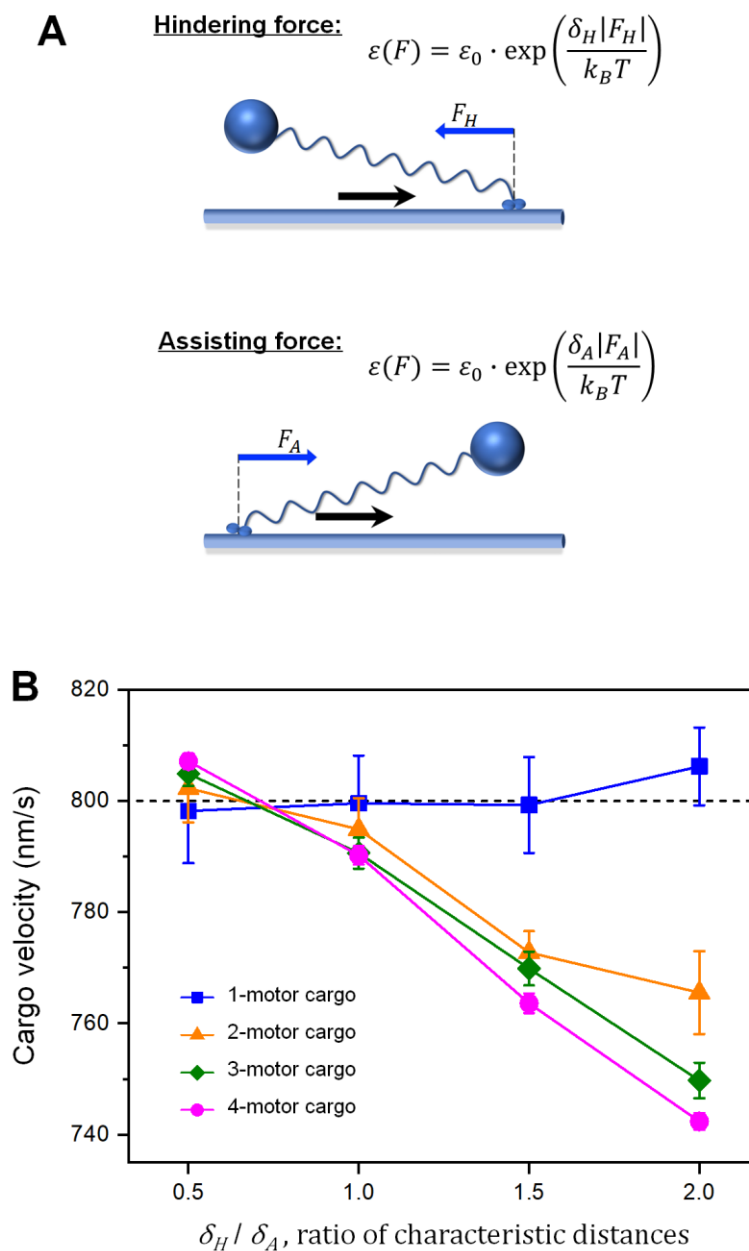
Figure 5.1: Multi-motor cargo velocity is sensitive to the single-motor detachment rate. (A) Schematic: of a cargo-mediated interaction between two motors. Each motor experiences a force proportional to its stiffness (k) and how much the motor is stretched past its rest length (L_r = 40 nm). The force increases the motors detachment rate (ε), this increase depends on the thermal energy (k_BT) and the motor's characteristic distance, δ_H for motors leading the cargos and which δ_A. Note the simulations are in one-dimension, the schematic is shown in 2D for illustration purposes. (B) Mean cargo velocity as a function of δ_H/δ_A for cargos

carried by 1–4 motors. The single-motor velocity is 0.8 nm/s for all motors, and there are no external forces on the cargo. Error bars are the variance of the cargo velocity (see Methods). For each condition, 1000 cargo trajectories were simulated.

We found that the velocity of multi-motor cargos decreased as δ_H increased (Figure 5.1B&C). We first examined the cumulative distribution of the cargos velocity for each condition tested. For multi-motor cargos, increasing the δ_H shifted the velocity distribution towards the left, indicating a decrease in the average velocity of multi-motor cargos (Figure 5.1B). The velocity distribution of cargos carried by one motor did not shift to the left, indicating no such reduction in the mean velocity (Figure 5.1B). We next found that the mean velocity of cargos carried by two motors decreased by 5% when δ_H/δ_A increased from 0.5 to 2 (Figure 5.1B). The cargo velocity was lower than the single-motor velocity when $\delta_H/\delta_A > 1$ (Figure 5.1C). Over the same range of δ_H/δ_A, cargos carried by three or four motors exhibited a similar reduction in cargo velocity, 7% and 8%, respectively. In contrast, cargos carried by a single motor did not exhibit a slow-down as δ_H/δ_A increased from 0.5 to 2. Thus, our data indicates that the velocity of cargos carried by two or more motors is sensitive to the single motor force-detachment rate.

5.3.2 Single-motor detachment kinetics influence the detachment probability of the leading versus lagging motor

We next examined how changes in the single-motor detachment rate impact detachment events of leading versus lagging motors for cargos carried by two motors. We hypothesized that increasing δ_H/δ_H would result in an increased frequency of detachment for leading motors versus lagging motors. For simplicity, we tested this hypothesis for cargos carried by two motors. We quantified two metrics of these detachment events to assess their impact on cargo velocity. First, we examined how the cargo position changes 5 ms after a detachment event (cargo flop) as a function of the separation between two engaged motors. Next, we compared the fraction of detachment events for leading versus lagging motors as a function of separation between the two engaged motors.

We found that the direction of cargo flops, but not their magnitude, depends on whether the leading or lagging motor detaches from the microtubule (Figure 5.2 top row). When the lagging motor detaches from the microtubule, the cargo position tends to increase (Figure 5.2, magenta top). Similarly, when the leading motor detaches from the cargo, the cargo position decreases (Figure 5.2, blue top). We found that the cargo flop magnitude is similar for leading versus lagging motor detachment events (Figure 5.2C, blue vs. magenta). We expected the cargo flop to be a direct result of the force on the cargo from the remaining motor. However, if this had been the case we would expect to see a sudden increase in the change in cargo position at a separation of 80 nm, corresponding to the motors being separated by twice their rest length. Instead, we see that the change in cargo

position increases at a constant rate with motor separation. This is consistent with the cargo's average position changing from the midpoint between the two attached motors to the position of the remaining motor. We examined the change in cargo position after a detachment event for δ_H/δ_A = 0.5 and 2 and found no significant difference for either leading or lagging motor detachment events (Figure 5.2 top, square vs. circle points).

Importantly, we found that when $\delta_H/\delta_A < 1$ the leading motor is more likely to detach from the microtubule than the lagging motor during force-based interactions. Two motors undergo forced-based interactions when they are separated by more than 80 nm because motors only experience a force when they are stretched passed their rest length. To quantify this, we considered the number of leading (or lagging) motor detachment events at a given motor separation divided by the total number of detachment events (detachment frequency). For a δ_H/δ_A = 0.5 force-based interactions were more likely to result in the lagging motor detaching (Figure 5.2A, bottom). For example, at a motor separation of 104 nm, the frequency of lagging motor detachments was 0.05 while the frequency of leading motor detachments was 0.01. However, when δ_H/δ_A = 0.5 the leading motors were more likely to detach during force-based interactions (Figure 5.2B, bottom). For instance, at a separation of 104 nm, the frequency of leading motor detachments was 0.10, while the frequency of lagging motor detachments was 0.01. Thus, as δ_H/δ_A increases it becomes more likely the cargo will flop backward after a detachment event, which is consistent with the decrease average velocity of the cargo over the same range.
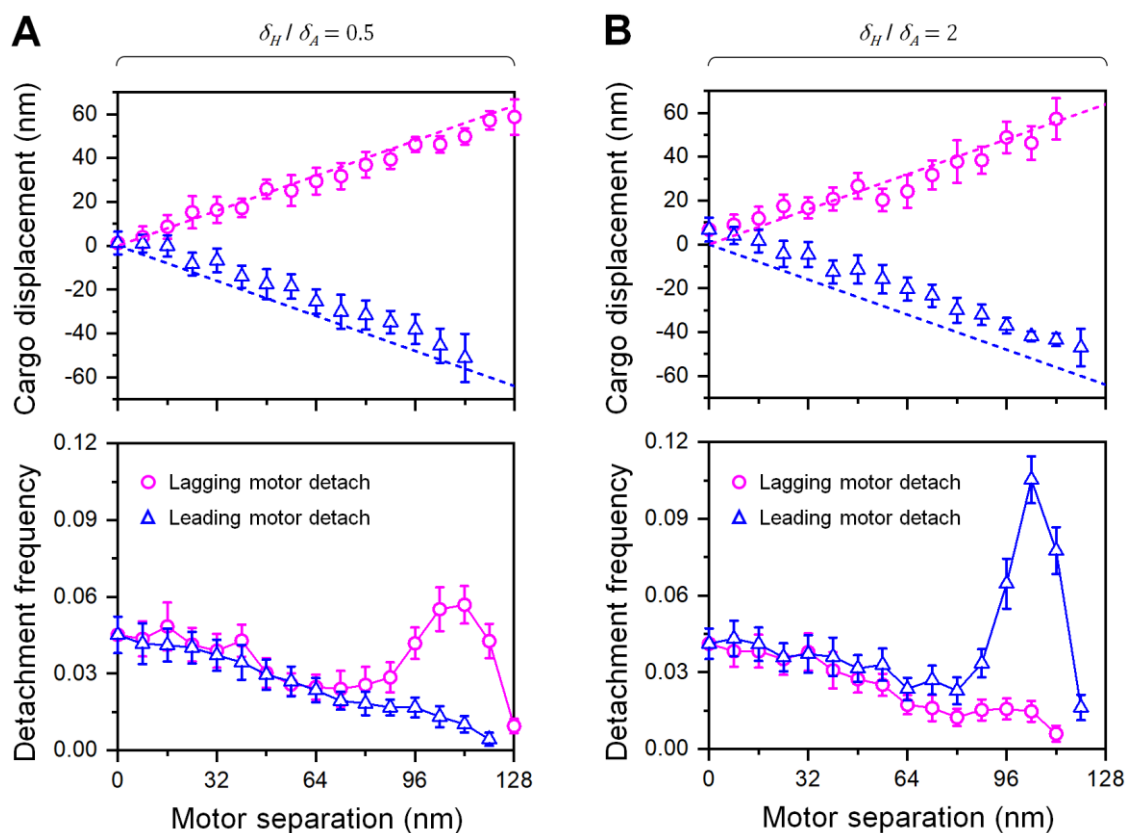
Figure 5.2: Single-motor detachment kinetics influence the probability that the leading versus lagging motor will detach from the microtubule. (A) Average change in cargo position 5 ms (top) after a detachment event for lagging (magenta) and leading (blue) motor detachment with $\delta_H/\delta_A = 0.5$. Fraction of detachment events (bottom) for a given motor separation with $\delta_H/\delta_A = 0.5$. (B) Average change in cargo position 5 ms (top) after a detachment event for lagging (magenta) and leading (blue) motor detachment with $\delta_H/\delta_A = 1$ Fraction of detachment events (bottom) for a given motor separation with $\delta_H/\delta_A = 1$. Error bars were calculated using bootstrapping (Methods). Cargos were carried by two motors and had the same unloaded single-motor velocity (0.8 μm/s). For each condition, 1000 cargo trajectories were simulated.

5.3.3 Heterogeneity in single-motor velocity increases the sensitivity of cargo velocity to single-motor detachment kinetics

In Sections 4.2.1 and 4.2.2, we examined cargos transported by motors with the same single-motor velocity; however, *in vivo*, variations arise among motors [145]. Variations in the single motor velocity will increase the frequency of force-based interaction. Thus, we examined how heterogeneity in single-motor velocities impacts the velocity of cargos carried by multiple motors. We hypothesized that when δ_H is high, as in

crowded conditions, heterogeneity would lead to a greater reduction in cargo velocity than that experienced by cargos carried by motors with the same velocity. To test our hypothesis, we simulated cargos carried by two motors, with each motor's velocity being randomly drawn from a normal distribution with a standard deviation (Δv) ranging from 0 to 0.2 µm/s. For each velocity distribution, we determined the average cargo velocity as a function of δ_H.

We found that increasing the standard deviation in the motor velocity (Δv) led to a larger decrease in cargo velocity compared with the change observed for a homogeneous population of motors (Figure 5.3A). For a low value of $\delta_H/\delta_A < 1$, the average cargo velocity equals the average single-motor velocity for both heterogeneous and homogeneous populations of motors. As δ_H/δ_A increased, the cargo velocity fell below the single-motor velocity for each Δv examined here; however, there was a greater reduction in cargo velocity for a heterogeneous population of motors. For example, for $\delta_H/\delta_A = 2$, a standard deviation of 0 µm/s in the single-motor velocity led to a decrease of 5% in the cargo velocity while a standard deviation of 0.2 µm/s led to a 12% decrease in the cargo velocity.

We found heterogeneity in kinesin's single motor velocity increased the frequency of force-based interactions between the motors, further increasing the frequency of leading motor detachment events (Figure 5.3B). As we increased Δv, the frequency of motors that detached with a separation of less than 80 nm (not undergoing forced-based interactions) decreased for all values of δ_H tested (Figure 5.3B). For example, at $\delta_H/\delta_A = 0.5$ and a motor separation of 8 nm, the combined frequency of leading and lagging motor detachment events decreased from 0.08 to 0.05 when Δv increased from 0 to 0.2 µm/s. This corresponds to an increase in the frequency of motors detaching during force-based interactions. When $\delta_H/\delta_A > 1$ there was a larger increase in detachment frequency for leading motors than for lagging motors, as Δv increased (Figure 5.3B, left column). Thus, there was both an increase in the frequency of force-based interactions, as well as an increase in the frequency of flops that were backward (Figure 5.3B, left column). This is consistent with the greater slowdown we observed for a heterogeneous population of kinesin with $\delta_H/\delta_A = 2$ versus the homogeneous population of kinesin under the same conditions.
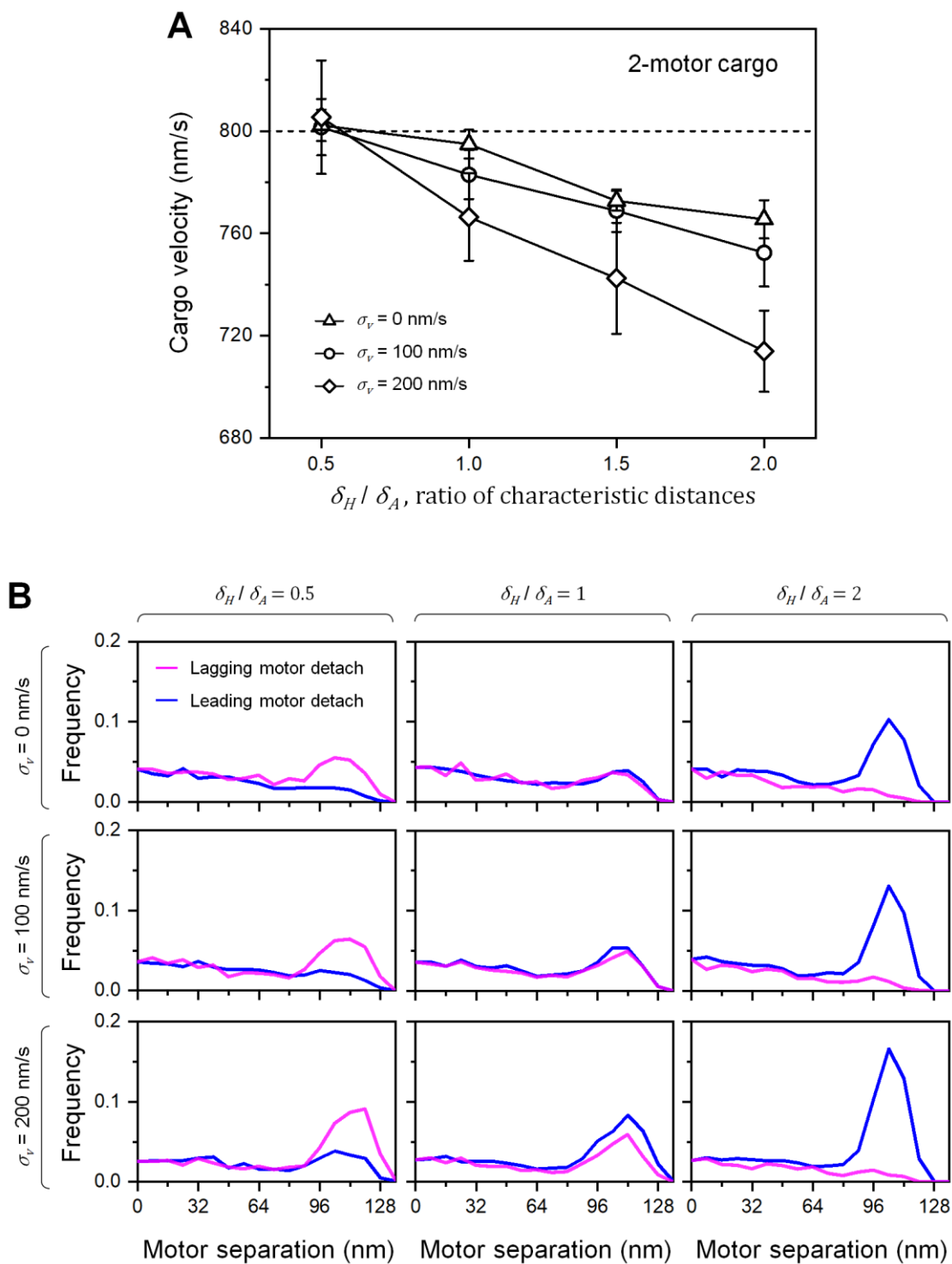
Figure 5.3: Heterogeneity in the single-motor velocity increases the sensitivity of cargo velocity to single-motor detachment kinetics. **(A)** Cargo velocity as a function of δ_H/δ_A for three standard deviations (Δv) in single-motor velocity. Error bars are the variance in cargo velocity. **(B)** Detachment fraction of leading (blue)

and lagging (magenta) motors for δ_H/δ_A = 0.5, 1, or 2 and Δv = 0, 0.1, or 0.2 μm/s as a function of motor separation. In both (A) and (B), cargos were carried by two motors. For each condition, 1000 cargo trajectories were simulated.

5.3.4 Low-to-moderate external forces on the cargo amplify the impact of crowding by increasing the frequency of leading motor detachment

In cells, cargos are often subject to forces opposing their motion, such as drag on the cargo and other motors pulling the cargo in the opposite direction. Here we consider the impact of these external forces which cause the cargo position to be behind the central position of the motors. For motors separated on the microtubule, this change in cargo position will cause the hindering force on the leading motor to be greater than the assisting force on the lagging motor. We hypothesized that these forces would amplify the slow-down caused by cellular crowding by increasing the frequency at which leading motors detach from the microtubule. Thus, we examined how low-to-moderate forces (0–1 pN) on the cargo impact the slow-down caused by leading motor detachments. For each external force tested, we determined the average velocity of cargos carried by two motors as δ_H/δ_A increased from 0.5 to 2 (Figure 5.4A).

We found that increasing δ_H/δ_A resulted in a greater slow-down when the cargo was subjected to an external load (Figure 5.4A). Consistent with previous findings, when δ_H/δ_A > 1, the cargo velocity decreased as the load on the cargo increased. As we increased δ_H/δ_A, we found that the velocity of cargos subject to an external load was more sensitive to δ_H/δ_A than cargos without an external force. For example, for an external force of 0.5 pN, the cargo velocity decreased by 7% as δ_H/δ_A increased from 0.5 to 1. In contrast, for an external force of 0 pN, the cargo velocity decreased by only 5% as δ_H/δ_A increased from 1 to 2.

We found that the decrease in velocity was associated with a further increase in the frequency of leading motor detachments versus when no force was present (Figure 5.4B, top versus bottom 2 rows). Further, this increase included motors not undergoing force-based interactions as δ_H/δ_A was increased from 0.5 to 1 (Figure 5.4B, bottom 2 rows). Indicating an increase in motors under hindering forces due to the load on the cargo.
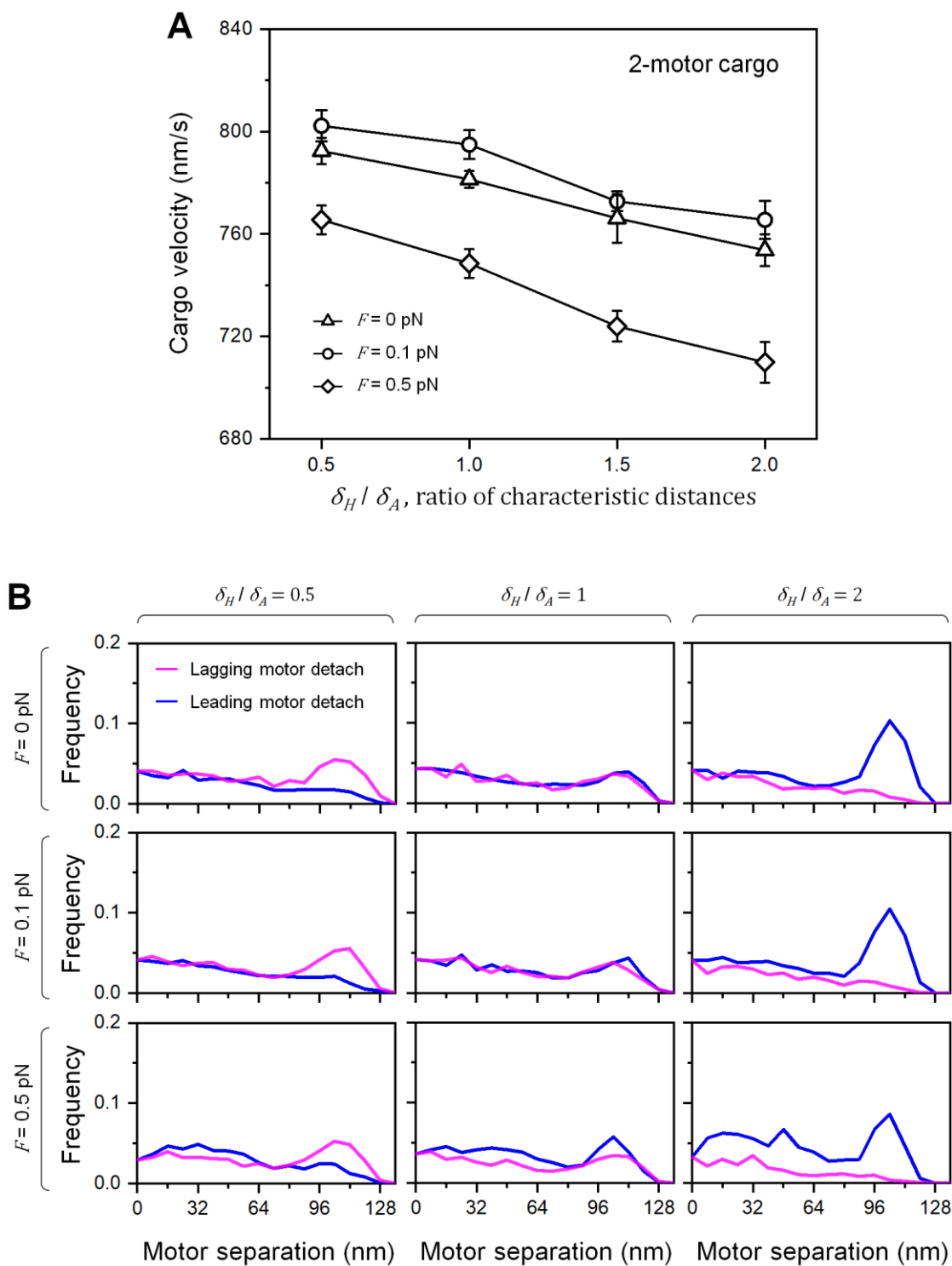
Figure 5.4: Low-to-moderate forces on the cargo amplify the impact of crowding by increasing the frequency of leading motor detachment. **(A)** Cargo velocity as a function of δ_H/δ_A for four external forces (F) on the cargo. Error bars are the variance in cargo velocity. (B) Frequency of leading (blue) and lagging (magenta)

motor detachments for δ_H/δ_A = 0.5, 1, or 2 and F = 0.1, 0.5, or 1.0 pN. In both (A) and (B), cargos were carried by two motors and had the same unloaded single-motor velocity (0.8 μm/s). For each condition, 1000 cargo trajectories were simulated.

5.4 Discussion

Here, we have presented in silico evidence that the force-based detachment rates of kinesin is an important and sensitive tuning parameter influencing the velocity of cargos transported by multiple motors in a cell. In contrast to the velocity of cargos transported by a single motor, the velocity of cargos transported by multiple motors is sensitive to alterations in kinesin's force-dependent detachment rate. Specifically, we found that when the motors are more likely to detach under hindering forces than assisting forces, the cargos velocity slows down when compared with the single motor velocity under identical conditions. This discrepancy in the team motor velocity and the single motor velocity arises because of force-based interactions between the motors as they become separated along the microtubule. When motors are more likely to detach under hindering loads the cargo will flop backward more often than it will flop forwards reducing the average velocity of the cargo. Furthermore, we found heterogeneity in the single motor velocity increased the occurrence of these detachment events amplifying the slowdown in cargo velocity. We also found that external forces, opposing the motion of the cargo, can amplify the slowdown because the cargo will on average be behind the central position of the motors.

In part, our study aimed to capture the slowdown in the cargos average velocity from macromolecular crowding by including the increased force-detachment rate under hindering load observed in experiments. While our simulations did confirm that the cargo does indeed slow down under these conditions due to the cargo flopping backward, our simulations did not capture the magnitude of the slowdown observed in experiments. Our simulations found a slowdown of 12% of the single motor velocity (with crowding and heterogeneity in single motor velocity) while the experiments indicate a 28% slowdown [14]. A slight external load, which has a negligible impact on the single motor velocity was not enough to account for this difference. Thus, our study suggests that the change in the detachment rate of the motors is an important factor in explaining the slowdown from macromolecular crowding, but it is likely not the only important factor.

Taken together our findings provide strong evidence that cellular factors that alter the details of force-dependent kinesin detachment can substantially influence the velocity of cellular cargos. More generally our study adds to the mounting evidence of the importance of force-based interactions on the transport of cargos by multiple motors [9, 14, 15, 20]. Factors impacting either the frequency of force-based interaction or their outcome, are likely to impact the velocity of multi-motor cargos. For instance, cellular cargos are enclosed in a lipid membrane, recent work suggests that this membrane might delay force-based interactions leading to an increase in cargo velocity [15]. Further, the

frequency of force-based interactions could be impacted by microtubule-associated proteins which can impact the rate motors bind to the microtubule [13, 48-51]. Overall, our study suggests that understanding the details of force-based interaction and the factors that impact them, such as kinesins force detachment kinetics, may provide rich insight into the velocity of cellular cargos transported by small teams of motors.

Chapter 6 Future direction/conclusion

The primary driving factor behind my research has been understanding how kinesin's single motor detachment kinetics impacts the transport of its cargo. In my first project, I examined the interplay between cargo diffusion and the motor's force-based detachment kinetics over a large parameter space of viscosities and cargo sizes. I found that at low viscous drag, there is a shoring of the cargo's run length leading to a non-monotonic response to viscosity. In my second project, I explored, how the fractional changes in the number of motors on the cargo can change the impact. I found that these changes are highly sensitive to both the motor's detachment rate and the on rate of the motors. Finally, I explored how the motor's force detachment kinetics can impact the cargo's velocity. I found that, for cargos carried by more than one motor, the asymmetric detachment kinetics can have a significant impact on the cargo's velocity. For example, if the motors are more sensitive to hindering loads, this can slow the cargo's velocity significantly. This effect is greatly amplified by heterogeneity in the motor's unloaded velocity.

Overall, my work has indicated that single motor detachment kinetics may play a central role in regulating cargo transport in cells. However, we are still learning more about the detachment kinetics of molecular motors, and how they are impacted by cellular conditions. For example, kinesin's detachment rates in the hindering direction are increased by macromolecular crowding [66]. Another study indicates that the vertical component of the detachment kinetics may be import.

Future work could incorporate these new findings into the simulations and explore how they impact transport dynamics. Another possibility direction to go with these simulations is to explore the role of detachment kinetics in regulating the transport of cargos with different types of motors. For example, cargos that are transported by both kinesin and dynein. An emphasis could be placed on how changes in environmental factors influence the direction of the cargos motion.

Chapter 7 Educational Guide

Mentoring undergraduate students has been a major part of my PhD experience. As such I would like to write a guide to introduce students to performing simulation-based research. My goal is for this guide to be useful for either a student first getting into research or someone mentoring a student in research.

In this guide, I will start with an introduction to python. Here I will start with setting up python, and then cover enough about python for a student to get started with a simulation project. Next, introduce the idea of simulations to students including starting with dynamic simulations for a deterministic system. I will then move on to cover simulating non-deterministic systems using stochastic and Monte-Carlo simulations.

7.1 Introduction to python

Here I give a comprehensive introduction to python. First, I will go over installing python and then get into a few of the basics such as using python as a simple calculator. I will discuss how we can expand pythons' capabilities by importing a library. Then I will cover a few data types in python along with a few basic operators. Next, I will discuss how we can store value in a variable. Finally, I will cover some more intermediate topics such as conditional statements, arrays, loops, and functions.

7.1.1 Installing python

There are many ways we can set up python on our own computers. I believe the most useful is using what is called the anaconda framework. Not only does this give us python but it gives us several useful tools along with python. We won't use them all, but there are several we will use, so it saves us from needing to install them all separately.

To install anaconda all we need to do is go to https://www.anaconda.com/ and click the download link. If prompted select the appropriate system (windows, macintosh, or linux). Once downloaded open the link and follow the installation prompts. I would recommend sticking with all recommended settings.

Anaconda will install several programs along with python, we will use the one called Spyder to use python. To open Spyder you can search for it on your computer, you might want to set up a shortcut to it.

7.1.2 Using Spyder

Spyder is what is called an integrated development environment (IDE). It provides a nice user interface for writing and running python code. Strictly speaking, we don't need this to use python, but it will make our lives simpler to use it.

Spyder has three panels. On the left we have the text editor; this is where we can write code that we can save for later use. On the bottom right is the console, this is where we can input code for immediate execution. On the upper right is where we can view various pieces of information as indicated by the tabs at the bottom of this panel. For example, this is where we can view plots.

7.1.3 Python as a simple calculator

To get started we will use the console on the bottom right. Let's start with a basic calculation such as 5+5. On the line that has "In [1]:" immediately following the colon. We can then press enter to execute it and get the expected value of 10. Now I would suggest trying out a few more complex expressions. At this point the console supports a few of the basic operations we are familiar with (addition, subtraction, multiplication, and division, and exponents). Notably we input exponents using "**" We can also use parenthesis to make more complex statements (see below).

```
In [2]: 5**2
Out [2]: 25
```

As you were trying out the trying out the console, you may have tried to use a function you know from math such as the sin function. If you did you will have gotten an error. This is because by default python only has a small set of things it knows how to do. So, if we want to use this function we need to import it from a library of functions. There are a few ways we can do this, here I will go over the easiest to understand. When I talk about python code files (7.1.5) I will introduce another approach.

The first way is to make an import statement that allows us to use the function directly. In the example below I am first importing the sin function from the NumPy library (this is a library we will use frequently). We also imported the value of π from the same library. We can see the value of π by typing pi into the console (as shown below). Next, we evaluate the $\sin(\pi)$ (note that the sin function assumes an input in radians). You were likely

expecting a value of 0, though we get a value extremely close to zero we are not getting exactly zero. This has to do with how the computer represents number which have decimal points, which I will not go into here. But if you are interested, you can look into what are called floating point numbers.

```
In [6]: from numpy import sin, pi

In [7]: pi
Out [7]: 3.141592653589793

In [8]: sin(pi)
Out [8]: 1.2246467991473532e-16
```

7.1.4 Types

We have already seen that we can use numbers in python. There are two types of numbers. The first is numbers that have decimal points (floating point numbers) and the other is integers. Python is reasonably forgiving about switching between these types of numbers, so I won't go into any of the nuances here. But this is something to watch out for, especially if you decide to program in another programming language such as java or c. The different types of numbers are two examples of what are called data types. Python has other data types as well.

In addition to the two already covered, we will use strings, Boolean, and lists. Strings are a data type the represents text. One common way we will use this data type is for keeping track of file and folder names. These values are entered as inside quotation marks. Boolean is a data type that can only have *True* or *False*. This will be useful to decide whether we take a certain action or not. And finally, lists are exactly as their name implies a list of values (which can be any of the data types mentioned). There are other data types that we won't be using such as complex numbers.

Each of these data types has operations associated with it. The Boolean type has four operators associated with it: *comparison (multiple)*, *not*, *and*, and *or*. The comparison operators compares two values and outputs a Boolean value. For example, to check if two values are the same, we would use two equal signs (==). We can also compare if something is less than (<), greater than (>), less than or equal (<=), or greater than or equal (>=). These two inputs don't need to be Boolean values. The *not* operator, takes a Boolean value and changes it to the opposite value. And takes in two Boolean values and outputs *True* if they are both *True*, otherwise it outputs *False*. Or takes in two Boolean values and outputs *True* if either one is *True*, otherwise it outputs *Fales*. Using the console to help, I suggest making a table for both *and* and *or* operations containing all four possible inputs for each. Some

examples with Boolean operations are shown below. We will return to dealing with strings and lists latter.

7.1.6 Variables

We can also have python store information for use. There are several reasons we might want to do this. First, it can make our code easier to read if we use given values relevant names. For instance, consider the value π, we all know that this represents a very specific number that shows up all over the place. Similarly in code if we want to use the same value in multiple locations it is cleaner to give that value a name. This is also useful for setting initial parameters before running our code (see *7.1.5*). We might also want to store the output of some operations for later use. Finally, we might not even know the value ahead of time, the value might be read from a file or input by the user.

Storing values into a variable is straight forward, we just use the equal symbol we use the equal symbol with the variable name to the left and the value to be stored on the right. In the example below x is given a value of 3, and why is the assigned the outcome of the expression 4**2. Next, we multiply x by 2 adding the result to y, and store the result in z. Finally, we print the result to the console using the print statement. Print is a function we will use all the time, which prints its input to the console. This will be useful latter on when we aren't running our code in the console.

```
In [16]: y = 4**2
In [17]: z = 2*x + y
In [18]: print(z)
22
```

7.1.5 Python code files

So far, we have just been entering code in the console and having each input statement executed immediately. However, our ultimate goal is to have code that we can execute multiple times and often with different starting values. To do this we will want to write our code in a file and have python execute that code line by line.

To see how this can be useful, imagine we are conduction an experiment to measure the period of an oscillating spring with a mass attached to it. We are given its spring constant and mass, so we can calculate a theoretical value. We measure the time it takes to complete 10 oscillations, allowing use to compute an experimental value for the period.

Finally, we can compute the percent error in the period, using the theoretical and experimental values of the period.

Below I have included some sample code that does exactly this, with its console output below it. This code would be typed in the left panel of Spyder. To run the code, you will press the large green arrow about it. The output will then appear in the console.

```python
import numpy as np

# our input values
mass = 0.15; # (kg)
k_spring = 3; # (N/m)

t_measured = 14.5
num_osc = 10;

T_theory = 2*np.pi*np.sqrt(mass/k_spring); # (s)
T_exp = t_measured/num_osc

p_error = 100*(T_exp - T_theory)/T_theory

print("Experimental Period:", T_exp, "s");
print("Theoretical Period:", np.round(T_theory,2), "s");
print("Percent Error:", np.round(p_error,2), "%")
```

```
Experimental Period: 1.45 s
Theoretical Period: 1.4 s
Percent Error: 3.21 %
```

In this code start by importing the numpy library. Notice that instead of importing individual items, I have imported the entire library. At the end of the import statement I have included the as np, this allows me to create a shorthand for numpy so now instead of typing numpy every time I want to access the library, I can just type np. So, to access the value of π, I would type *np.pi*. Next, I set up all of my input values. I then calculate the theoretical and experimental periods. After that, I use those values to calculate the percent error. Finally, I print out all the results to the console. Notice, I can give the print statement multiple values all separated by commas. In the last two print statements, I round the values to keep the output clean.

7.1.7 Conditional statements

Often, we want to do something only under a specific condition. For instance, continuing from our previous example, we might want our program to warn us if the percent error is too large. Otherwise, we just print our output as usual. To do this we will use if else statements. In the if statement we evaluate a condition and execute a set of statements if the condition is *True*. We can also chain multiple conditions using the else if statements.

Below I have modified our previous example to check if the percent error is a bit high or very high. I set two thresholds for these *error_mid* and *error_high*. Before printing the value of the percent error, I check if it is above either of these values. If it is I modify the enter a matching conditional statement. Notice at the end of the line for the if, elif, and else statements there is a colon. The statements to be executed under that condition are indented. This will also be the case for functions and loops.

```python
import numpy as np

# our input values
error_mid = 5;
error_high = 10;

mass = 0.15; # (kg)
k_spring = 3; # (N/m)

t_measured = 15
num_osc = 10;

T_theory = 2*np.pi*np.sqrt(mass/k_spring); # (s)
T_exp = t_measured/num_osc

p_error = 100*(T_exp - T_theory)/T_theory

print("Experimental Period:", T_exp, "s");
print("Theoretical Period:", np.round(T_theory,2), "s");
if p_error >= error_high:
  print("Double check your measurements.")
  print("The percent error is very high: ", np.round(p_error,2), "%")
elif p_error >= error_mid:
  print("The percent error is a bit high: ",  np.round(p_error,2), "%")
else:
  print("Percent Error:", np.round(p_error,2), "%")
```

```
Experimental Period: 1.5 s
Theoretical Period: 1.4 s
The percent error is a bit high: 6.76 %
```

7.1.6 Functions

Often when we have a calculation, we don't want to include the details of the calculation in our main code. To hide the details, we can use functions. We might also make a function if we are going to reuse a bit of code often. For example, we might be doing many experiments and need to calculate the percent error in each experiment. In that case, it might make sense to move this into a function. We have two choices as to where we can put the function at the top of the file (before it gets used), or in a new file. I will demonstrate putting it in a new file.

In this example, I will put this function in a file called "Experimental_analysis.py". the other file ("Spring_experiment.py") will be in the same folder. Below I show each of these in the order mentioned.

Notice that to define the function we used the key word *def*, we then have the name of the function (which we choose), then in parentheses, we list all the inputs and then end the line with a colon. Note inputs are not required, in that case, we will just have an empty set of parentheses.

```
def percentError(T_exp, T_theory):
    return 100*(T_exp - T_theory)/T_theory;

#using the function
p_error = percentError(T_exp, T_theory);
```

7.1.8 Lists and Loops

Let's consider that in the spring-mass experiment, we have now repeated our measurement several times. If we want to have the output printed for each of these trials, we could of course run our code multiple times. A better approach is to store each of these values in a list, and then we can use a loop to repeat the calculations and print the results of each.

In this case instead of having a single value for the time, we now have 5. To make a list we put all of these values in brackets. Now in order to go through and do our calculations and print our output for each of these, we will wrap the code we want to repeat in a for statement. This statement repeats itself for each value in the list. So as a result we perform our calculations for all of our time values using the same piece of code.

Note there is another important type of loop called a while loop. This loop repeats until some condition is not longer true.

```python
import numpy as np
from Experimental_analysis import percentError

# our input values
error_mid = 5;
error_high = 10;

mass = 0.15; # (kg)
k_spring = 3; # (N/m)

t_list = [13,14.5,13.9,15,16.1];
num_osc = 10;

for t_measured in t_list:
  T_theory = 2*np.pi*np.sqrt(mass/k_spring); # (s)
  T_exp = t_measured/num_osc

  p_error = percentError(T_exp,T_theory)

  print("Experimental Period:", T_exp, "s");
  print("Theoretical Period:", np.round(T_theory,2), "s");
  print("Percent Error:", np.round(p_error,2), "%")

  print("")
```

7.2 Introduction to simulations

One of our goals in science is to create a model that represents the most important aspects of the system we are studying. Creating these models allows us to gain a deeper understanding of a system and allows us exam the behavior of the system under a wide range of conditions. Creating a model for a specific system might entail starting with a set of laws the system obeys and using these laws to determine how that system changes over time.

For example, consider a spring-mass system. In this system, the forces experienced by the mass can be determined using Hooke's law, while Newton's Law will tell us how this force impacts the motion of the object. We can use these two laws to find an analytical solution for the position of the mass over time.

We could instead create a simulation to model the position of the mass, in the spring-mass system, changes over time. To do this we would use Hooke's law to determine the force on the mass at a given time and assume this force remains constant over a short

time. We could then use the standard kinematics equations (for a small time period) for an object under constant acceleration to update the position and velocity of the mass. Repeating this for many time steps we could determine how the position of the object changes over time.

The spring-mass system is an example of a deterministic system, meaning we can determine the exact position of the mass at any given time. Indeed, the analytical model for this system does exactly that. Similarly, we can make the simulation model as accurate as we need by making the time steps arbitrarily small.

Since the spring-mass system does have an analytical solution, modeling this system with a simulation is not strictly necessary. However, not all systems have an analytical solution. For example, for the N-body gravitational system, there is no known analytical solution. Thus, creating a simulation model for this system can be helpful in better understanding the system. In this case, the system is still deterministic. In principle, with the proper initial conditions we can determine the exact position of each of the objects at any given time.

7.3 Stochastic Simulations

Many systems don't behave deterministically and instead contain a certain amount of randomness. In these cases, modeling the system using only deterministic equations will not be sufficient, as it fails to capture the inherent randomness and uncertainty present in the system. In these situations, stochastic simulation can be used to capture the probabilistic nature of the system.

For example, in the case of Brownian motion, the motion of a small particle suspended in a fluid is affected by random collisions with the fluid molecules. These random collisions can cause the particle to move in random directions, which are uncorrelated with its previous movement. This process is called a random walk. A stochastic simulation uses random numbers to model the random motions of this particle. To see how this works we can consider the Brownian motion of a particle in two dimensions.

To simulate Brownian motion in one dimension, we can start by defining the initial position of the particle, say at the origin. We can then use a random number generator to determine the direction and magnitude of the particle's displacement in a small-time interval. This random displacement can be modeled as a Gaussian distribution centered at zero with a certain standard deviation, which determines the average distance the particle travels in a given time interval. This distance is proportional to the square of the elapsed time. This is given by $\Delta x = \sqrt{2D \cdot \Delta t}$ where Δx is the standard deviation of the Gaussian distribution, D is the diffusion constant of the particle, and Δt is the time interval over which the position of the particle is updated.

After determining the random displacement, we can update the position of the particle by adding the displacement to its previous position. We can repeat this process over many time steps to model the Brownian motion of the particle. If we run this simulation again, we can see that each time we end up with a distinct trajectory despite initial starting conditions. Figure 7.1 shows and example of the output from this simulation.
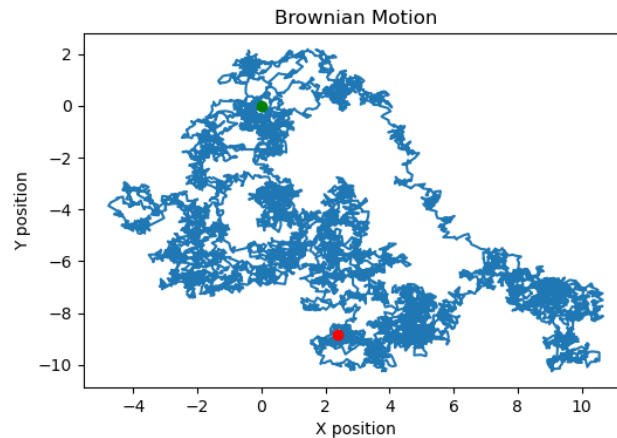
Figure 7.1 Example trajectory from Brownian motion simulation.

```python
import numpy as np
import matplotlib.pyplot as plt

# Define the simulation parameters
num_steps = 1000   # number of time steps
delta_t = 0.1   # time step size
diff_coef = 0.1   # diffusion coefficient


# Initialize an arrays for the position and time
X = np.zeros(num_steps + 1)
T = np.zeros(num_steps + 1)
# Generate random displacement at each time step using the normal
distribution
for i in range(num_steps):
    X[i+1] = X[i] + np.random.normal()*np.sqrt(2 * diff_coef * delta_t)
    T[i+1] = T[i] + delta_t

# Plot the particle trajectory
plt.plot(X, T)
plt.xlabel('Position')
plt.ylabel('Time')
plt.title('Brownian Motion')
plt.show()
```

7.4 Monte-Carlo Simulations

Often, we want to model a system in which the outcome of a given event is determined by a probability distribution. Simulations of this nature are called monte-Carlo simulations. For example, we might simulate the chance of a kids making it across a set of monkey bars. To keep things simple, we could say that there are two possibilities each time the kid attempts to reach the next bar; they either reach the bar, or they fall off entirely. To make things more interesting, we can consider that the kid gets tired as they go, so the probability of reaching the next bar goes down as they get further across the monkey bars.

To simulate this scenario using a Monte Carlo simulation, we can define a probability distribution for each attempt based on the distance from the starting point. For example, the probability of making the next bar might be relatively constant, to begin with, and then begin to decrease after some number of bars. At each attempt to reach the next bar, we could calculate the probability of reaching the next bar based on this probability. By comparing this probability to a random number, we can determine whether the kid makes it to the next bar or falls off.

If we repeat this simulation 100 times, we can then determine the percentage of kids who make it across the monkey bars. An example, of this simulation is provided below.

```python
from numpy.random import rand
import numpy as np

# Define the probability distribution for each attempt
# Based on the distance (in bars) crossed so far.
def success_prob(distance, p0, bars_at_p0, prob_drop_rate):

    # p0 : Starting probability of success.
    # bars_at_p0 : The bar the probability starts decreasing.
    # Prob_drop_rate : rate probability decreases.

    if distance <= bars_at_p0:
      # probability steady
      return p0;
    else:
      # probability decreasing
      prob = p0 + bars_at_p0*prob_drop_rate - prob_drop_rate*distance

      return max(prob,0);

# Define the simulation parameters
num_trials = 100  # Number of times to run the simulation
p0 = 0.9
bars_at_p0 = 5;
```

```python
prob_drop_rate = 0.01
bars_reached_list = np.zeros(num_trials);
total_bars = 10;
kids_reached = 0;

# Run the simulation
for trial in range(num_trials):
    reached_bar = True;
    bars_reached = 0;
    while reached_bar:
       # Calculate the success probability for this attempt
       prob = success_prob(bars_reached, p0, bars_at_p0, prob_drop_rate)
       if rand() <= prob:
         bars_reached += 1;
       else:
         reached_bar = False;

    if bars_reached >= total_bars:
      kids_reached += 1;

percent_accross = kids_reached/num_trials
print("Percent of kids who make it accross: %0.1f"%percent_accross)
```

Chapter 8 Appendix

8.1 Kinesin simulation code

```python
# Multi-motor Kinesin transport on a single microtubule
# Date : 03/09/2023

from os import path
from numpy import zeros, sqrt, random, sign, sum, save, ceil, floor, exp,
pi

def kinSim( simDir, sampleSize, fileNum_start, numMots, Pon, L0_nm,
delta_hind, velStdev, extForce ):

  KBT = 4.11 # (pN*nm)

  L0 = L0_nm*1e-6; # Unloaded run length of the motor (m)
  kmot = 0.32; #pN/nm
  Kmotor= kmot*1e-3  #motor stalk stiffness (N/m)
  Lmot= 40e-9  # Rest length of the motor (m)
  v_mean = 8*1e-7; # Mean unloaded motor velocity (m/s)
  velStdev  = velStdev*1e-6;
  dx = 8e-9  # Motors step size (m)
  Fs = 7.0e-12  # Stall force of single Kinesin (N)
  w = 2  # Power-law for loaded kinesin can be either [1/2 ,1 ,2]
  delta_assist = 2 # (nm)
  Fd_hind = KBT/delta_hind*1e-12; # (N)
  Fd_assist = KBT/delta_assist*1e-12; # (N)
  R = 2.5e-7 #cargo of radius (m)

  dt = 1e-5 # (s)
  t_max = 50000000; # Max time steps
  sampleRate = 1000; # How often to write to the file

  extForce_pN = extForce*1e-12 #pN (positive for hindering forces)

  etaFactor = 1; #1 for the viscosity of water
  #viscosity is twice bulk near surface and three times right at the
surface
  ksi = 6*pi*1e-3*R*3*etaFactor
  D = (1.38e-23)*295/ksi  # Einstein Diffusion constant

  notAttached = -100;
  takeStep = 1;
  pMotNum = False; # Is the motNums the mean number of motors?

  for fileNum in range( fileNum_start , sampleSize + fileNum_start ):
    # Motor number drawn from a poisson distribution.
    if pMotNum:
      Nmean = numMots
      numMots = random.poisson(Nmean);
```

```python
    while numMots == 0:
      numMots = random.poisson(Nmean);

  f_index = 1;
  d_index = 0;
  trajectory_data = zeros((int(t_max/sampleRate) + 1, numMots+2) );
  detach_data = zeros((int(t_max/sampleRate) + 1, numMots+3) );

  trajectory_file = "%scargoTajectory_%i.npy"%(simDir,fileNum)

  if path.isfile(trajectory_file):
    continue;

  cargoPosition = 0

  # Keeping track of lattice postioin.
  motLatPos = zeros(numMots,dtype=int)
  motLatPos[:] = notAttached
  vMot = zeros((numMots,1));
  motAction = zeros(numMots) # no action, take a step, or fall off

  for motNum in range(numMots):
    # Motor velocities are pulled from a normal distribution.
    vMot[motNum] = random.randn()*velStdev+v_mean;
    # The first row of the trajecory data will contain the velocity
    # of each motor.
    trajectory_data[0,motNum+2] = vMot[motNum];

  engMots = 0 #start with no engMotsaged motors

  # At least one motor needs to attach to the MT
  # before the cargos trajectory is started.
  while engMots == 0:
    for motNum in range(numMots):
      # See if any motors attach to the microtubule.
      # If any attached then set the starting locations.
      if random.rand() < Pon*dt:
        # Lbind is how far the motor can reach
        Lbind = min( abs(Lmot/2*random.randn()) ,Lmot);
        maxLatPos = ceil( (cargoPosition + Lbind)/dx );
        minLatPos = floor( (cargoPosition - Lbind) /dx);
        motLatPos[motNum] = random.randint(minLatPos,maxLatPos+1);
        engMots += 1;

  #Start of simulation.
  t_index = 0
  while t_index < t_max and engMots > 0:
    Fmot=zeros(numMots) #running tally of motor forces on cargo
    detachedMot = -1;
    #################################################
    # Loop through motors.
    # If unattached roll a dice to determine if the should be
    # reattached.
    # If they are attached make sure that they don't land on another
    # motor.
```

```python
    for motNum in range(numMots):
      if motLatPos[motNum] == notAttached and random.rand() < Pon*dt:
        # Determine how far the motor is currently stretched.
        Lbind = min ( abs(Lmot/2*random.rand()),Lmot);
        maxLatPos = ceil( (cargoPosition + Lbind)/dx );
        minLatPos = floor( (cargoPosition - Lbind) /dx);
        motLatPos[motNum] = random.randint(minLatPos,maxLatPos+1);
        engMots = engMots + 1

    # Go through all the motors that were attached before this time
    # step.
    for motNum in range(numMots):

      if motLatPos[motNum] != notAttached:
        #Define motor-cargo separation and which direction it is in.
        dLmot = cargoPosition - motLatPos[motNum]*dx
        sgn = sign(dLmot) # Negative if the motor is leading.

        # If the motor is longer than the natural length of the motor,
        # then it is stretched.
        # Otherwise it is not stretched and will not exert a
        # force on the cargo.
        if abs(dLmot) > Lmot:
          dLmot=(abs(dLmot)-Lmot)*sgn
        else:
          dLmot = 0

        Fmot[motNum] = Kmotor*dLmot # Compute the force on the motor

        if Fmot[motNum] <= 0:
          # off rate for opposing forces.
          offrate = exp(abs(Fmot[motNum])/Fd_hind);
        elif Fmot[motNum] > 0:
          # off rate for assisting forces larger than 2 pN.
          offrate = exp(Fmot[motNum]/Fd_assist);

        offrate = offrate*vMot[motNum]/L0;
        # The probability of the motor falling off the MT.
        prob = offrate*dt;

        # Determine if detachment occurs
        if (random.rand()<prob):
          motAction[motNum] = notAttached
          engMots = engMots-1
          detachedMot = motNum;

        # Find the probability of the motor stepping.
        if sign(Fmot[motNum]) < 0: # Hindering Force
          pf=1-exp(-(vMot[motNum]*dt/dx)*max(1-
(abs(Fmot[motNum])/Fs)**w,0))
        else:
          pf=1-exp(-(vMot[motNum]/dx)*dt) # Assisting Force

        # Roll some dice to see if the motors steps.
        if (random.rand() < pf) and motAction[motNum] != notAttached:
```

```python
        motAction[motNum] = takeStep; # motor steps

    # Balance forces on the cargo
    Fcargo = sum(Fmot) + extForce_pN
    # Compute new cargo position by adding thermal and drift components
    cargoPosition = cargoPosition+sqrt(2*D*dt)*random.randn() -
(Fcargo/ksi)*dt

    # Keep track of detachment events, to latter store in a file.
    # This needs to be done before the motors lattuce position is
    # updated
    # so we know where the detachmed motor was before it detached.
    if  detachedMot >= 0:
      detach_data[d_index,0] = t_index*dt;
      detach_data[d_index,1] = cargoPosition*1e9;
      detach_data[d_index,2] = detachedMot;
      for motNum in range(numMots):
        if motLatPos[motNum] == notAttached:
          detach_data[d_index,motNum+3] = notAttached;
        else:
          detach_data[d_index,motNum+3] = motLatPos[motNum]*dx*1e9;
      d_index = d_index+1;

    # Update motor lattuce position.
    for motNum in range(numMots):
      if motAction[motNum] == notAttached:
        motLatPos[motNum] = notAttached;
      elif motAction[motNum] == 1:
        motLatPos[motNum] = motLatPos[motNum]+1;
      motAction[motNum] = 0;

    #Store trajectory info to latter be written to a file.
    if t_index%sampleRate == 0 and engMots > 0:
      trajectory_data[f_index,0] = t_index*dt;
      trajectory_data[f_index,1] = cargoPosition*1e9;
      for motNum in range(numMots):
        if motLatPos[motNum] == notAttached:
          trajectory_data[f_index,motNum+2] = notAttached;
        else:
          trajectory_data[f_index,motNum+2] = motLatPos[motNum]*dx*1e9
      f_index += 1

    t_index = t_index+1

save(trajectory_file, trajectory_data[0:f_index,:]);
detach_output_file = "%sdetachment_%i.csv"%(simDir,fileNum);
save(detach_output_file, detach_data[0:d_index,:]);
```

8.2 Method Code

8.2.1 Obtain a list of run length and velocities

```python
def get_vel_Dist_npy(simDir,numSamps, remake = True, RL_cutoff = 0.1):

    if not os.path.exists(simDir):
        print("does not exist: %s"%simDir);
        return None;

    vCount = 0;
    RL_list_file = "%srunLenList.csv"%simDir
    vel_list_file = '%svelList.csv'%simDir;

    if os.path.exists(vel_list_file) and not remake:
        velocityList = np.loadtxt(vel_list_file);
        RL_list = np.loadtxt(RL_list_file);
        return velocityList,RL_list;
    velocityList = np.zeros(numSamps);
    RL_list = np.zeros(numSamps)

    for simNum in range(numSamps):
        beadFile = '%sdet.%imot.npy'%(simDir,simNum+1)

        if not os.path.exists(beadFile):
            beadFile = '%stimeOut.%imot.npy'%(simDir,simNum+1)
        if not os.path.exists(beadFile):
            print(beadFile)
            continue;

        beadData = np.load(beadFile);
        if len(beadData)>5:
            RL = (beadData[-1,1]-beadData[1,1])/1000;
            if RL > RL_cutoff:
                fit = np.polyfit(beadData[1:,0],beadData[1:,1]/1000,1)
                velocityList[vCount] = fit[0]
                RL_list[vCount] = RL;
                vCount = vCount + 1;

    if vCount > 0:
        np.savetxt(vel_list_file,velocityList[0:vCount])
        np.savetxt(RL_list_file,RL_list[0:vCount])

    return velocityList[0:vCount],RL_list[0:vCount];
```

8.2.2 Fitting a run length distribution

```python
def fitExpDist(rawData, plot=False,figNum=1):
    cumDist = binCumDist(rawData);
    initVals = [1,np.median(cumDist)]
    fitVals = curve_fit(exp_fit,cumDist[:,0],cumDist[:,1],p0=initVals);

    return fitVals[1]

def exp_fit(x,A,D):
   return 1-A*np.exp(-(x)/D);
```

8.2.3 Fitting a velocity distribution

```python
def fit_cumNorm_dist(rawVel_dist):
    cDist = binCumDist(rawVel_dist);
    initVals = [np.mean(rawVel_dist),np.std(rawVel_dist)];
    fitVals = curve_fit(cumNorm_fit,cDist[:,0],cDist[:,1],p0=initVals);
    return fitVals

def cumNorm_fit(x,m,stdev):
    return 0.5*(1+erf((x-m)/(stdev*np.sqrt(2))) );
```

8.2.4 Bootstrapping code

```python
def RL_bootStrap(rawData, subSampSize = 200, repSamp = 10):
    RL_BS_list = np.zeros(repSamp);
    for ii in range(repSamp):
        RL_subSample = randSubSamp(rawData,subSampSize)
        RL_BS_list[ii] = fitExpDist(RL_subSample)
    RL_mean = np.mean(RL_BS_list)
    RL_error = np.std(RL_BS_list)
    return RL_mean, RL_error;
```

References

1.   Ridley, A.J., *Life at the leading edge.* Cell, 2011. **145**(7): p. 1012-22.

2.   Lauffenburger, D.A. and A.F. Horwitz, *Cell migration: a physically integrated molecular process.* Cell, 1996. **84**(3): p. 359-69.

3.   Beeby, M., et al., *Propulsive nanomachines: the convergent evolution of archaella, flagella and cilia.* FEMS Microbiology Reviews, 2020. **44**(3): p. 253-304.

4.   Fletcher, D.A. and J.A. Theriot, *An introduction to cell motility for the physical scientist.* Physical Biology, 2004. **1**(1): p. T1.

5.   Cretel, E., et al., *How Cells feel their environment: a focus on early dynamic events.* Cell Mol Bioeng, 2008. **1**(1): p. 5-14.

6.   Hirokawa, N. and Y. Noda, *Intracellular transport and kinesin superfamily proteins, KIFs: structure, function, and dynamics.* Physiol Rev, 2008. **88**(3): p. 1089-118.

7.   Vale, R.D., *The molecular motor toolbox for intracellular transport.* Cell, 2003. **112**(4): p. 467-480.

8.   Nirschl, J.J., A.E. Ghiretti, and E.L.F. Holzbaur, *The impact of cytoskeletal organization on the local regulation of neuronal transport.* Nature Reviews Neuroscience, 2017. **18**(10): p. 585-597.

9.   Lodish, H., A. Berk, and S. Zipursky, *Molecular Cell Biology*. 2000.

10.   Hirokawa, N., et al., *Kinesin superfamily motor proteins and intracellular transport.* Nature reviews Molecular cell biology, 2009. **10**(10): p. 682-696.

11.   Millecamps, S. and J.-P. Julien, *Axonal transport deficits and neurodegenerative diseases.* Nature Reviews Neuroscience, 2013. **14**(3): p. 161-176.

12.   Brady, S.T. and G.A. Morfini, *Regulation of motor proteins, axonal transport deficits and adult-onset neurodegenerative diseases.* Neurobiology of disease, 2017. **105**: p. 273-282.

13.   Sleigh, J.N., et al., *Axonal transport and neurological disease.* Nature Reviews Neurology, 2019. **15**(12): p. 691-703.

14.   Gordon, D., et al., *Single-copy expression of an amyotrophic lateral sclerosis-linked TDP-43 mutation (M337V) in BAC transgenic mice leads to altered stress*

granule dynamics and progressive motor dysfunction. Neurobiol Dis, 2019. **121**: p. 148-162.

15. Moller, A., et al., *Amyotrophic lateral sclerosis-associated mutant SOD1 inhibits anterograde axonal transport of mitochondria by reducing Miro1 levels.* Hum Mol Genet, 2017. **26**(23): p. 4668-4679.

16. Gauthier, L.R., et al., *Huntingtin Controls Neurotrophic Support and Survival of Neurons by Enhancing BDNF Vesicular Transport along Microtubules.* Cell, 2004. **118**(1): p. 127-138.

17. Gunawardena, S. and L.S.B. Goldstein, *Disruption of Axonal Transport and Neuronal Viability by Amyloid Precursor Protein Mutations in Drosophila.* Neuron, 2001. **32**(3): p. 389-401.

18. Reid, E., et al., *A kinesin heavy chain (KIF5A) mutation in hereditary spastic paraplegia (SPG10).* Am J Hum Genet, 2002. **71**(5): p. 1189-94.

19. Weedon, M.N., et al., *Exome sequencing identifies a DYNC1H1 mutation in a large pedigree with dominant axonal Charcot-Marie-Tooth disease.* Am J Hum Genet, 2011. **89**(2): p. 308-12.

20. Aulchenko, Y.S., et al., *Genetic variation in the KIF1B locus influences susceptibility to multiple sclerosis.* Nature Genetics, 2008. **40**(12): p. 1402-1403.

21. Filges, I., et al., *Exome sequencing identifies mutations in KIF14 as a novel cause of an autosomal recessive lethal fetal ciliopathy phenotype.* Clinical genetics, 2014. **86**(3): p. 220-228.

22. Moawia, A., et al., *Mutations of KIF14 cause primary microcephaly by impairing cytokinesis.* Annals of neurology, 2017. **82**(4): p. 562-577.

23. Zhao, C., et al., *Charcot-Marie-Tooth disease type 2A caused by mutation in a microtubule motor KIF1Bβ.* Cell, 2001. **105**(5): p. 587-597.

24. He, M., et al., *The kinesin-4 protein Kif7 regulates mammalian Hedgehog signalling by organizing the cilium tip compartment.* Nature Cell Biology, 2014. **16**(7): p. 663-672.

25. Marszalek, J.R., et al., *Novel dendritic kinesin sorting identified by different process targeting of two related kinesins: KIF21A and KIF21B.* J Cell Biol, 1999. **145**(3): p. 469-79.

26.   Yu, W.-X., et al., *Kinesin-5 Eg5 is essential for spindle assembly, chromosome stability and organogenesis in development.* Cell Death Discovery, 2022. **8**(1): p. 490.

27.   Sleiman, P.M.A., et al., *Loss-of-Function Mutations in KIF15 Underlying a Braddock-Carey Genocopy.* Hum Mutat, 2017. **38**(5): p. 507-510.

28.   Kalantari, S. and I. Filges, *'Kinesinopathies': emerging role of the kinesin family member genes in birth defects.* J Med Genet, 2020. **57**(12): p. 797-807.

29.   Andreasson, J.O., et al., *Examining kinesin processivity within a general gating framework.* Elife, 2015. **4**.

30.   Milic, B., et al., *Kinesin processivity is gated by phosphate release.* Proc Natl Acad Sci U S A, 2014. **111**(39): p. 14136-40.

31.   Schnitzer, M.J. and S.M. Block, *Kinesin hydrolyses one ATP per 8-nm step.* Nature, 1997. **388**(6640): p. 386-90.

32.   Schnitzer, M.J., K. Visscher, and S.M. Block, *Force production by single kinesin motors.* Nat Cell Biol, 2000. **2**(10): p. 718-23.

33.   Svoboda, K. and S.M. Block, *Force and velocity measured for single kinesin molecules.* Cell, 1994. **77**(5): p. 773-84.

34.   Coy, D.L., M. Wagenbach, and J. Howard, *Kinesin takes one 8-nm step for each ATP that it hydrolyzes.* Journal of Biological Chemistry, 1999. **274**(6): p. 3667-3671.

35.   Wade, R.H. and A.A. Hyman, *Microtubule structure and dynamics.* Current Opinion in Cell Biology, 1997. **9**(1): p. 12-17.

36.   Chrétien, D., et al., *Lattice defects in microtubules: protofilament numbers vary within individual microtubules.* The Journal of cell biology, 1992. **117**(5): p. 1031-1040.

37.   Arnal, I. and R.H. Wade, *How does taxol stabilize microtubules?* Current biology, 1995. **5**(8): p. 900-908.

38.   Dogterom, M. and G.H. Koenderink, *Actin–microtubule crosstalk in cell biology.* Nature Reviews Molecular Cell Biology, 2019. **20**(1): p. 38-54.

39.   Ray, S., et al., *Kinesin follows the microtubule's protofilament axis.* The Journal of cell biology, 1993. **121**(5): p. 1083-1093.

40. Miller, R.H. and R.J. Lasek, *Cross-bridges mediate anterograde and retrograde vesicle transport along microtubules in squid axoplasm.* The Journal of cell biology, 1985. **101**(6): p. 2181-2193.

41. Franker, M.A. and C.C. Hoogenraad, *Microtubule-based transport–basic mechanisms, traffic rules and role in neurological pathogenesis.* Journal of cell science, 2013. **126**(11): p. 2319-2329.

42. Steinhauer, J. and D. Kalderon, *Microtubule polarity and axis formation in the Drosophila oocyte.* Developmental Dynamics, 2006. **235**(6): p. 1455-1468.

43. Derr, N.D., et al., *Tug-of-war in motor protein ensembles revealed with a programmable DNA origami scaffold.* Science, 2012. **338**(6107): p. 662-665.

44. Hendricks, A.G., et al., *Motor coordination via a tug-of-war mechanism drives bidirectional vesicle transport.* Current Biology, 2010. **20**(8): p. 697-702.

45. Kunwar, A., et al., *Mechanical stochastic tug-of-war models cannot explain bidirectional lipid-droplet transport.* Proceedings of the National Academy of Sciences, 2011. **108**(47): p. 18960-18965.

46. Kural, C., et al., *Kinesin and dynein move a peroxisome in vivo: a tug-of-war or coordinated movement?* Science, 2005. **308**(5727): p. 1469-1472.

47. Liang, W.H., et al., *Microtubule defects influence kinesin-based transport in vitro.* Biophysical journal, 2016. **110**(10): p. 2229-2240.

48. Hirokawa, N., *Microtubule organization and dynamics dependent on microtubule-associated proteins.* Current opinion in cell biology, 1994. **6**(1): p. 74-81.

49. Vershinin, M., et al., *Tuning microtubule-based transport through filamentous MAPs: the problem of dynein.* Traffic, 2008. **9**(6): p. 882-92.

50. Chaudhary, A.R., et al., *MAP7 regulates organelle transport by recruiting kinesin-1 to microtubules.* Journal of Biological Chemistry, 2019. **294**(26): p. 10160-10171.

51. Hooikaas, P.J., et al., *MAP7 family proteins regulate kinesin-1 recruitment and activation.* Journal of Cell Biology, 2019. **218**(4): p. 1298-1318.

52. Tymanskyj, S.R., et al., *MAP7 regulates axon morphogenesis by recruiting kinesin-1 to microtubules and modulating organelle transport.* Elife, 2018. **7**: p. e36374.

53. Xu, J., et al., *Interplay between velocity and travel distance of kinesin-based transport in the presence of tau.* Biophysical journal, 2013. **105**(10): p. L23-L25.

54.   Vershinin, M., et al., *Multiple-motor based transport and its regulation by Tau.* Proc Natl Acad Sci U S A, 2007. **104**(1): p. 87-92.

55.   Li, Q., et al., *Cholesterol in the cargo membrane amplifies tau inhibition of kinesin-1-based transport.* Proceedings of the National Academy of Sciences, 2023. **120**(3): p. e2212507120.

56.   Miki, H., Y. Okada, and N. Hirokawa, *Analysis of the kinesin superfamily: insights into structure and function.* Trends in cell biology, 2005. **15**(9): p. 467-476.

57.   Mandelkow, E. and K.A. Johnson, *The structural and mechanochemical cycle of kinesin.* Trends in biochemical sciences, 1998. **23**(11): p. 429-433.

58.   Yildiz, A., et al., *Kinesin walks hand-over-hand.* Science, 2004. **303**(5658): p. 676-678.

59.   Hackney, D.D., *Highly processive microtubule-stimulated ATP hydrolysis by dimeric kinesin head domains.* Nature, 1995. **377**(6548): p. 448-450.

60.   Cross, R.A., *The kinetic mechanism of kinesin.* Trends in biochemical sciences, 2004. **29**(6): p. 301-309.

61.   Block, S.M., L.S. Goldstein, and B.J. Schnapp, *Bead movement by single kinesin molecules studied with optical tweezers.* Nature, 1990. **348**(6299): p. 348-352.

62.   Andreasson, J.O., et al., *The mechanochemical cycle of mammalian kinesin-2 KIF3A/B under load.* Current Biology, 2015. **25**(9): p. 1166-1175.

63.   Xu, J., et al., *Tuning multiple motor travel via single motor velocity.* Traffic, 2012. **13**(9): p. 1198-205.

64.   Yajima, J., et al., *Direct long-term observation of kinesin processivity at low load.* Current biology, 2002. **12**(4): p. 301-306.

65.   Kunwar, A., et al., *Stepping, strain gating, and an unexpected force-velocity curve for multiple-motor-based transport.* Current biology, 2008. **18**(16): p. 1173-1183.

66.   Nettesheim, G., et al., *Macromolecular crowding acts as a physical regulator of intracellular transport.* Nature Physics, 2020. **16**(11): p. 1144-1151.

67.   Feng, Q., et al., *Motor Reattachment Kinetics Play a Dominant Role in Multimotor-Driven Cargo Transport.* Biophysical Journal, 2018. **114**(2): p. 400-409.

68.   Jiang, R., et al., *Microtubule binding kinetics of membrane-bound kinesin-1 predicts high motor copy numbers on intracellular cargo.* Proceedings of the National Academy of Sciences, 2019. **116**(52): p. 26564-26570.

69.   Jiang, R., et al., *Slow Microtubule Binding Kinetics of Membrane-bound Kinesin Predicts High Motor Copy Numbers on Intracellular Cargo.* bioRxiv, 2019: p. 627174.

70.   Li, Q., et al., *Quantitative determination of the probability of multiple-motor transport in bead-based assays.* Biophysical journal, 2016. **110**(12): p. 2720-2728.

71.   Rank, M. and E. Frey, *Crowding and Pausing Strongly Affect Dynamics of Kinesin-1 Motors along Microtubules.* Biophysical Journal, 2018. **115**(6): p. 1068-1081.

72.   Seitz, A., et al., *Single-molecule investigation of the interference between kinesin, tau and MAP2c.* The EMBO journal, 2002. **21**(18): p. 4896-4905.

73.   Maday, S., et al., *Axonal transport: cargo-specific mechanisms of motility and regulation.* Neuron, 2014. **84**(2): p. 292-309.

74.   Margraves, C., et al., *Simultaneous measurements of cytoplasmic viscosity and intracellular vesicle sizes for live human brain cancer cells.* Biotechnol Bioeng, 2011. **108**(10): p. 2504-8.

75.   Shubeita, G.T., et al., *Consequences of motor copy number on the intracellular transport of kinesin-1-driven lipid droplets.* Cell, 2008. **135**(6): p. 1098-1107.

76.   Wilson, J., et al., *Cargo diffusion shortens single-kinesin runs at low viscous drag.* Scientic reports, 2019.

77.   Kalwarczyk, T., et al., *Comparative analysis of viscosity of complex liquids and cytoplasm of mammalian cells at the nanoscale.* Nano letters, 2011. **11**(5): p. 2157-2163.

78.   Kuimova, M.K., et al., *Imaging intracellular viscosity of a single cell during photoinduced cell death.* Nat Chem, 2009. **1**(1): p. 69-73.

79.   Luby-Phelps, K., et al., *A novel fluorescence ratiometric method confirms the low solvent viscosity of the cytoplasm.* Biophys J, 1993. **65**(1): p. 236-42.

80.   Hunt, A.J., F. Gittes, and J. Howard, *The force exerted by a single kinesin molecule against a viscous load.* Biophysical journal, 1994. **67**(2): p. 766.

81.   Beausang, J.F., et al., *Elementary simulation of tethered Brownian motion.* American Journal of Physics, 2007. **75**: p. 520–523.

82. Li, Q., et al., *A fluid membrane enhances the velocity of cargo transport by small teams of kinesin-1.* The Journal of Chemical Physics, 2018. **148**(12): p. 123318.

83. Sarpangala, N. and A. Gopinathan, *Cargo surface fluidity can reduce inter-motor mechanical interference, promote load-sharing and enhance processivity in teams of molecular motors.* PLOS Computational Biology, 2022. **18**(6): p. e1010217.

84. Verhey, K.J. and J.W. Hammond, *Traffic control: regulation of kinesin motors.* Nature Reviews Molecular Cell Biology, 2009. **10**(11): p. 765-777.

85. Monroy, B.Y., et al., *A combinatorial MAP code dictates polarized microtubule transport.* Developmental cell, 2020. **53**(1): p. 60-72. e4.

86. Telley, I.A., P. Bieling, and T. Surrey, *Obstacles on the microtubule reduce the processivity of Kinesin-1 in a minimal in vitro system and in cell extract.* Biophysical journal, 2009. **96**(8): p. 3341-3353.

87. Ferro, L.S., et al., *Structural and functional insight into regulation of kinesin-1 by microtubule-associated protein MAP7.* Science, 2022. **375**(6578): p. 326-331.

88. Wilson, J.O., A.D. Zaragoza, and J. Xu, *Tuning ensemble-averaged cargo run length via fractional change in mean kinesin number.* Phys Biol, 2021. **18**(4).

89. Kerssemakers, J., et al., *The distance that kinesin-1 holds its cargo from the microtubule surface measured by fluorescence interference contrast microscopy.* Proceedings of the National Academy of Sciences, 2006. **103**(43): p. 15812-15817.

90. Coppin, C.M., et al., *Detection of sub-8-nm movements of kinesin by high-resolution optical-trap microscopy.* Proceedings of the National Academy of Sciences, 1996. **93**(5): p. 1913-1917.

91. Coppin, C.M., et al., *The load dependence of kinesin's mechanical cycle.* Proceedings of the National Academy of Sciences, 1997. **94**(16): p. 8539-8544.

92. Kawaguchi, K., S. Uemura, and S.i. Ishiwata, *Equilibrium and transition between single-and double-headed binding of kinesin as revealed by single-molecule mechanics.* Biophysical journal, 2003. **84**(2): p. 1103-1113.

93. Leduc, C., et al., *Cooperative extraction of membrane nanotubes by molecular motors.* Proceedings of the National Academy of Sciences, 2004. **101**(49): p. 17096-17101.

94. Dix, J.A. and A.S. Verkman, *Mapping of fluorescence anisotropy in living cells by ratio imaging. Application to cytoplasmic viscosity.* Biophys J, 1990. **57**(2): p. 231-40.

95. Visscher, K., M.J. Schnitzer, and S.M. Block, *Single kinesin molecules studied with a molecular force clamp.* Nature, 1999. **400**(6740): p. 184-189.

96. Valentine, M.T., et al., *Precision steering of an optical trap by electro-optic deflection.* Opt Lett, 2008. **33**(6): p. 599-601.

97. Clancy, B.E., et al., *A universal pathway for kinesin stepping.* Nat Struct Mol Biol, 2011. **18**(9): p. 1020-7.

98. Manly, B.F.J., *Randomization, Bootstrap and Monte Carlo Methods in Biology, Third Edition*. 2006: Chapman and Hall/CRC.

99. Kovesi, P., *Good colour maps: How to design them.* arXiv preprint arXiv:1509.03700, 2015.

100. Alcocer, M., *Convert matlab colormap to binary.pal format.* https://www.mathworks.com/, 2013.

101. Einstein, A., *Investigations on the theory of brownian movement.* Annalen der Physik, 1905: p. 549–560.

102. Turing, A.M., *The chemical basis of morphogenesis. 1953.* Bull Math Biol, 1990. **52**(1-2): p. 153-97; discussion 119-52.

103. Gregor, T., et al., *Diffusion and scaling during early embryonic pattern formation.* Proc Natl Acad Sci U S A, 2005. **102**(51): p. 18403-7.

104. McMurtrey, R.J., *Roles of Diffusion Dynamics in Stem Cell Signaling and Three-Dimensional Tissue Development.* Stem Cells Dev, 2017. **26**(18): p. 1293-1303.

105. Rohde, R.A. and P.B. Price, *Diffusion-controlled metabolism for long-term survival of single isolated microorganisms trapped within ice crystals.* Proc Natl Acad Sci U S A, 2007. **104**(42): p. 16592-7.

106. Sozański, K., et al., *Small crowders slow down kinesin-1 stepping by hindering motor domain diffusion.* Physical review letters, 2015. **115**(21): p. 218102.

107. Bergman, J.P., et al., *Cargo navigation across 3D microtubule intersections.* Proceedings of the National Academy of Sciences, 2018: p. 201707936.

108. Mogilner, A., et al., *Molecular motors: Theory.*, in *Joel Keizer's Computational Cell Biology*, C. Fall, et al., Editors. 2002. p. 321–355.

109. Suhling, K., et al., *Time-resolved fluorescence anisotropy imaging applied to live cells.* Opt Lett, 2004. **29**(6): p. 584-6.

110. Zhang, B., et al., *Synaptic vesicle size and number are regulated by a clathrin adaptor protein required for endocytosis.* Neuron, 1998. **21**(6): p. 1465-75.

111. Casley-Smith, J.R., *The dimensions and numbers of small vesicles in cells, endothelial and mesothelial and the significance of these for endothelial permeability.* J Microsc, 1969. **90**(3): p. 251-68.

112. Bakker, A.C., et al., *Homotypic fusion between aggregated lysosomes triggered by elevated [Ca2+]i in fibroblasts.* J Cell Sci, 1997. **110 (Pt 18)**: p. 2227-38.

113. Wiemerslage, L. and D. Lee, *Quantification of mitochondrial morphology in neurites of dopaminergic neurons using multiple parameters.* J Neurosci Methods, 2016. **262**: p. 56-65.

114. Keller, S., K. Berghoff, and H. Kress, *Phagosomal transport depends strongly on phagosome size.* Sci Rep, 2017. **7**(1): p. 17068.

115. Lorenz, T. and M. Willard, *Subcellular fractionation of intra-axonally transport polypeptides in the rabbit visual system.* Proc Natl Acad Sci U S A, 1978. **75**(1): p. 505-9.

116. Tytell, M., et al., *Axonal transport: each major rate component reflects the movement of distinct macromolecular complexes.* Science, 1981. **214**(4517): p. 179-81.

117. Opper, M. and D. Saad, *Advanced Mean Field Methods: Theory and Practice.* 2001: The MIT Press.

118. Rogers, A.R., et al., *Negative interference dominates collective transport of kinesin motors in the absence of load.* Physical Chemistry Chemical Physics, 2009. **11**(24): p. 4882-4889.

119. Ando, D., et al., *Cooperative protofilament switching emerges from inter-motor interference in multiple-motor transport.* Sci Rep, 2014. **4**: p. 7255.

120. Erickson, R.P., et al., *How molecular motors are arranged on a cargo is important for vesicular transport.* PLoS computational biology, 2011. **7**(5): p. e1002032.

121. Holzwarth, G., K. Bonin, and D.B. Hill, *Forces required of kinesin during processive transport through cytoplasm.* Biophys J, 2002. **82**(4): p. 1784-90.

122. Vale, R.D., et al., *Direct observation of single kinesin molecules moving along microtubules.* Nature, 1996. **380**(6573): p. 451-3.

123. Ross, J.L. and R. Dixit, *Multiple color single molecule TIRF imaging and tracking of MAPs and motors.* Methods Cell Biol, 2010. **95**: p. 521-42.

124. Nelson, S.R., K.M. Trybus, and D.M. Warshaw, *Motor coupling through lipid membranes enhances transport velocities for ensembles of myosin Va.* Proc Natl Acad Sci U S A, 2014. **111**(38): p. E3986-95.

125. Andreasson, J.O.L., *Single-Molecule Biophysics of Kinesin Family Motor Proteins.* 2013, Stanford University, Stanford, CA.

126. Nicholas, M.P., et al., *Cytoplasmic dynein regulates its attachment to microtubules via nucleotide state-switched mechanosensing at multiple AAA domains.* Proc Natl Acad Sci U S A, 2015. **112**(20): p. 6371-6.

127. Carter, N.J. and R.A. Cross, *Mechanics of the kinesin step.* Nature, 2005. **435**(7040): p. 308-12.

128. Schief, W.R., et al., *Inhibition of kinesin motility by ADP and phosphate supports a hand-over-hand mechanism.* Proc Natl Acad Sci U S A, 2004. **101**(5): p. 1183-8.

129. Liepelt, S. and R. Lipowsky, *Kinesin's network of chemomechanical motor cycles.* Phys Rev Lett, 2007. **98**(25): p. 258102.

130. Jamison, D.K., et al., *Two kinesins transport cargo primarily via the action of one motor: implications for intracellular transport.* Biophysical journal, 2010. **99**(9): p. 2967-2977.

131. Furuta, K.y., et al., *Measuring collective transport by defined numbers of processive and nonprocessive kinesin motors.* Proceedings of the National Academy of Sciences, 2013. **110**(2): p. 501-506.

132. Belyy, V., et al., *The mammalian dynein-dynactin complex is a strong opponent to kinesin in a tug-of-war competition.* Nat Cell Biol, 2016. **18**(9): p. 1018-24.

133. Norris, S.R., et al., *A method for multiprotein assembly in cells reveals independent action of kinesins in complex.* J Cell Biol, 2014. **207**(3): p. 393-406.

134. Katrukha, E.A., et al., *Probing cytoskeletal modulation of passive and active intracellular dynamics using nanobody-functionalized quantum dots.* Nat Commun, 2017. **8**: p. 14772.

135. Nam, W. and B.I. Epureanu, *The effects of viscoelastic fluid on kinesin transport.* J Phys Condens Matter, 2012. **24**(37): p. 375103.

136. Rai, A.K., et al., *Molecular adaptations allow dynein to generate large collective forces inside cells.* Cell, 2013. **152**(1-2): p. 172-82.

137. Dixit, R., et al., *Differential regulation of dynein and kinesin motor proteins by tau.* Science, 2008. **319**(5866): p. 1086-9.

138. McVicker, D.P., L.R. Chrin, and C.L. Berger, *The nucleotide-binding state of microtubules modulates kinesin processivity and the ability of Tau to inhibit kinesin-mediated transport.* J Biol Chem, 2011. **286**(50): p. 42873-80.

139. Monroy, B.Y., et al., *Competition between microtubule-associated proteins directs motor transport.* Nat Commun, 2018. **9**(1): p. 1487.

140. Beeg, J., et al., *Transport of beads by several kinesin motors.* Biophysical journal, 2008. **94**(2): p. 532-541.

141. Li, Q., S.J. King, and J. Xu, *Native kinesin-1 does not bind preferentially to GTP-tubulin-rich microtubules in vitro.* Cytoskeleton, 2017. **74**(9): p. 356-366.

142. Klumpp, S. and R. Lipowsky, *Cooperative cargo transport by several molecular motors.* Proceedings of the National Academy of Sciences of the United States of America, 2005. **102**(48): p. 17284-17289.

143. Klein, S., C. Appert-Rolland, and L. Santen, *Environmental control of microtubule-based bidirectional cargo transport.* Eur Phys J, 2014. **107**: p. 18004.

144. Kunwar, A. and A. Mogilner, *Robust transport by multiple motors with nonlinear force–velocity relations and stochastic load sharing.* Physical biology, 2010. **7**(1): p. 016012.

145. Reddy, B.J., et al., *Heterogeneity in kinesin function.* Traffic, 2017. **18**(10): p. 658-671.

146. Jamison, D.K., J.W. Driver, and M.R. Diehl, *Cooperative responses of multiple kinesins to variable and constant loads.* Journal of Biological Chemistry, 2012. **287**(5): p. 3357-3365.

147. Berger, F., S. Klumpp, and R. Lipowsky, *Force-dependent unbinding rate of molecular motors from stationary optical trap data.* Nano letters, 2019. **19**(4): p. 2598-2602.

148. Ellis, R.J., *Macromolecular crowding: obvious but underappreciated.* Trends in biochemical sciences, 2001. **26**(10): p. 597-604.

149.   Gierasch, L.M. and A. Gershenson, *Post-reductionist protein science, or putting Humpty Dumpty back together again.* Nature chemical biology, 2009. **5**(11): p. 774-777.

150.   Gnutt, D. and S. Ebbinghaus, *The macromolecular crowding effect–from in vitro into the cell.* Biological chemistry, 2016. **397**(1): p. 37-44.

151.   Minton, A.P., *The influence of macromolecular crowding and macromolecular confinement on biochemical reactions in physiological media.* Journal of biological chemistry, 2001. **276**(14): p. 10577-10580.

152.   Ellis, R.J. and A.P. Minton, *Join the crowd.* Nature, 2003. **425**(6953): p. 27-28.

153.   Zhou, H.X., G. Rivas, and A.P. Minton, *Macromolecular crowding and confinement: biochemical, biophysical, and potential physiological consequences.* Annu Rev Biophys, 2008. **37**: p. 375-97.

154.   Ge, J., et al., *Macromolecular crowding modulates actomyosin kinetics.* Biophysical journal, 2016. **111**(1): p. 178-184.

155.   Chase, K., F. Doval, and M. Vershinin, *Enhanced stability of kinesin-1 as a function of temperature.* Biochemical and biophysical research communications, 2017. **493**(3): p. 1318-1321.